Ph. D. DISSERTATION

Low Power Design and LCP Packaging

for Photodiode-based Retinal Prosthesis System

광 다이오드 기반 인공 망막 시스템을 위한

저전력 설계 및 LCP 패키징에 대한 연구

By

JEONG HOAN PARK

FEBRUARY 2017

**DEPARTMENT OF ELECTRICAL ENGINEERING AND
COMPUTER SCIENCE
COLLEGE OF ENGINEERING
SEOUL NATIONAL UNIVERSITY**

Low Power Design and LCP Packaging

for Photodiode-based Retinal Prosthesis System

지도 교수 김 성 준

이 논문을 공학박사 학위논문으로 제출함
2017년 2월

서울대학교 대학원
전기 · 컴퓨터공학부
박 정 환

박정환의 공학박사 학위논문을 인준함
2017년 2월

위 원 장	조	동	일	
부위원장	김	성	준	
위　　원	서	종	모	
위　　원	송	윤	규	(인)
위　　원	전	상	범	(인)

Abstract

The retinal prosthesis is an implantable electronic device that delivers electrical stimuli containing visual information to the retina for the visual restoration of the blinds. The currently available retinal prostheses have several problems in the number of pixels. They are limited in the number of pixels, which restricts the amount of visual information they can deliver. Many research groups are trying to improve their device in this aspect. In order to achieve a significant number of pixels, retinal prosthesis needs large stimulus power dissipation. A typical device consumes more than 20 mW of power to drive 1000 channels. Some of this power can lead to temperature rise which is a safety issue. As the power dissipation scales up with the increase in the number of channels, it is desired to minimize the power per channel as much as possible. Another problem is the absence of a suitable packaging material for the long-term reliable optical window. Due to the curved and narrow implant space available for this kind of device, as well as the transparency required for the incoming wavelengths of lights, it is quite difficult to choose a material that satisfies all requirements of long-term hermetic packaging with optically transparent window. Sapphire glass with titanium metal package are too bulky and rigid, and flexible transparent polymers such as polyimide and parylene-C have high moisture absorption for the implant.

This dissertation proposes strategies and methods to solve the problems mentioned above. Two stimulation strategies are proposed. One strategy is to confine the stimulus level with a threshold that cell is activated. Thus we coin it as

'thresholding strategy.' The other strategy is to reduce the number of stimulation channels by using only outlines of images ('outline extraction strategy'). Prototype IC's were designed and fabricated for the verification of the effects of these strategies. The simulation and the measurement agree to show that retinal implant with the thresholding and outline extraction strategies consumes below one-third of the stimulus power of the conventional photodiode-based devices.

Area-efficient designs of the voltage-controlled current source are also adopted to increase the number of channels. The unit pixel area of the fabricated prototype IC was 0.0072 mm^2, expanding up to 1200-channels in the macular area.

Liquid crystal polymer (LCP) is proposed as the long-term implantable packaging material with an optical window. It is an inert, biocompatible, and flexible polymer material that has a moisture absorption rate similar to Pyrex glass. We showed that an LCP film with a thickness less than 10 μm allows transmission of the lights in the visible wavelengths by more than 10 %, as the rate increases with thinner films. Thus a thinning process was developed. O$_2$ DRIE was shown effective in reducing the roughness of the film, and the corresponding light scattering. The spatial resolution of LCP with 8.28 μm thickness showed a minimum distinguishable pitch of 90 μm, allowing a 1200 channel integration within a macular area.

Keyword: retinal prosthesis, photodiode-based retinal prosthesis, low power design, liquid crystal polymer, long-term implantable optical window

Student Number: 2011-20843

Contents

List of Tables

List of Figures

Notes

Some parts of this dissertation are extracted and adapted from the journal publications that were published or submitted during this study:

1) J. H. Park, J. Jeong, H. Moon, C. Kim, and S. J. Kim, "Feasibility of LCP as an Encapsulating Material for Photodiode-Based Retinal Implants," IEEE Photonics Technol. Lett., vol. 28, no. 9, pp. 1018–1021, 2016.

2) J. H. Park *et al.*, "A distributed current stimulator ASIC for high-density neural stimulation," 2016 38th Annu. Int. Conf. IEEE Eng. Med. Biol. Soc., pp. 1770–1773, 2016.

3) J. H. Park *et al.*, "Design of an Analog Front End for a Bio-Inspired Auditory Sensor of a Novel Totally Implantable Cochlear Implant," Sensors Mater., vol. 25, no. 8, pp. 553–565, 2013.

4) J.H. Park *et al.*, "A Multi-Photodiode Array-based Retinal Implant IC with On/off Stimulation Strategy to Improve Spatial Resolution" Journal of Semiconductor Technology and Science, to be published.

Chapter 1: Introduction

Loss of sensory or motor modality results in inconvenience and devastation of human life. Such neuronal disorder leads many types of researchers to study the human nervous system to substitute damaged neurons. Technological advancement of electrical engineering encourages to understand the nervous system, and neural prosthesis has been investigated to restore the human nervous system by electrical stimulation. The cochlear implant, which stimulates spiral ganglion cells to restore hearing, became one of the most popular neural prostheses in the 1980s [1]–[5]. This success inspired other neural prostheses such as deep brain stimulation (DBS) [6]–[8] and spinal cord stimulation [9], [10].

The retinal prosthesis has also been developed like other neural prostheses inspired by the success of cochlear implant, and a recent FDA approval of a commercial retinal prosthesis showed the possibility of vision recovery of the blinds.

This introductory chapter describes the retinal prosthesis and focuses on the conventional retinal prosthesis, its challenges, and proposals towards the future high-resolution retinal prosthesis.

1.1. Retinal Prosthesis – State of the Arts

Retinal Prosthesis is aimed to give adequate visual information to the blinds with retinal degenerative diseases. The retinal degenerative diseases occupy 30 % of adult blindness, and most common retinal degenerative diseases that the blind patients have are retinitis pigmentosa (RP) and age-related macular degeneration (AMD). 3500 live births get the inherited RP around the worlds [11], and one in five hundred patients between the age of 55-64 years and one of eight patients with age over 85 years in the developed countries suffer from AMD [12]. RP and AMD results in the progressive death of photoreceptor, still there remains inner retinal structure.

The principle of the retinal prosthesis is to replace the function of degenerated photoreceptors. The retinal prosthesis activates the survived inner retinal cells with electrical stimulation containing visual information. Recent clinical trials showed that the blind patients consistently perceive spatial and temporal modulated light using the retinal prosthesis, and they could achieve several tasks such as reading characters, grating patterns, and localization of objects [13]–[16].

Most popular state-of-the-art retinal prostheses are Argus II and Alpha IMS

acquiring the US FDA approval and European CE mark, respectively. Argus II and Alpha IMS are different regarding the position of the image sensor and processor, implant place, and so on. For these reasons, we describe the difference of the system structures in following two chapters.

1.1.1. Retinal Prosthesis with External Camera

Argus II is the representative example of the retinal prosthesis with an external camera. Figure 1-1 shows the block diagram of the retinal prosthesis with an

Table 1-1 Comparison of the camera-based retinal prostheses

Device	Second Sight (Argus II) [17]–[19]	Boston Retinal Implant Project [21]	T. Fujikado et al. [20]
Position	Epiretinal	Epiretinal	Suprachoroidal
Pulse Type	Biphasic current pulse	Biphasic current pulse	Biphasic current pulse
# of Channels	60	256	49
Package Material	Titanium	Titanium	Titanium
Electrode Substrate	Parylene-C	Polyimide + SiC	parylene
Stimulus Condition	DR: 0.45 ms, PR:3-60 Hz, AMP: 4 – 677 µA,	DR: 4.5 ms, AMP: 1 – 127 µA,	DR: 0.5 ms, PR:20 Hz, AMP: 0 – 1000 µA,
Power Consumption	Received power: < 100 mW	Received power: < 30 mW Standby mode: 0.1 mW	N/A
Image Processing	Capture image and digital processing (External device)	Capture image and digital processing (External device)	Capture image and digital processing (External device)

DR: duration, PR: Pulse rate, AMP: Amplitude
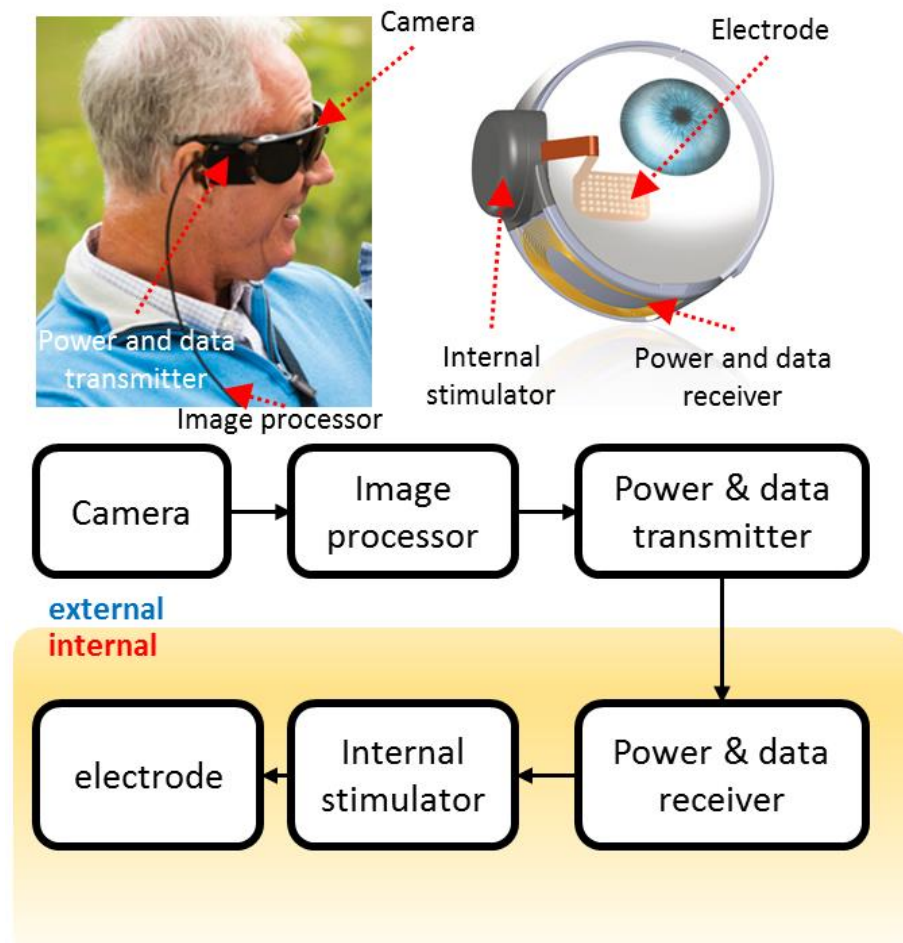
Figure 1-1 Block diagram of the camera-based retinal prosthesis (ARGUS II, Second Sight, USA) [17]-[19]

external camera. The external camera captures the incident light, and the image processor converts the captured image into data to control the internal stimulator. The inductive link, which is adaptive for wireless telemetry in biomedical devices, transfers the power and data to the internal circuit. The internal stimulating circuit generates the electrical pulses to stimulate the retina cells. Microelectrode array delivers the electrical pulses to retinal cells from the internal stimulator circuit. Titanium metal or near hermetic polymer materials hermetically seal the internal

4

circuits [17]–[19]. Table 1-1 shows the comparison of the representative retinal prostheses with external camera [17]–[21]. The retinal prosthesis with the external camera has the advantage in easy customization to each blind patients by changing stimulus parameter via the camera and the image processor outside that is located the body. However, it has a fatal disadvantage that the number of activating channels is limited owing to the data bandwidth. Several researchers tried to find another way to use an optical receiver inside the body to overcome these limited number of channels that provides low-resolution visual information to the blind patients.

1.1.2. Retinal Prosthesis with Internal Photodiode Array

An internal photodiode array was used to solve data bandwidth of the inductive link. E. Zrenner *et al.* developed the retinal prosthesis with photodiode array (ordinarily called by photodiode-based retinal prosthesis) named as Alpha IMS which has image processor inside the body [22], [23]. In Figure 1-2, An IC includes a multi-photodiode array (MPDA) responding to the incident light intensity, and stimulator circuits generating electrical pulses to stimulate retinal cells. The IC needs power and global control signals that enable to increase the number of channels limited by data bandwidth of the inductive link. As a result, the
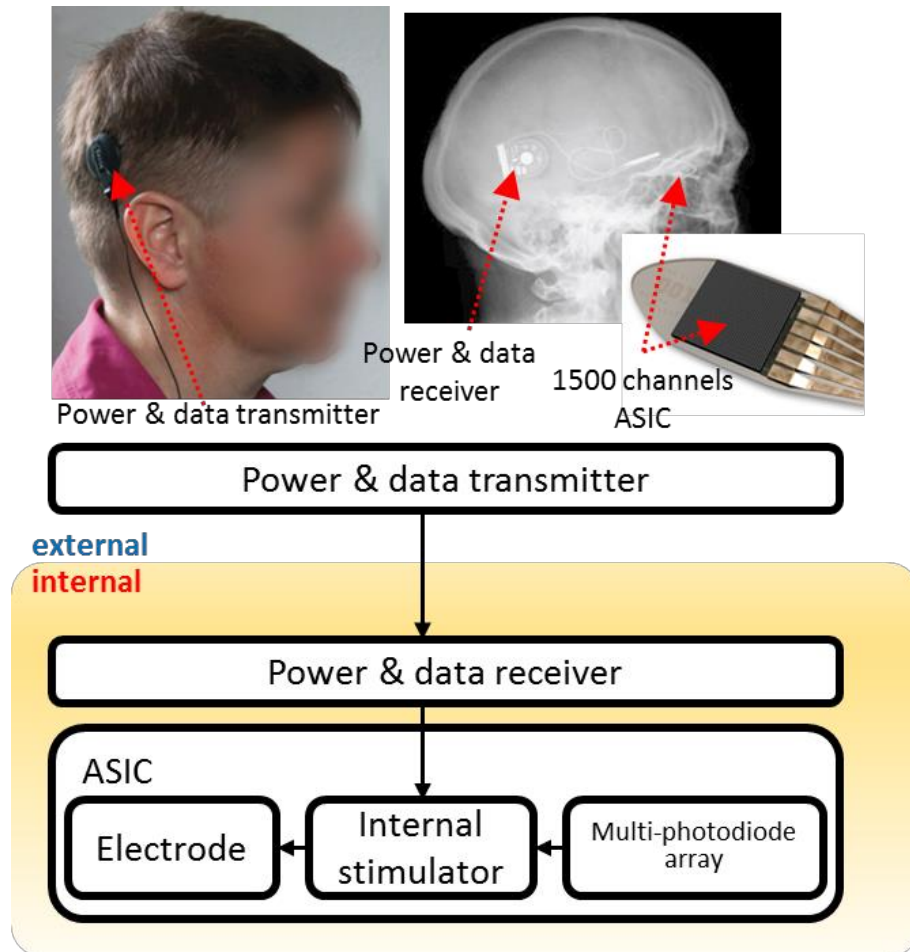
Figure 1-2 Block diagram of the photodiode-based retinal prosthesis (Alpha IMS, Germany) [22], [23]

Alpha IMS has 1500 activating channels, compared with 60 channels of Argus II, and the clinical study was reported that the blind patients had the visual acuity of 20/546.

Palanker *et al.* tried a different optical telemetry. They implanted microfabricated arrays of photodiodes driven photovoltaically [24], [25]. These components use near infrared as power and data source to generate stimuli. The internal device doesn't need any internal peripheral circuits for power and data telemetry; they

Table 1-2 Comparison of the photodiode-based retinal prostheses

Device	E. Zrenner *et al.* (Alpha IMS) [22], [23]	D. Palanker *et al.* [24], [25]
Pixel Size	72 μm square (1500 channels)	58 μm hexagon
Package Material	Metal, polyimide	SU-8
Pulse Type	Monophasic Voltage pulse (induced biphasic current pulse)	Monophasic Voltage pulse (induced biphasic current pulse)
Stimulus Condition	DR: 0.5 - 1 ms, PR: < 20 Hz AMP 2 V, Charge: 1 – 40 nC	DR: 0.5 ms, PR: 25 Hz AMP < 1.4 V, Charge: 1 – 40 nC
Internal Device Power Consumption	< 10 mW (Condition: DR: 1 ms, PR: 5 - 7 Hz, AMP: 2 V, Charge: 1-5 nC) Temperature rise: < 0.5 K	No power requirement due to the only existence of photodiodes Average irradiance: 13 μW/mm^2 (DR: 0.5 ms, PR: 25 Hz, Charge 1-9 nC)
Image Processing	Conversion of light intensity into voltage level directly (in the internal device)	Capture image and digital processing (In the external device)

DR: duration, PR: Pulse rate, AMP: Amplitude

need the external light source that generates near infrared patterns containing visual information. Pixel size is small enough to implant thousands of stimulation channels, and *in vivo* tests verified their functionality. Table 1-2 shows the comparisons of two representative photodiode-based retinal prostheses.

1.2. Photodiode-based Retinal Prosthesis

The photodiode-based retinal prosthesis is the most probable high-resolution retinal prosthesis. Despite the clinical successes of the photodiode-based retinal prosthesis, there remain challenges to provide high-resolution visual information. Following three chapters describe each problem, as shown in Figure 1-3.

1.2.1. Problems

1.2.1.1. The Number of Pixels

The number of pixels (stimulating channels) is crucial for delivering effective visual information to the blinds. Simulation result of the minimum pixel to recognize a face or letters was 600 – 1000 [16]. Thus recent studies were focused on increasing the number of pixels, and Alpha IMS was developed with 1500-indivisual pixels including photodiode and stimulator. However, a clinical study showed that visual acuity didn't dramatically increase, as the number of the pixels
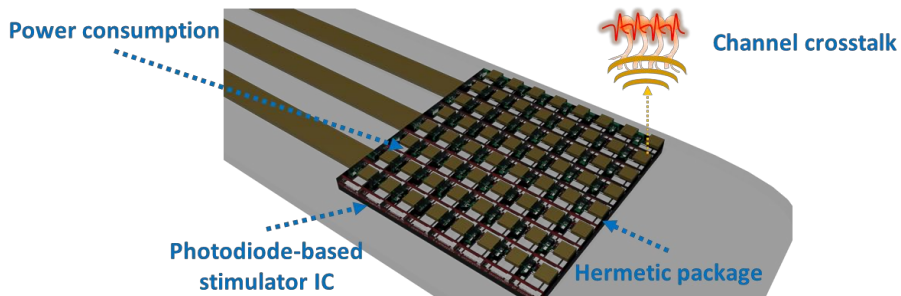
Figure 1-3 Challenges towards high-resolution retinal prosthesis

Table 1-3 Power consumption to generate 1000 stimulation pulses

The number of channels	1000
Threshold Charge (duration=1 ms)	100 nC
Pulse rate	20 Hz
Current consumption	>2 mA
Power consumption ($V_{DD} = 10$ V)	>20 mW

increases from 60 to 1500. This result was due to the crosstalk where a current pulse activates not only the target nerve but also neighboring nerves caused by current spread via the electrolyte [26]. New technologies are needed to minimize the current spread, not increasing pixel area of 0.01 mm^2 to guarantee the number of pixels above 1000. Still, there are other problems to increase the number of pixels.

1.2.1.2. Power Dissipation

A large number of stimulating channels can provide high-resolution visual information to the blind patients, and it takes a lot of electrical power as well. Cochlear implant with 16 channels, for example, needs finger size battery for one-day life. Owing to the similarity between the cochlear implant and retinal prosthesis, 1000 channels of the retinal prosthesis will need about 50 finger-size

batteries for one-day life which can be a significant inconvenience. The excessive

power consumption causes heat dissipation that can lead to inner retinal cell death.

For instance, a power dissipation of 80 mW/cm^2 causes necrosis in muscle tissue

owing to heat flux [27]. In other words, maximum power consumption is 8 mW in

the macular area of 10 mm^2 to avoid cell death. Another case reported that

temperature increase of more than 1 ℃ may damage the brain tissue [28]. Thus

retinal prosthesis should be designed to limit the temperature increases above 1 ℃,

although there are no reports of retinal tissue effects to chronic higher temperature

than that of body. A clinical report showed that safe power consumption of the

implanted IC with a volume of 6 mm × 6 mm × 2 mm was 10 mW,

corresponding to the temperature increase of 0.5 ℃ *in vivo* test [29]. From this

result, the power consumption of the photodiode-based retinal prosthesis should

not exceed 20 mW.

Power dissipation can be calculated on the stimulation condition from

physiological results. Table 1-3 is a mathematical analysis of the power

consumption to generate 1000 stimulation pulses using the stimulation condition of

[28], [30], [31]. The calculated value is above 20 mW that is higher than maximum

power consumption not to lead the cell death.

Conventional retinal prosthesis limits power consumption. ARGUS II limits to

transfer power for safety, which is not suitable for the high- resolution retinal

prosthesis. Alpha IMS has a low pulse rate of 5 – 7 Hz that supports sparse visual

Table 1-4 Comparison of the optical window materials used in neural prosthesis

Device	E. Zrenner *et al.*	D. Palanker *et al.*	Borton *et al.*
Package Material	polyimide	SU-8	Metal & sapphire
Advantage	Flexible, thin High transparency	Flexible, thin High transparency	Hermetic High transparency
Disadvantage	High water absorption 2.8 (%)	High water absorption 0.65 (%)	Rigid, bulky (> 1mm)

information, compared with other prostheses. Digital controller and peripheral circuits consume less power than power generating stimulus. Thus new strategies are needed to reduce stimulus power.

The reduction of power consumption can also be considered regarding specific absorption rate (SAR). SAR is an important factor to guarantee safety. The maximum SAR is 1.6 W/kg in the US, and 2 W/kg in Europe and Japan, [32]. As power delivery of the internal device is based on the inductive link, SAR is proportional to power consumption.

1.2.1.3. Hermetic Packaging

The photodiode-based retinal prosthesis so far could not be chronically implanted for more than a year due to the absence of suitable packaging technologies that can provide both hermeticity and optical transparency for encapsulation of the photodiode-based retinal prosthesis and unaffected photovoltaic performance,

11

respectively. Long-term durability in the implanted condition has remained a significant limitation for the photodiode-based retinal prosthesis despite their high scalability of channels compared with other approaches using an external camera and 60-channel stimulating electronIC's in a metallic package [17]–[19].

Major requirements of long-term implantable packaging with light windows for photodiode-based retinal implants include hermeticity, transparency, flexibility, and capability of integration with surrounding circuits.

Although the conventional biocompatible polymers such as polyimide and parylene have a light transmittance higher than 70 % for the visible spectrum, they do not guarantee long-term reliability due to relatively high moisture absorption rate [33]. A recently developed titanium package with optical windows of sapphire glass [34] can achieve good hermeticity, but the package is too bulky and stiff to be applied for subretinal devices which are implanted within thin, soft and curvilinear retinal tissues. It also requires brazing and welding techniques which are expensive and laborious. Comparison of these materials is shown in Table 1-4.

1.2.2. Possible Solutions

To solve the problems of the conventional photodiode-based retinal prosthesis, we focused on the reduction of power consumption generating stimulus, and long-term reliable packaging materials. In addition, we also use current spread to increase the number of stimulating channels than that of physical electrodes. Following
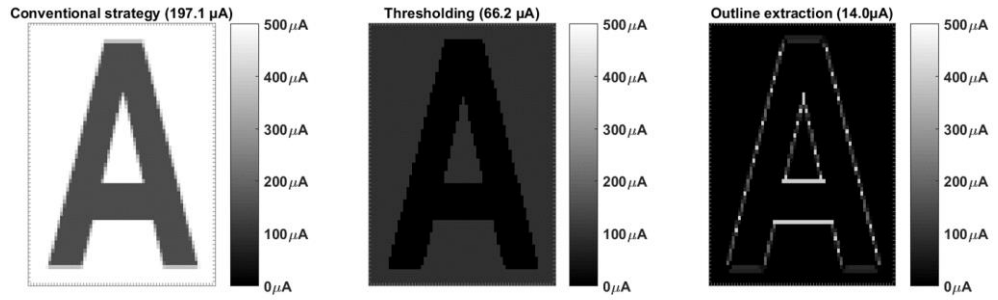
Figure 1-4 Simulation result of average power generating stimulus using conventional strategy, thresholding and outline extraction

chapters describe the proposed strategies, material, and circuit scheme.

1.2.2.1. Thresholding

One of the proposed strategies is thresholding that generates electrical pulses in response to incident light only above a designated intensity threshold. The thresholding allows the stimulus level to be set at a minimum value. As a result, all channels are activated with a minimum current level, reducing power consumption. Figure 1-4 shows an example that the average power decreases compared with that of conventional stimulation strategy. Also, reduction of power consumption has another advantage of less cell damage. Excessive current stimulation leads to cell damage by exceeding water window that changes the pH concentration near the electrode [35] as well as increasing temperature. To adapt the thresholding strategy into the photodiode-based retinal prosthesis, we designed the circuit and verified by prototype IC.

1.2.2.2. Outline Extraction

Another strategy is the outline extraction that generates electrical pulses in response to the image shape. In high-resolution retinal prosthesis, the outline extraction activates less activating channels, compared with level based stimulation strategy that conventional photodiode-based retinal prosthesis uses, as shown in Figure 1-4. Although power consumption is reduced in generating stimulus, an additional image processor for outline extraction should be integrated into the ASIC, resulting in more power consumption. We design low power image processor with dynamic operation, inspired by the human retinal network. The detailed design and circuit implementation are explained in the method.

1.2.2.3. Virtual Channel

In order to achieve more stimulation channels than physical channels of the IC, the two-dimensional virtual stimulation channel using current spread can be implemented by the modification of [36], [37]. The delicate electrical field can be generated by the sum of the four current spreads, resulting in a small region of the high electrical field. The virtual channel has another advantage regarding power consumption. Electrode area decreases in order to integrate a large number of electrodes. For example, the electrode area of 1000 channel retinal prosthesis in the macular area of 10 mm^2 is 100 μm $\times$ 100 μm. Table 1-5 shows the electrode

Table 1-5 Electrode impedance and cathodic charge storage capacity of gold and EIROF electrode

	Electrochemical impedance at 1 kHz (kΩ)	Cathodic charge storage capacity (CSC$_c$)(mC/cm^2)
Gold	26.65 $\pm$ 6.93	0.32 $\pm$ 0.05
EIROF	1.41 $\pm$ 1.1	24.19 $\pm$ 6.21

impedances of gold and EIROF with a diameter of 300 μm [38], [39], and electrochemical impedance increases when the electrode area decreases. This impedance increase results in the large compliance voltage that needs high supply voltage. Novel metal like EIROF and geometrically porous polymer such as PEDOT can be a solution to decrease impedance. However, these materials are expensive or have weak mechanical property. The two-dimensional virtual stimulation channel using current spread can solve this problem to increase the number of pixels without electrode area decrease.

1.2.2.4. Polymer Packaging

Recently, liquid crystal polymer (LCP) has gained increasing attention as a packaging material for long-term implantable biomedical devices [40], [41]. Compared with other optical packaging materials as listed in Table 1-4, low moisture absorption rate (<0.04 %) and gas permeability that is comparable to Corning glass [41] are expected to realize a long-term reliable encapsulation, and yet it retains desirable features of polymeric material being thin, light-weight and

flexible. The LCP encapsulation of the photodiode-based retinal prosthesis can offer another advantage of the possibility to be integrated with the surrounding circuitry such as a coil, chip and interconnects, constituting a monolithically integrated device in a homogeneous LCP package as demonstrated in a recent study [42]. A photodiode-based ASIC can be encapsulated by thermally laminating between two LCP films, followed by partial thinning for optical windows and exposing electrode sites for charge injection, which is low cost, and simple process compared to brazing and welding of sapphire and titanium process. While LCP has been primarily studied as an encapsulation material so far, its optical properties such as transmittance and scattering have not been investigated yet. Although the semi-crystalline structure of LCP results in lower light transmittance compared with amorphous polymers like polyimide and parylene [43], the transmittance of LCP could increase by using thinner LCP films. Our preliminary test methods and results are described.

The rest of this thesis describes the design, circuit implementation, and test results of the two proposed stimulation strategies and the optical properties and fabrication of LCP for a packaging material with an optical window. Moreover, a new system architecture for the two-dimensional virtual channel is explored to increase the number of channels with a small number of the physical electrode for the low supply voltage.

Chapter 2: Methods

This chapter describes methods for the verification of the proposed strategies and materials. In the strategies parts, strategy explanation and its circuit design are described. In the packaging parts, we briefly explain the test methods optical property of LCP and compare fabrications of the LCP thinning.

2.1. Thresholding

2.1.1. Concept

The thresholding stimulation strategy (thresholding) generates biphasic current pulses in response to incident light only above a designated intensity threshold, thus allowing excitation of retinal neurons with minimum current level for low power consumption. Figure 2-1 explains the thresholding.
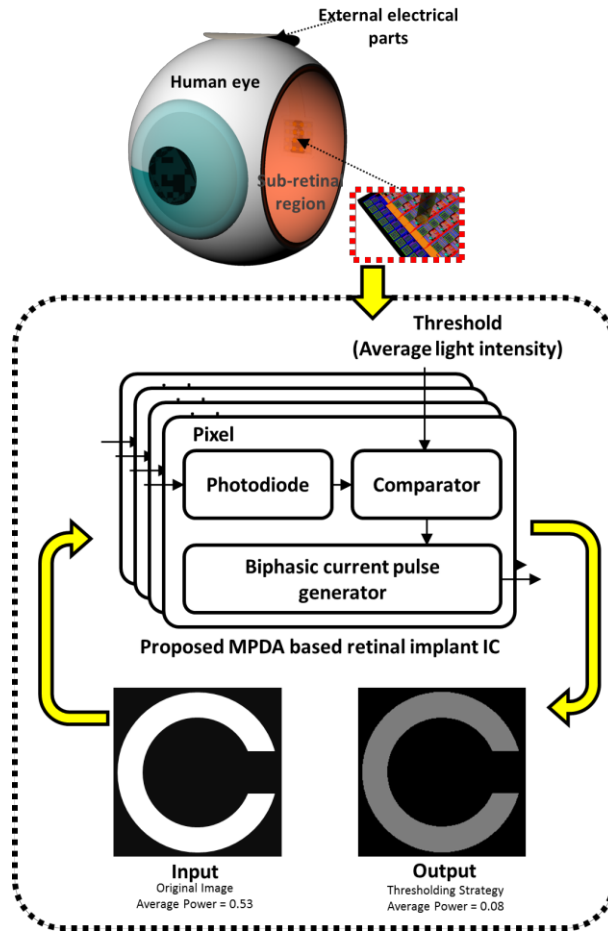
Figure 2-1 Concept of the retinal prosthetic IC using thresholding stimulation strategy

The electrical signal obtained by conversion of light intensity information is input to a comparator with a threshold value that is obtained using the average background light intensity throughout the array. Thus only the light intensity that surpasses background intensity can elicit biphasic current pulses. This operation allows the stimulus level to be set at a minimum value. The thresholding operation can be expressed by the complicated equation (1). Total stimulus power of the

conventional retinal prosthesis ($P_{total,conventional}$) and that of the proposed retinal prosthesis with thresholding strategy ($P_{total,threshold}$) can be expressed as

$$P_{total,conventional} = \sum P_{<threshold} + \sum P_{>threshold} \geq \sum P_{>threshold,min} = P_{total,threshold} \quad (1)$$

Where $P_{<threshold}$ is the stimulus power in response to a light intensity below the threshold, $P_{>threshold}$ is the stimulus power above the threshold, and $P_{>threshold,min}$ is the minimum stimulus power to activate retinal cells in response to light intensity above the threshold. As a result, the benefits of lower power consumption can be achieved, compared with the conventional photodiode-based retinal prosthesis strategy.

2.1.2. Circuit Descriptions

To implement the thresholding, a photodiode-based retinal prosthetic IC was designed, as shown in Figure 2-2. The IC consists of a bias generator, a digital controller, and an array of multi-channel pixels. Each pixel has a photosensor combined with a comparator, a voltage-controlled current source (VCCS), and a biphasic current generator (BCG). The digital controller provides signals to control the photodiode-based retinal prosthetic IC. BCG converts the output current of VCCS into the biphasic current pulse using signals of the digital controller when
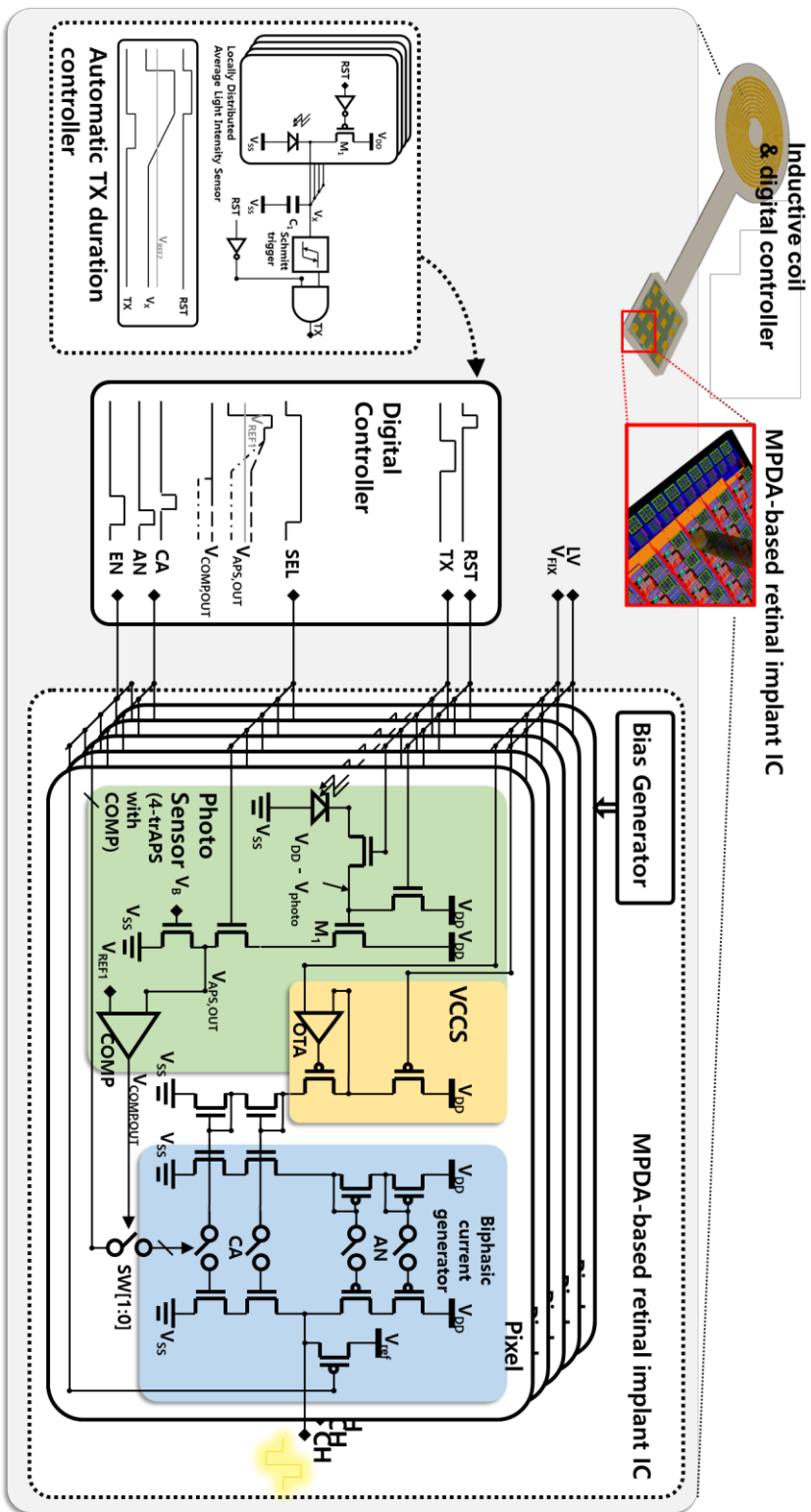
Figure 2-2 Schematic of the photodiode-based retinal prosthetic IC using thresholding

the incident light level is above the threshold. Following chapters demonstrates each part.

2.1.2.1. Low-power Photosensor for Thresholding Strategy

A 4-transistor active pixel sensor (4-tr APS) combined with a latched comparator (COMP) was adopted for the thresholding of the photosensor [44], [45]. The 4-tr APS allows the change of photo-sensitivity via discharging time (TX) and provides excellent noise characteristics as compared with other types of CMOS image sensors. The output voltage of the 4-tr APS ($V_{OUT,APS}$) decreases during TX, and this relation can be expressed as

$$V_{OUT,APS} = V_{DD} - V_{TH} - V_{photo} \cdot TX = V_{DD} - V_{TH} - k \cdot L \cdot TX \qquad (2)$$

where V_{photo} is a voltage induced by the photodiode, L is a light intensity, k is a responsivity (V/lx·s), and V_{TH} is the threshold voltage of the MOSFET M_1, as shown in Figure 2-2. At the comparator (COMP), if $V_{OUT,APS}$ is below the reference voltage (V_{REF1}), digital signals (AN, CA) that control the switching of BCG pass through the SW[1:0], enabling biphasic pulse generation. Using this property and equation (2), we can express the light intensity threshold ($L_{threhold}$) for generating current stimulus as equation (3) and equation (4)
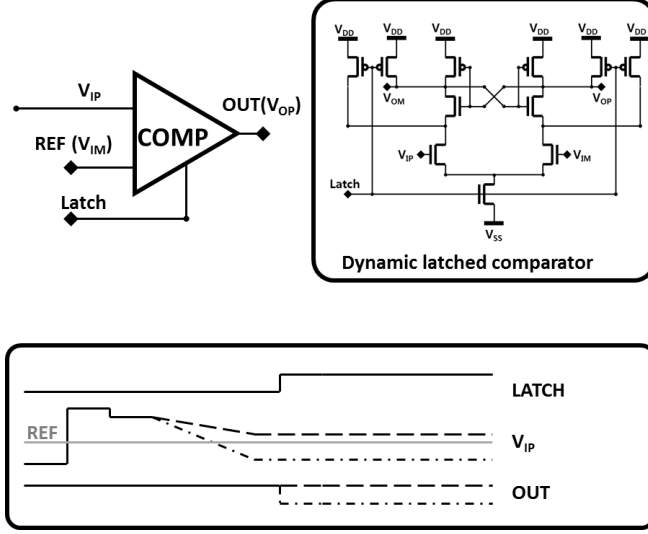
Figure 2-3 Schematic of the dynamic latched comparator and its signal flow

$$V_{REF1} = V_{OUT,APS} = V_{DD} - V_{TH} - k \cdot L_{threshold} \cdot TX \qquad (3)$$

$$L_{threshold} = \frac{(V_{DD} - V_{REF1} - V_{TH})}{(k \cdot TX)} \qquad (4)$$

From equation (4), it is found that $L_{threshold}$ is inversely proportional to TX. Thus $L_{threshold}$ can be adjusted by varying TX, making this type of photosensor uniquely applicable to various light intensity environments. The comparator has the structure of a dynamic latched comparator for low power consumption as shown in Figure 2-3 [44]. When LATCH is V_{SS}, the output voltages (V_{OP}, V_{OM}) is set to V_{DD}. If the LATCH is changed into V_{SS}, current starts to flow, and the input voltages (V_{IP}, V_{IM}) determines the output voltages. If the V_{IP} is higher than V_{IM}, the V_{OP} is V_{DD} and V_{OM} is V_{SS}. The comparator consumes power only when LATCH is V_{DD}. Thus power consumption can be reduced by using this comparator.

22
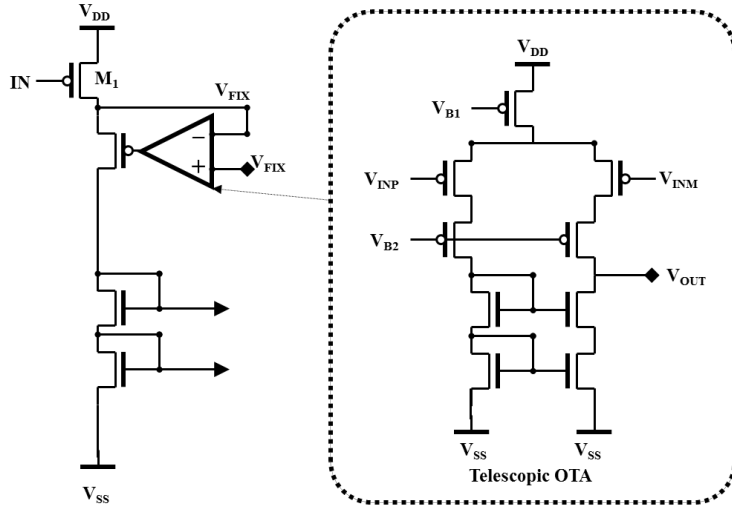
Figure 2-4 Schematic of the VCCS and telescopic OTA used in the VCCS.

2.1.2.2. Voltage Controlled Current Source (VCCS)

The VCCS based on the MOS resistor was used to control the current stimulus level efficiently [46]. An OTA retains drain voltage of M_1 to a fixed voltage of V_{FIX} forcing M_1 to remain in the triode region, as shown in Figure 2-4. As a result, the gate voltage of M_1 can linearly change the drain current (I_D) of M_1. The telescopic OTA optimized using g_m/I_D is operated in weak inversion region [47]. Telescopic OTA is a suitable choice as this structure doesn't need large output swing with high open-loop gain. Operating in weak inversion region can achieve the high g_m/I_D, leading to reduced power consumption with the same transconductance.

2.1.2.3. Biphasic Current Generator (BCG)

Simultaneous monopolar stimulation was used for reduction of the number of electrodes, and for ease of scaling up the stimulation channels without modification of the digital controller. The N-channel monopolar stimulation needs N+1 electrodes, compared with bipolar stimulation that needs 2·N electrodes. As most photodiode-based retinal implant IC's include the stimulating electrodes, reduction of the number of electrodes increases the geometrical area of the electrodes, which results in decreasing electrode impedance and the circuit compliance voltage. The decrease of compliance voltage affects to reduce the power consumption owing to using low V_{DD}.

As control signals are shared by all the pixels during simultaneous stimulation, it is possible to increase stimulation channels without modification of the digital circuit. Simple digital controller is also suitable for reducing power consumption

The BCG was designed to have two independent current sources, one for anodic phase and the other for cathodic phase, for safety reason [48]. In a structure that employs single current source and the monopolar stimulation, amplitudes of simultaneous multichannel biphasic stimulation pulses can be affected by the electrode-cell impedance, as shown in Figure 2-5. The simultaneous stimulation with the single current source can result in unsafe retinal stimulation due to excess charge used. Two independent current sources are designed to deliver predictable and safe stimulation to retinal neurons regardless of electrode-cell impedance.

24
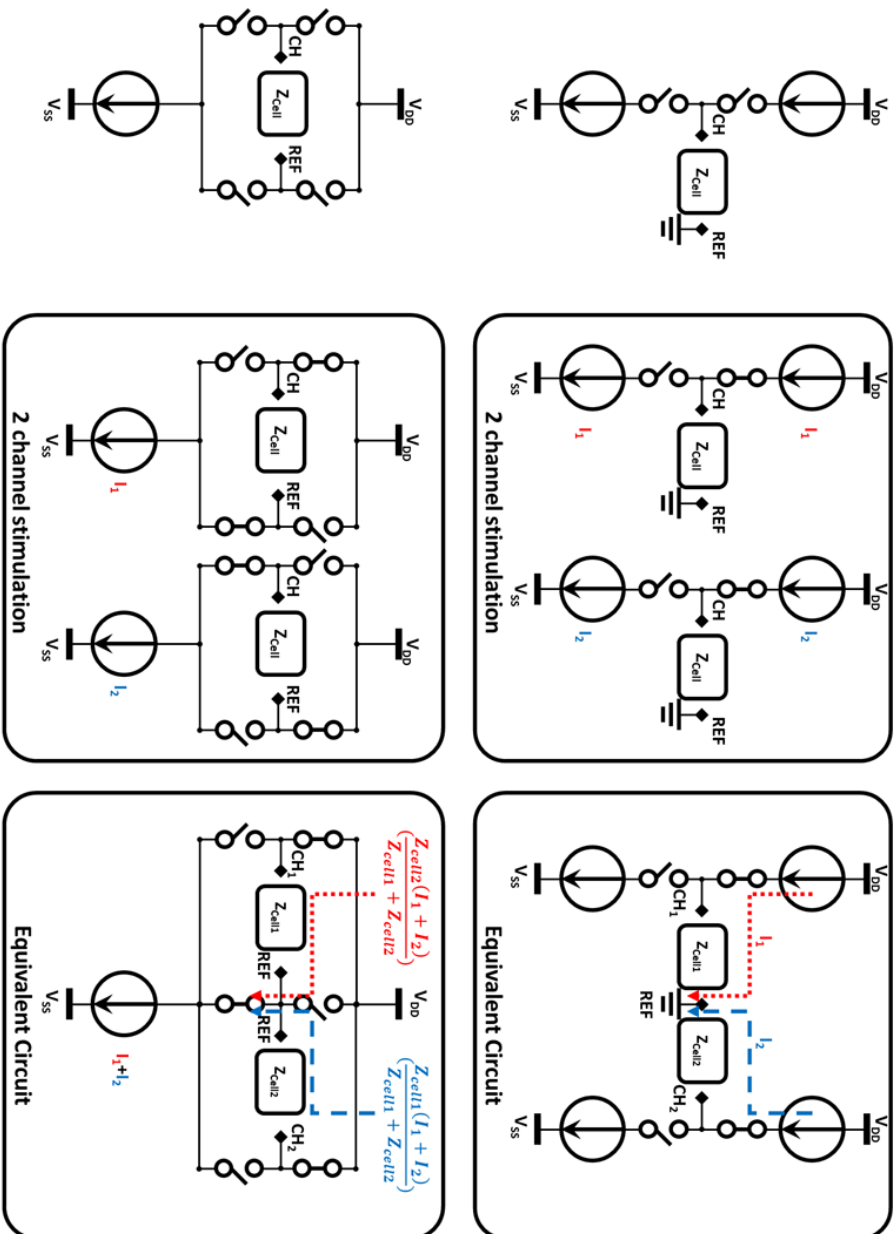
Figure 2-5 Comparison between BCG with two independent current sources and BCG with a single current source
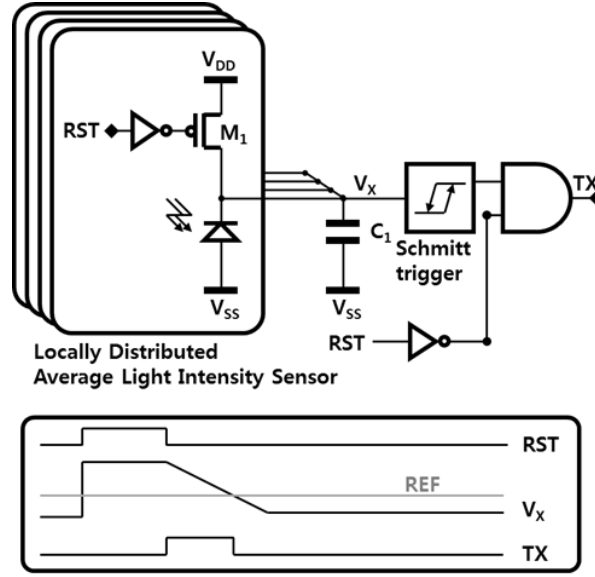
Figure 2-6 Schematic of the automatic TX controller

2.1.2.4. Digital Controller

The digital controller has five states of photo-sensing state, comparing state, cathodic stimulating state, anodic stimulating state, and resting state.

In the photo-sensing state, the digital controller determines TX time to control the photosensor sensitivity. The prototype of the digital controller digitally modulates TX, and this operation has to be controlled manually in order to adapt to various light environments. Thus we propose the automatic TX controller to control the light intensity threshold for efficient image processing of thresholding, as shown in Figure 2-6. The distributed photodiodes discharge the capacitor, decreasing the voltage. As the voltage is below the specified voltage that we set (REF), the output of Schmitt trigger becomes V_{SS}. The value of TX is calculated with RST and

26

the capacitor voltage via the AND gate. Thus the circuit in Figure 2-6 can perform automatic control of the TX value according to the average light intensity. In the comparing state, the output voltage of 4-tr active pixel sensor is compared with V_{REF1} of the comparator. The transition of LATCH occurs in this state. The cathodic and anodic stimulation state generates control signals of BCG. The signals can transfer to the BCG in the condition of the light intensity above the threshold ($L_{threshold}$). In the resting state, the residual charge is, for safety concern, removed by shorting CH node and REF node.

As mentioned above, control signals are shared by all the pixels. Thus, we can expand the number of pixels without modification of digital controller. The design of the digital controller was described by the Verilog HDL that can be converted into FPGA and IC easily

2.2. Outline Extraction

2.2.1. Concept

Figure 2-7 shows the human retinal network and its behavior schematic [49]. The human retina is sensitive to spatial difference of light intensity. This mechanism arises via the parallel connection of horizontal cells and photoreceptor terminals. Despite ambiguous details of horizontal cells' behavior, it is clear that horizontal cells regulate the amount of transmitter (output signal) that the photoreceptor releases onto bipolar cell dendrites. This behavior can be briefly expressed as
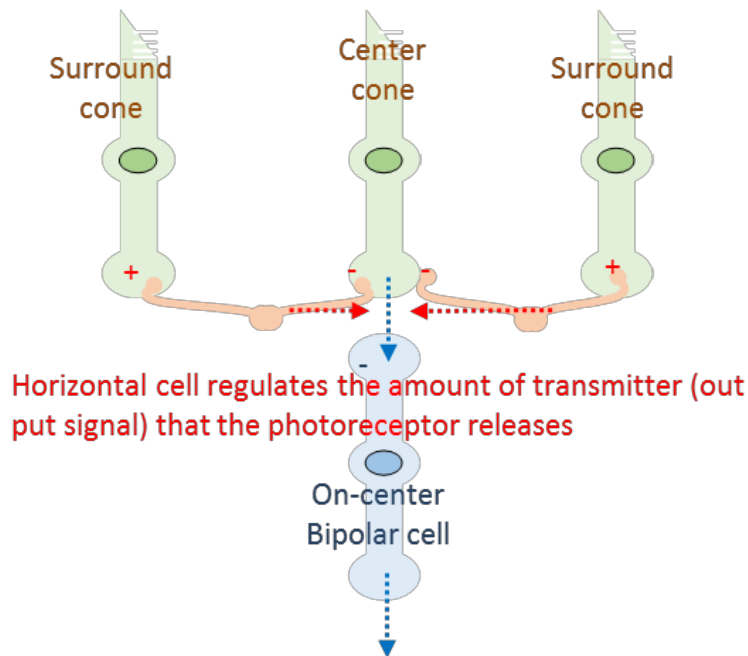
Figure 2-7 Human retinal network and its behavior

$$V_{bipolar} = V_{photoreceptor,center} - f(V_{photoreceptor,surround}) \tag{5}$$

where $V_{biopolar}$ is the field potential of the bipolar cell, $V_{photoreceptor,center}$ is the field potential from the center photoreceptor, and $f(V_{photoreceptor,surround})$ is the influence of the field potential from the surround photoreceptors (minus sign means inhibitory synaptic response).

Image outline can be extracted using edge detection algorithm such as the Laplacian operator [50]. This operator is expressed as

$$(\nabla^2 f)(x,y) = \frac{\partial^2 f}{\partial^2 x}(x,y) + \frac{\partial^2 f}{\partial^2 y}(x,y) \tag{6}$$

In the discrete domain, (6) can be rewritten as

$$(\nabla^2 f)(x,y) = -4f(x,y) + [f(x-1,y) + f(x+1,y) + f(x,y-1) + f(x,y+1)] \tag{7}$$

where (x,y) is the center inputs, and the others are the surrounding inputs. From the equation (7), the outline can be calculated by the difference between the center and the surrounding. We designed a low-power image processor for outline extraction mimicking the human retinal network and spike based neural circuit.

2.2.2. Circuit Descriptions

2.2.2.1. System Overview

Figure 2-8 schematically represents the MPDA-based retinal prosthetic IC and the flow of signals. The IC consists of a data receiver, a global controller, and many unit pixels including a photosensor with a pulsatile output, an image processor, a voltage-controlled current source (VCCS), and a biphasic current pulse generator (BCG).

Figure 2-8 Schematic of the proposed circuit

31
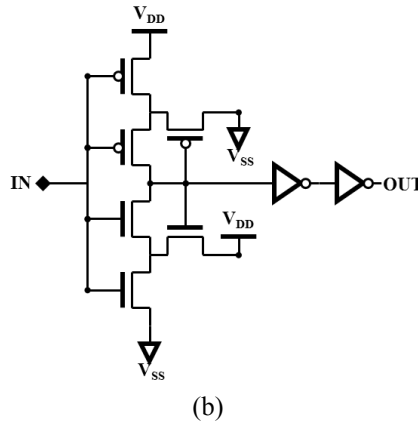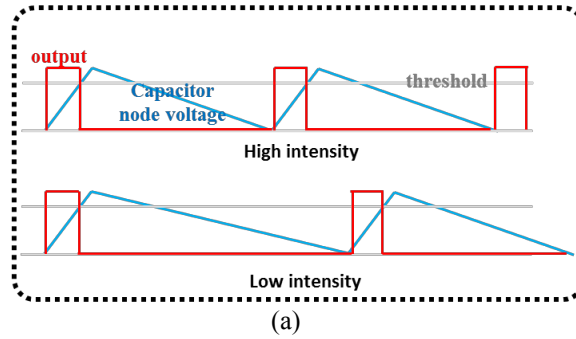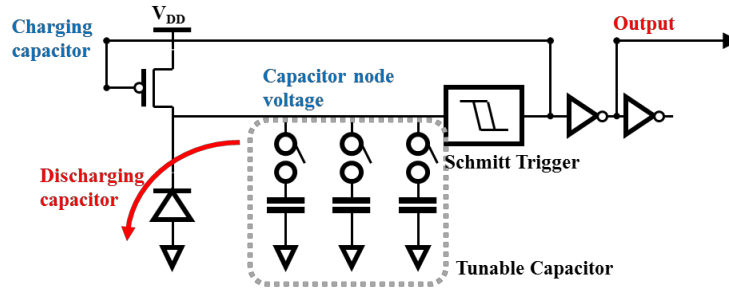
Figure 2-9 (a) Operation of the photosensor and output and capacitor node voltage at the high and low light intensities (b) Schematic of the conventional CMOS Schmitt trigger

2.2.2.2. Photosensor with Pulsatile Output

The photosensor modulates output pulse rate in response to incident light intensity. This property leads the image processor with the dynamic operation, achieving low power consumption. Figure 2-9 (a) shows the operation of the proposed

32

photosensor. A photodiode discharges the tunable capacitor, and PMOS charges the capacitor when the output voltage of the capacitor is below certain voltage by changing the Schmitt trigger's state. The light intensity determines the discharging duration. The discharging duration, for example, decreases as the light intensity increases. The intrinsic output driving force of the Schmitt trigger fix the charging duration. Thus the photosensor can generate the fixed pulse trains with the modulated pulse rate by the light intensity. A conventional CMOS Schmitt trigger was used, which is a very useful regenerative circuit as shown in Figure 2-9 (b) [51].

2.2.2.3. Image Processor with Outline Extraction

The image processor extracts the image outline adopting the Laplacian operator. Figure 2-10 (a) shows the schematic, the block diagram, and voltage operation of the image processor. In the sampling time, the photosensor output of the pixel itself discharges the capacitor of the image processor with a particular current level. Otherwise, the photosensor outputs of its surrounding pixels (top, bottom, left, and right side) charge the capacitor with a particular current level. Thus output capacitor includes the information of the difference between the light intensity of the center pixel and those of the surrounding pixels. A mathematical analysis is also conducted, as shown in Figure 2-10 (b). The output voltage is determined when charging current and discharging current are the same value as

33
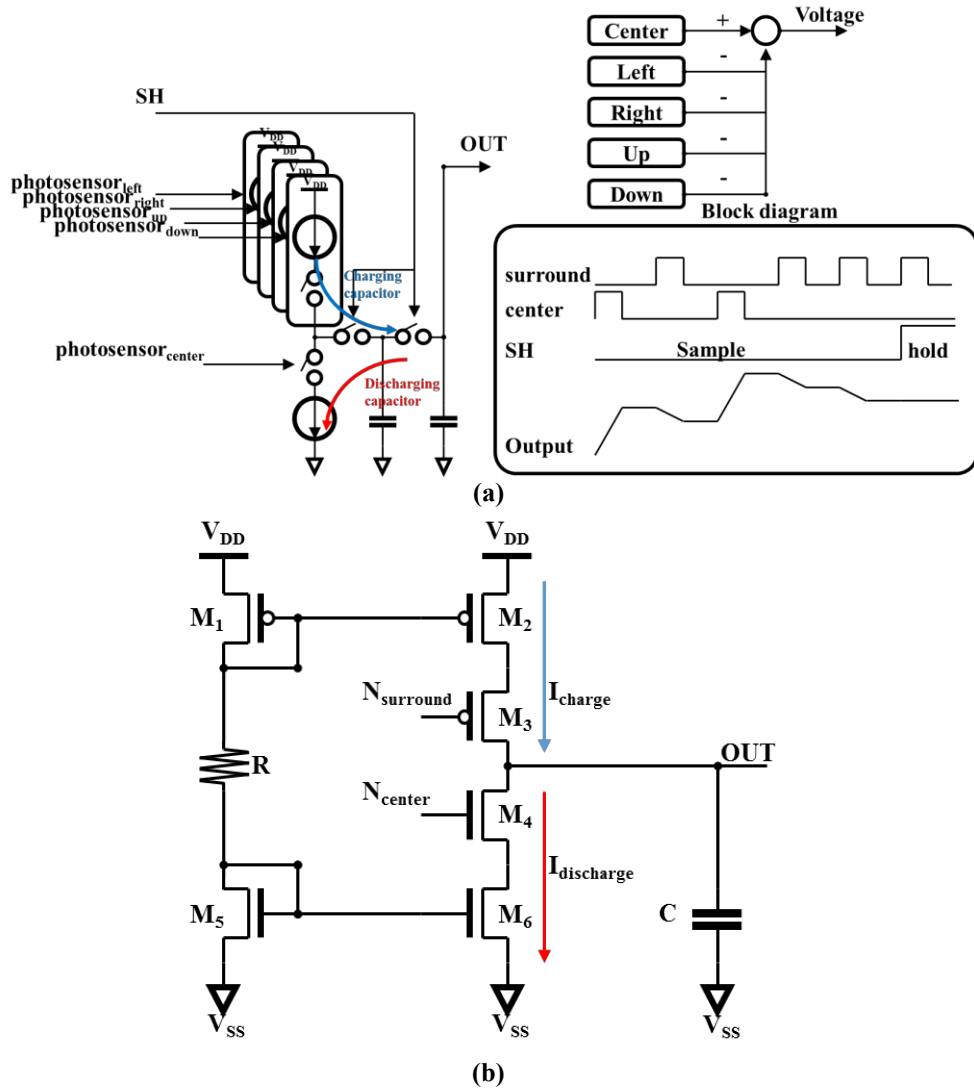
Figure 2-10 (a) Block diagram and operation of the image processor (b) Schematic of the image processor during sampling time

$$I_{charge} \cdot (N_{up} + N_{down} + N_{left} + N_{down}) = I_{discharge} \cdot N_{center} \qquad (8)$$

where $V_{capacitor}$ is the output voltage of the capacitor in the image sensor, I_{charge} and $I_{discharge}$ is the charging and discharging current level, respectively, and N is the pulse rate ratio between up, down, left, down, and center pixels. Equation (8) can

be rewritten as

$$4 \cdot I_{ch \arg e} \cdot N_{surroun(average)} = I_{disch \arg e} \cdot N_{center}$$

$$4 \cdot \frac{\mu_p C_{ox}}{2} \cdot \frac{W_p}{L_p} \cdot V_{OVP}^2 \cdot (1 + \lambda_p (V_{DD} - V_{out})) \cdot N_{surroun(average)} \qquad (9)$$

$$= \frac{\mu_n C_{ox}}{2} \cdot \frac{W_n}{L_n} \cdot V_{OVM}^2 \cdot (1 + \lambda_n (V_{out})) \cdot N_{center}$$

where $N_{surrounding, the\ average}$ is the average of N_{up}, N_{down}, N_{left}, and N_{down}, μ is mobility, C_{ox} is oxide capacitance, W and L are width and length of MOSFET, respectively, and λ is a constant due to channel length modulation effect. The sizes of M_2 and M_6 are determined by the condition that V_{DD}-V_{out} is the threshold voltage of the VCCS when $N_{center}/N_{surround,average}$ of 1. From Figure 3-4 (b), (9) can be simplified as

$$4 \cdot \frac{W_2}{L_2} \cdot I_U \cdot (1 + \lambda_p (V_{DD} - V_{out})) \cdot N_{surroun(average)}$$

$$= \cdot \frac{W_6}{L_6} \cdot I_U \cdot (1 + \lambda_n (V_{out})) \cdot N_{center} \qquad (10)$$

where I_U is unit drain current that is determined by M_1, R, and M_5, and the equation (10) can be written as

$$K(1 + \lambda_p (V_{DD} - V_{out}))(N_{surroun(average)}) = (1 + \lambda_n (V_{out})) \cdot N_{center} \qquad (11)$$

where K is the 4-fold ratio M_2 to M_6, V_{out} can be rewritten as

$$V_{out} = \frac{(K + K\lambda_p V_{DD} - N_{center}/N_{surround,average})}{(\lambda_n \cdot N_{center}/N_{surround,average} + K\lambda_p)} \quad (12)$$

$$= f(N_{center}/N_{surround,average})$$

From the equation (12), the output voltage (V_{out}) is not determined by the light intensity, but the ratio between N_{center} and $N_{surrouond}$, N_{center} / $N_{surround,average}$. This mathematical analysis has limit due to use of continuous current model of I_{charge} and $I_{discharge}$. But this circuit uses a pulsatile current. Thus V_{out} is not determined as a single value, but as a range. In the holding time, the output voltage is fixed in the range of V_{out} at the sampling time by the switch opening. The series-connected capacitors can reduce transition noise of sampling and hold state. Current mirror circuit determines the charging and discharging current level, and pulsatile input that needs no static current reduces power consumption.

2.2.2.4. Area Efficient Voltage Controlled Current Source (VCCS)

Figure 2-11 illustrates the voltage-controlled current source (VCCS) based on the MOS resistor to control the current stimulus level efficiently, modified by [46]. M_2 applying gain boosting retains drain voltage of M_1 to a fixed voltage when I_{D2} is
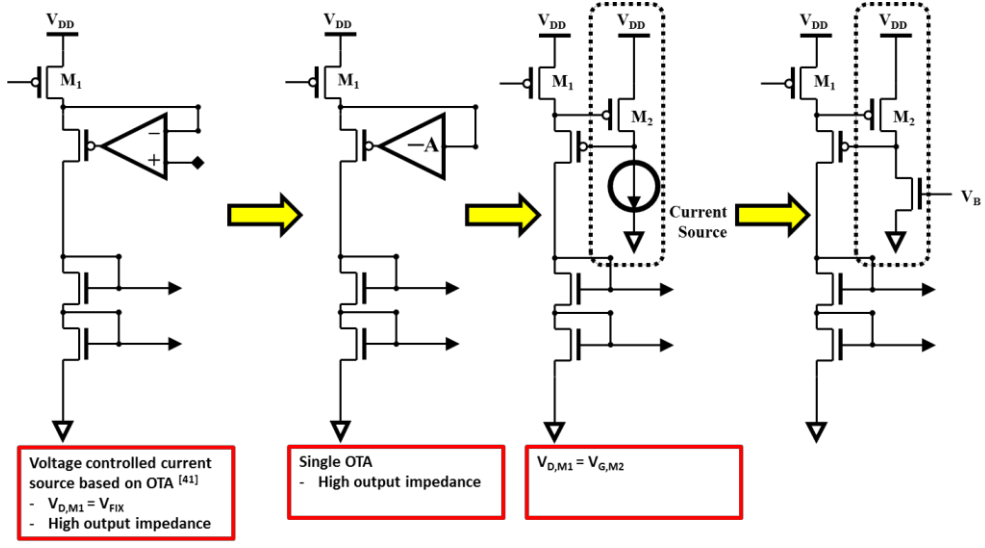
Figure 2-11 Operating mechanisms of area-efficient VCCS

the same as the current source in the BCG, forcing M_1 to remain in adjacent triode region for acting as the MOS resistor. This structure can save area by replacing OTA in Figure 2-11 into using only 2 MOSFETs.

2.2.2.5. Biphasic Current Generator (BCG)

For simultaneous monopolar stimulation, the biphasic current generator (BCG) was designed to have two independent current sources, one for anodic phase and the other for cathodic phase, for safety reason, explained in 2.1.2.3 [48], [52]. Two independent current sources were designed to deliver predictable and safe stimulation to retinal neurons regardless of electrode-cell impedance.

2.2.2.6. Digital Controller

Data Receiver converts the amplitude-modulated data into the clock and the control
signals as shown in the Figure 2-12. The data receiver generates the clock from the
amplitude modulated data using the envelope detection. Thus IC can use the first
rising edge of input. Logical data is generated using pulse width modulation
(PWM) and pulse counting. As a result, the global digital controller can analyze the
logical values and the end of frame (EOF). Decoding the serial data, the global
digital controller sends signals to change the state of SH, AN, and CA of each
pixel.

The global digital controller has four states that itemize sampling phase, cathodic
phase, anodic phase, and resting phase. The sampling phase is when photosensor
output is input to the image processor to calculate the outline. The cathodic phase is
generating a negative current pulse, and the anodic phase is creating a positive
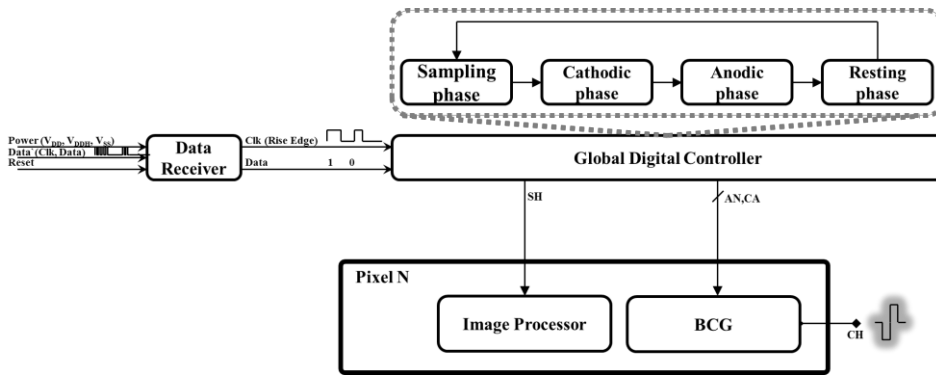
Figure 2-12 Schematic of the digital controller

current pulse. The resting phase is shorting CH to ground, removing residual stimulus charge from the biological environments.

2.3. Average Stimulus Power Estimation

2.3.1. Stimulus Patterns Generation of Conventional and Proposed Strategies

From the simulation and measurement of the fabricated IC's using thresholding and outline extraction, expected stimulus patterns were generated varying the number of stimulation channels, using simple fitting models as shown in Figure 2-13 (a). We set maximum stimulus level of the conventional retinal prosthetic strategy to 500 µA due to average maximum stimulation charge of 500 nC. Threshold level
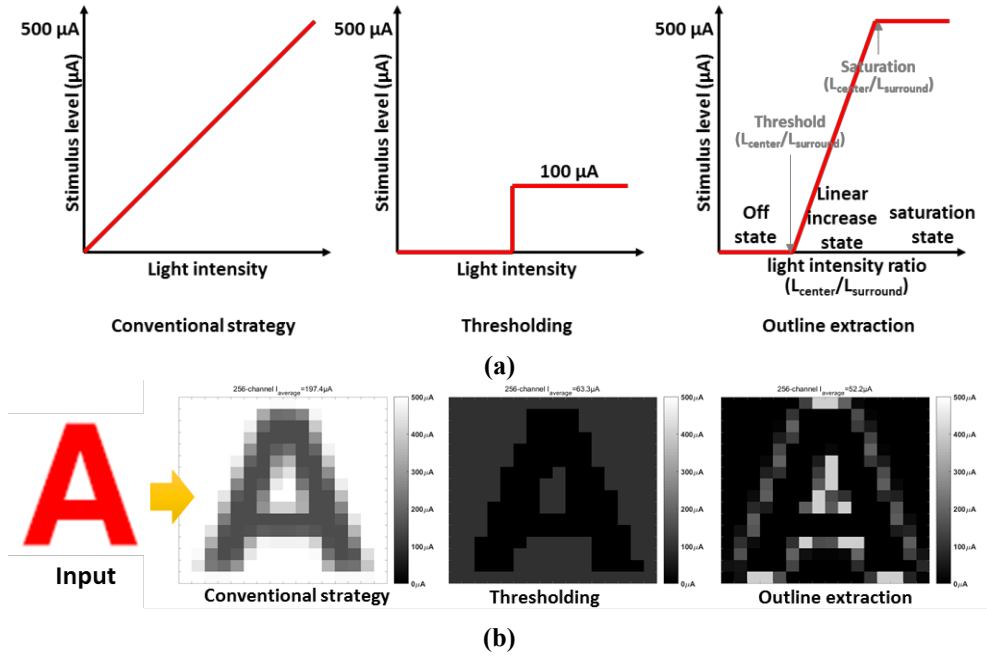
Figure 2-13 (a) Fitting model of three stimulation strategies: conventional, thresholding, and outline extraction strategies (b) Example of the generated stimulus patterns 32×32 channels

was set to 100 μA. The threshold of $L_{center}/L_{surround}$ is 1 and saturation of $L_{center}/L_{surround}$ are 1.2 from the simulation result. Alphabet characters were chosen as input images. Stimulus patterns were extracted from the each alphabet image using light-intensity, thresholding, and outline varying the number of channels (4×4, 8×8, 16×16, 32×32, 64×64 channels), and Figure 2-13 (b) shows the example of the test image with 32×32 channels, and all the test images are shown in Appendix. We calculate all stimulus power using generated stimulus patterns, and we can get average stimulus power by the number of channels in each strategy.

2.3.2. Minimum Distinguishable Channels to Recognize

Perceiving the minimum channels to recognize the image patterns by the conventional and proposed strategies, we conducted a preliminary test of question investigation. Four male subjects between the age of 24-27 with corrected vision of 1.1 ± 0.2 were asked minimum channels to recognize the images (all the images used are shown in Appendix). Visual angle of the picture was about 9 ° as shown in Figure 2-14, strategy order is conventional, thresholding, and outline extraction. Alphabet order was random, and the number of channels of each alphabet was from 16 (4×4) channels to 4096 (64×64) channels.
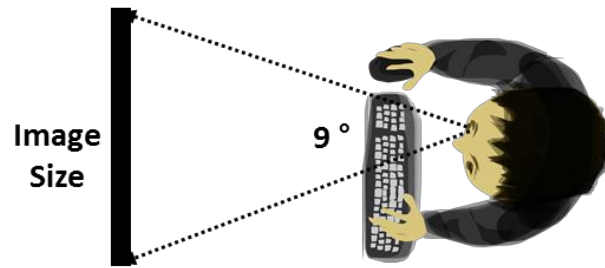
Figure 2-14 Question investigation setup

2.4. Virtual Channel

2.4.1. Concept

In order to achieve more stimulation channels than physical channels of the IC, the virtual stimulation circuit using current steering is adopted [36], [37]. Tripolar stimulation means that current from two electrodes with different ratio flow towards the one electrode. The tripolar stimulation is mainly used as one-

(a)

(b)
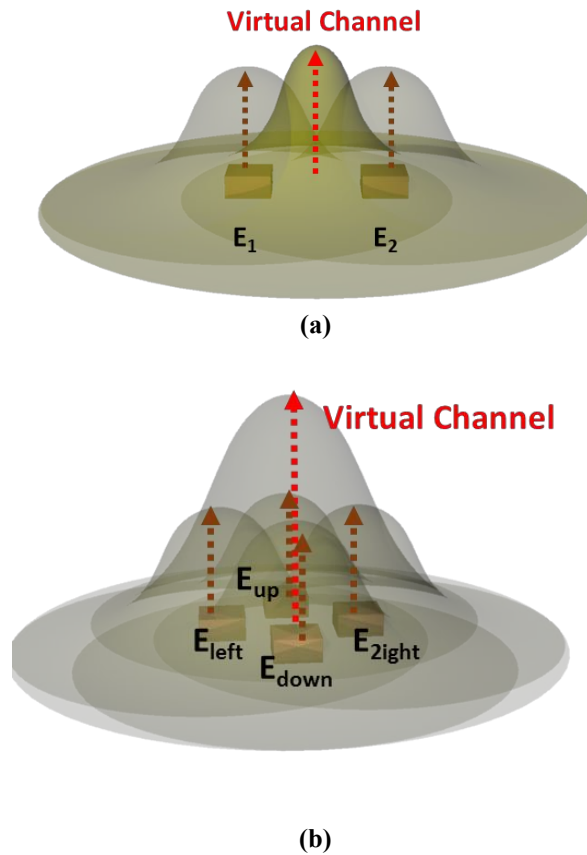
Figure 2-15 (a) Concept of the one-dimensional virtual channel (b) Concept of the two-dimensional virtual channel (one electrode, which is called reference electrode, is far from two electrodes. Thus it is not shown in the figure)

dimensional virtual channel generation in cochlear implant as shown in Figure 2-15 (a) [53]. The retinal prosthesis needs a different virtual channel scheme due to the two-dimensional retinal cell structure as illustrated in Figure 2-15 (b). We proposed two-dimensional virtual channel generation, combining two tripolar stimulation: one determines active field along up and down direction, the other does the effective area along left and right direction.

In this study, the design of the distributed current stimulator IC with the one-dimensional virtual channel was firstly explored to validate the feasibility for proposed neural prosthesis implementation. All circuits were simplified for smaller chip area. Multiplication structure of current digital to analog converter (DAC) for the reduction of IC area and simple virtual channel generator (VCG) for the channel increase were adopted. Fabrication and bench-top test were also conducted for the validation of design. Finally, the two-dimensional virtual channels were verified by combining two fabricated current stimulator IC with the one-dimensional virtual channel.

2.4.2. Circuit Descriptions

Figure 2-16 shows the block diagram of proposed neural stimulator and the distributed current stimulator IC with the one-dimensional virtual channel. The peripheral circuits consist of the regulator for the power management and the inductive link for power and data telemetry. The peripheral circuit receives the
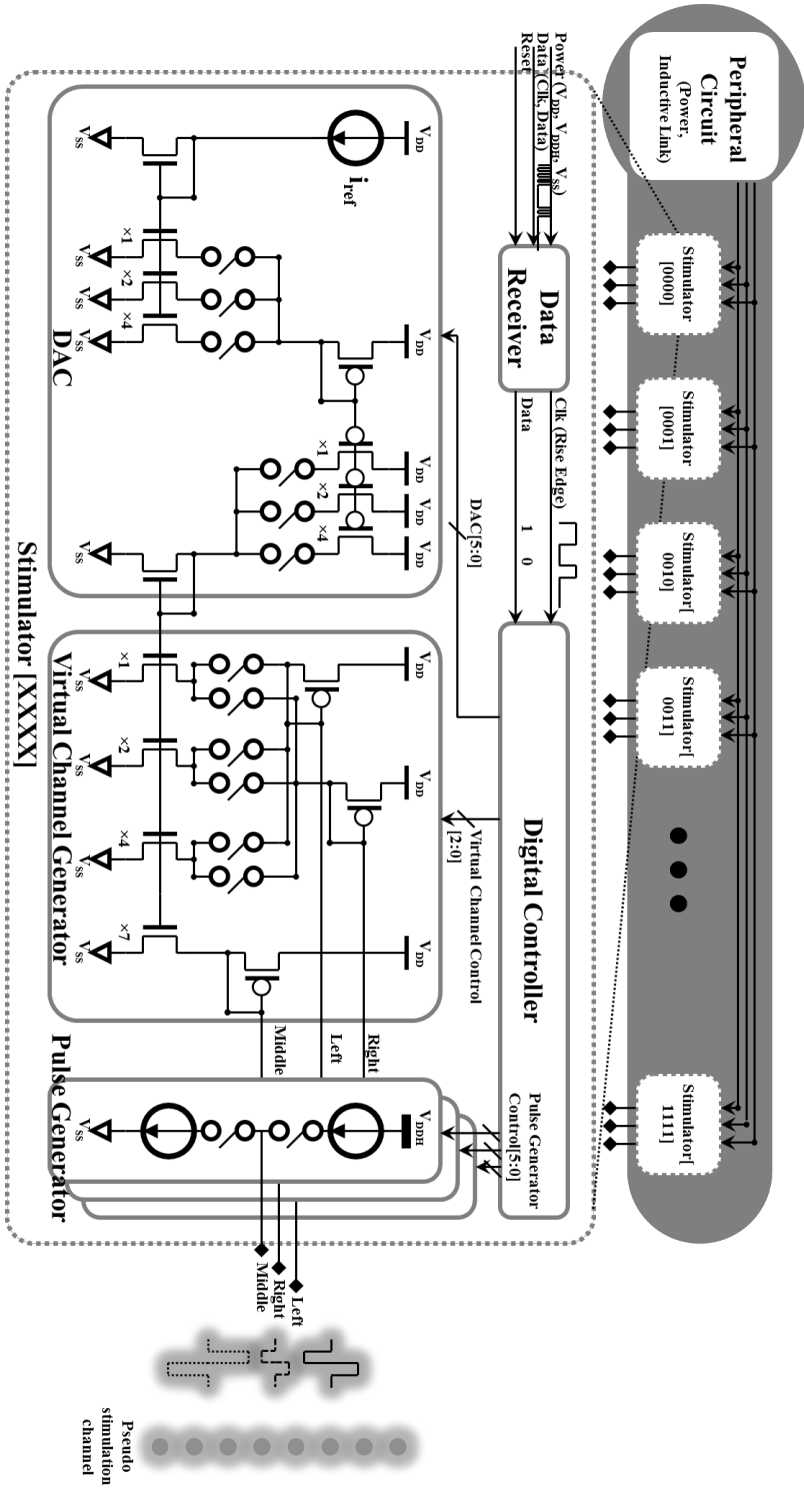
Figure 2-16 Block diagram of the proposed neural stimulator with distributed current stimulator ICs

amplitude modulated signals which are converted into power and control data. Then, data is transferred to all distributed current stimulator IC's (stimulator [XXXX]) using the shared metal line. All IC's have their 4-bit address which allows all IC's to be controlled individually. Thus the number of metal line can be a fixed value regardless of the increasing number of stimulation channels. When the address information of data matches the IC address, the matched IC receives the stimulation parameters (polarity, phase, duration, current level, virtual channel mode) and generates current pulses.

2.4.2.1. Data Receiver and Digital Controller

Data Receiver converts amplitude modulated data into clock and data. The clock is generated from amplitude modulated data using the envelope detection. Thus IC can use the first rising edge of input. Logical data is generated using pulse width modulation (PWM) and pulse counting. Thus digital controller can analyze the logical values and the end of frame (EOF) as shown in Figure 2-17 (a) [54]. Figure 2-17 (b) shows serial control data format which are composed of setup mode (MSB = 0) and stimulation mode (MSB = 1). The setup mode determines duration (Duration [4:0]) and current pulse type such as polarity, phasic type, and virtual channel mode (Mode [2:0]). The stimulation mode generates a current pulse with the current level determined by Level [5:0] after the EOF enters the digital controller. Then stimulation sites corresponding to Address[3:0] are activated

Figure 2-17 (a) PWM data structure (b) Serial data format
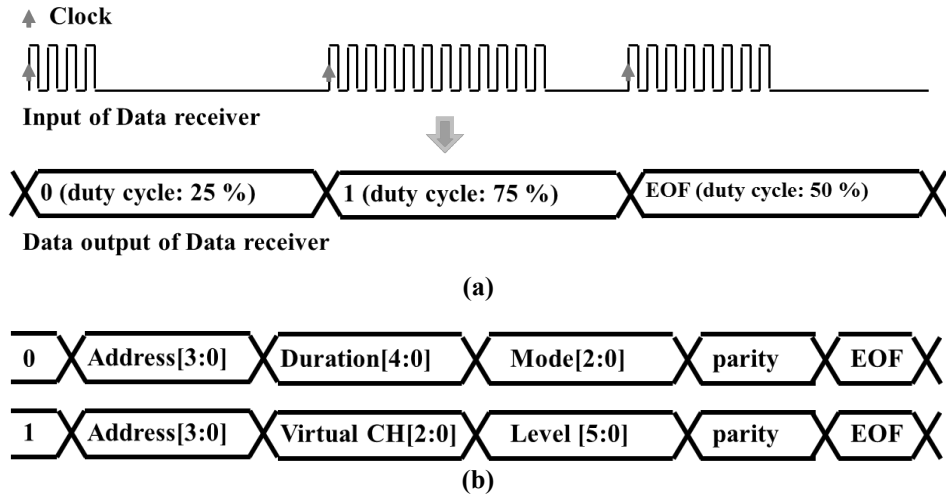
sequentially. If the virtual mode is active, Virtual CH [2:0] determines the ratio of left pulse generator current to right pulse generator current. Both modes have parity check bit that reduces data error rate. Frequencies of amplified modulated data, clock, and maximum stimulation pulse are set to 3 MHz, 192 kHz, and 11.3 kHz, respectively.

2.4.2.2. Current DAC

Current DAC is composed of two current DAC with 3-bit binary weighted transistors [55]. The first current DAC with 3-bit binary weighted transistors generates current up to 70 μA in 8 linear steps. The output current of the first current DAC is amplified by the second current DAC with a variable gain of 0 to 7, reducing chip area and retaining reasonable dynamic range compared with one

47

current DAC with a 6-bit binary weighted transistor with single bias.

2.4.2.3. Virtual Channel Generator

The VCG amplifies the output current of the current DAC with a gain of 1, 2, and 4. Each amplified current either chooses the left pulse generator or the right pulse generator, which make the ratio of the left pulse generator current to the right pulse generator current is from 0:7 to 7:0 in 8 steps. The amplified output current of the current DAC with a gain of 7 goes to the middle pulse generator, which makes current level be the sum of current from the left pulse generator and the right pulse generator while the virtual channel mode is active. As a result, the current generated by the left and right pulse generator can sink to the middle pulse generator without residual charge.

2.4.2.4. Biphasic Current Generator

Three output currents of the VCG are converted into the biphasic or monophasic current pulses in the pulse generator, as described in 2.1.2.4. Dual supplied with active cathodic, and active anodic phases are used to generate current irrespective of output impedance variability, provided that load voltage does not exceed the
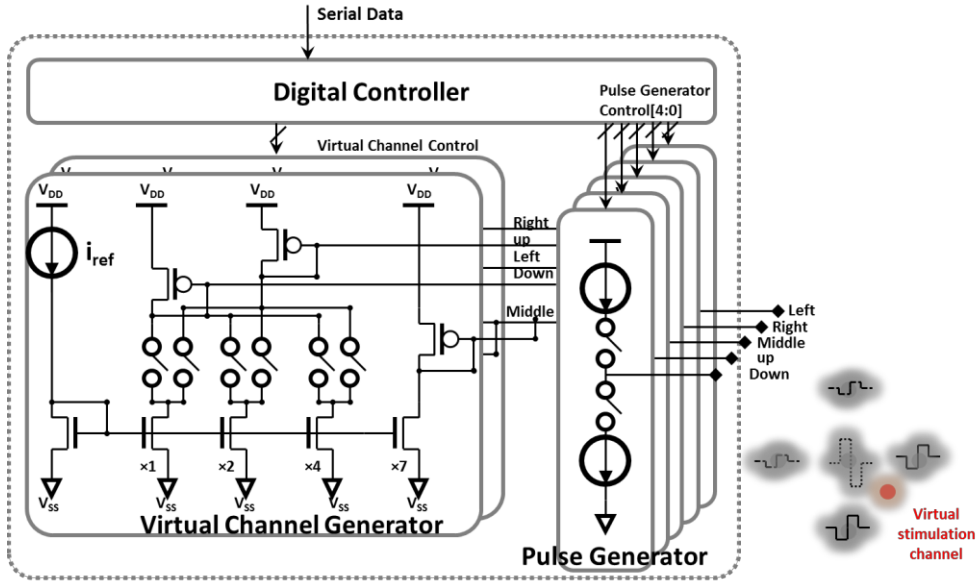
Figure 2-18 Schematic of the two-dimensional virtual channel generator

compliance voltage [56]. If the virtual channel mode is active, the phase of the left

and right pulse generator is opposite to that of the middle pulse generator. Thus the

sum of current from the left and right pulse generator can sink to the middle pulse

generator for safety. While virtual channel mode is inactive, current flows between

the output of the middle pulse generator and ground (GND). In resting state, all

electrodes are shorted to ground potential to remove residual charge [57].

2.4.2.5. Two-dimensional Virtual Channel Generator

As the human retinal network has a two-dimensional structure, virtual stimulus

should be generated with the two-dimensional axis. With designed current

stimulator chip, two-dimensional virtual channel generator can be created by

combining two customized stimulator chips, as shown in Figure 2-18. Digital

49

controller sends the signal to each current stimulator chips that one steers current along the horizontal axis (Left, Right), and the other along the vertical axis (Up, Down). Virtual stimulus is the sum of these two currents from two chips, containing two axis information. Middle channels of two IC's are connected, as all currents from the 4 channels (Left, Right, Up, Down) come together in the middle channel.

2.5. Polymer Packaging

Even though various biocompatible polymers had been researched as packaging and optical window materials for the photodiode-based retinal prosthesis, we proposed liquid crystal polymer (LCP) and explored the optical property for the feasibility of the long-term reliable optical window.

2.5.1. LCP as a Long-term Reliable Packaging Material

Recently, LCP has gained increasing attention as a substrate and packaging material for long-term implantable biomedical devices [58]. Low moisture absorption rate (< 0.04 %) and gas permeability that is comparable to Corning glass [41] of LCP are expected to realize a long-term reliable encapsulation, and yet it retains desirable features of polymeric material being thin, light-weight and flexible. The LCP encapsulation of MPDA can offer another advantage of the possibility to be integrated with the surrounding circuitry such as a coil, chip and interconnects, constituting a monolithically integrated device in a homogeneous LCP package as demonstrated in a recent study [59]. An MPDA can be encapsulated by thermally laminating between two LCP films, followed by partial thinning for optical windows and exposing electrode sites for charge injection as shown in Figure 2-19, which is low cost, and simple process compared with brazing and welding of sapphire and titanium process.
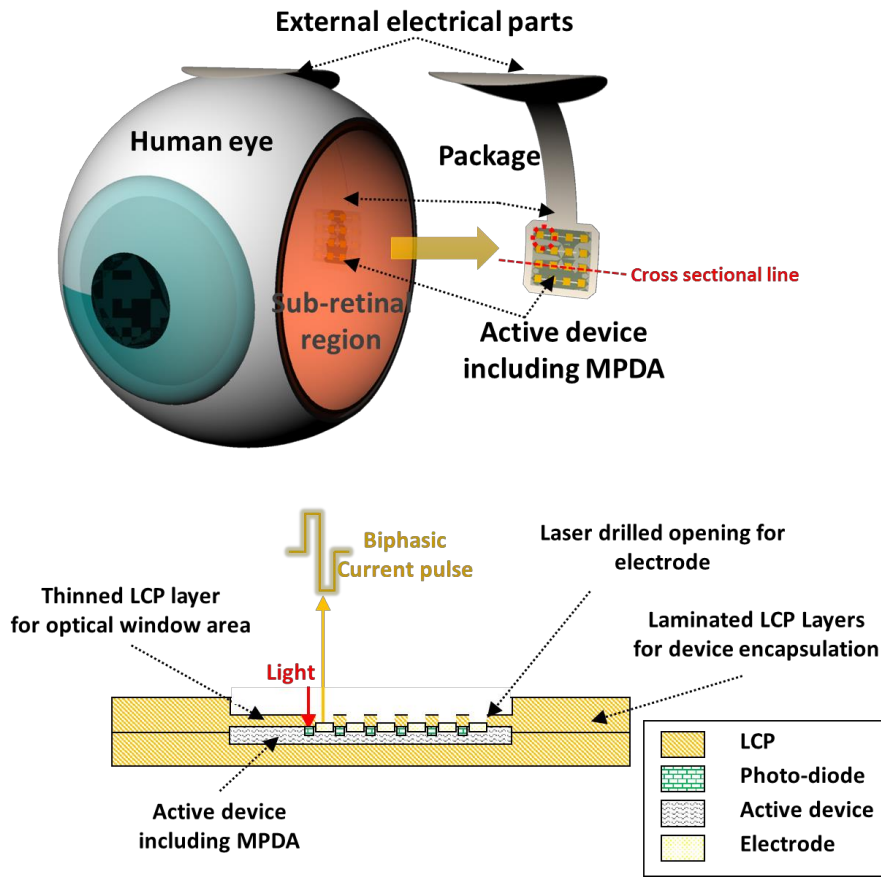
Figure 2-19 Concept of the LCP encapsulated photodiode-based retinal prosthetic IC

While LCP has been primarily studied as an encapsulation material so far, its optical properties such as transmittance and scattering have not been investigated yet. Although the semi-crystalline structure of LCP results in lower light transmittance compared with amorphous polymers like polyimide and parylene, our preliminary experiments showed transmittance could be increased by using thinner LCP films.

In this chapter, therefore, the feasibility of LCP as a transparent packaging material
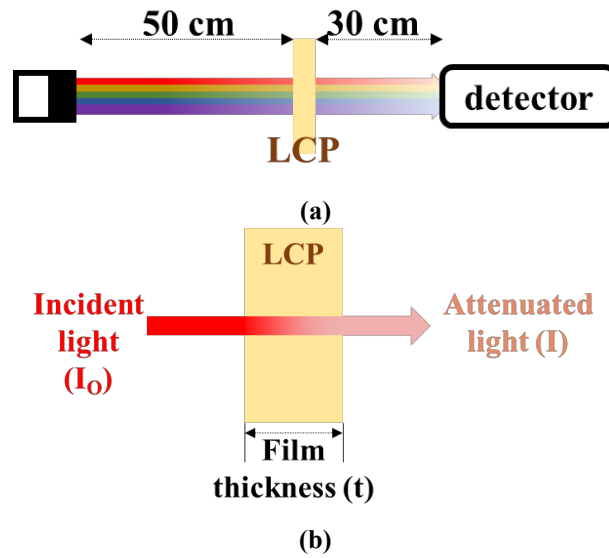
Figure 2-20 (a) Test methods of absorption coefficient (b) Coefficients of Lambert-Beer law

for an MPDA-based retinal prosthesis is explored by overcoming inherent low transmittance of LCP due to its semi-crystalline structure. The absorption characteristic of LCP is measured to estimate the film thickness below which 10 % of light transmittance is guaranteed. The etching process is developed to thin down the commercially available 25 μm-thick LCP film to several micrometers. The light scattering behavior is characterized using grating patterns projected on a CMOS image sensor covered by an LCP film to determine the maximum resolution.

2.5.2. Test Methods

2.5.2.1. Light Transmittance according to LCP Thickness

Table 2-1 Comparison of thinning LCP fabrication

	RIE Etching (O$_2$)	Wet Etching (KOH)	Thermal Pressing	Laser Ablation
Surface roughness	Flat[1]	Rough[1]	Flat	Rough
Thickness control	Easy	Easy	Hard	Hard
Etching time	Long	Long	Short	Short
Patterned etching	O	O	X	O

Light transmittance spectra of LCP films with varying thicknesses (25 μm, 50 μm, 100 μm; Vestar FA series, Kuraray, Japan) was measured using a spectrophotometer (UV-3101PC, Shimadzu, Japan) in order to calculate the absorption coefficient of LCP, as shown in Figure 2-20 (a). From the Lambert-Beer law, light transmittance can be written as

$$T = I / I_O = \exp(-\alpha t), \tag{13}$$

where T is the transmittance, I and I_0 are the intensity of the transmitted and incident light, respectively, α is the absorption coefficient, and t is the film thickness, as shown in Figure 2-20 (b) [60]. The absorption coefficient was acquired by fitting the measured transmittance data to (5-1) using the non-linear least square method of the curve-fitting tool provided by MATLAB.

2.5.2.2. Thickness Control of LCP

The etching process for thinning down an LCP layer was developed for lower scattering and higher light transmittance using a 25 μm-thick LCP film that is the thinnest among the commercially available LCP products. Reactive-ion etching (RIE) etcher (Plasmalab 80 plus, Oxford Instruments, UK) was used for LCP ablation since this process can provide higher flatness of the thinned surface than other thinning methods such as wet etching [61] and mechanical pressing so that light scattering can be minimized, compared in Table 2-1.

After a series of solvent cleaning, LCP film attached onto Si wafer was etched by oxygen plasma under the power of 199 W, the gas flow of 100 sccm, and the pressure of 0.1 torr for varying the time from 40 to 55 minutes with 5 minutes steps for controlling the final thickness.

2.5.2.3. Spatial Resolution of LCP

The resolution that can be achieved by an LCP-encapsulated MPDA was measured using LCP films of varying thicknesses. A customized optical experiment setup was built with a commercial CMOS image sensor (OV3640, OmniVision Technologies Inc., USA), half of which is covered by an LCP film while the other half of the area is uncovered as shown in Figure 2-21 (a). Black and white stripe of logarithmically varying pitches of an LCD monitor were projected on the image
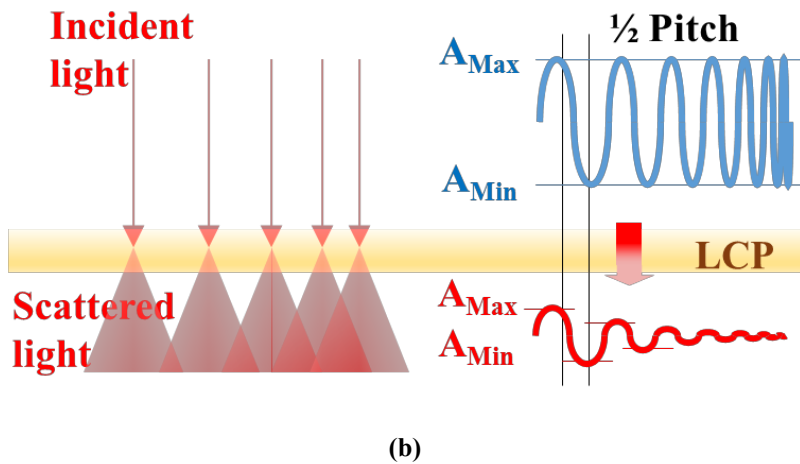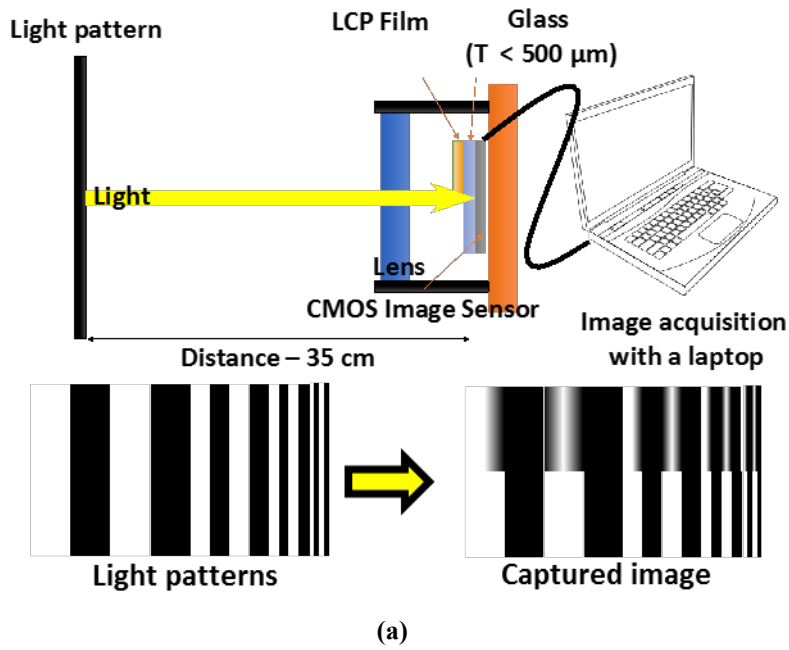
Figure 2-21 (a) Customized optical experiment setup for resolution test (b) Coefficient of modulation transfer function (MTF)

sensor so that the LCP-covered image and the uncovered image could be acquired at the same condition. With the captured images, the contrast was calculated from modulation transfer function (MTF) versus grating frequencies with modulation the

depth (M) written as

$$M = (A_{max} - A_{min})/(A_{max} + A_{min}), \tag{14}$$

$$MTF = M_{image}(\xi)/M_{object}, \tag{15}$$

where A is the amplitude of light intensity; M_{image} is the modulation depth of measured image; M_{object} is the modulation depth of input; ξ is the spatial frequency [62], as shown in Figure 2-21 (b). Higher spatial frequency leads to a lower M_{image} as a result of light scattering, thus a lower MTF. The MTFs of LCP-covered images were compared with that of an uncovered image to determine the maximum resolution of LCP encapsulation, defined as the grating frequency above which the contrast (MTF) is less than the arbitrarily set threshold of one tenth of the MTF from an uncovered image.

Chapter 3: Results

The chip designs with thresholding, outline extraction, and virtual channels were implemented and measured for the verification. Also, the optical properties of LCP were explored using test methods above. This chapter describes the prototype   IC fabrication, test setup, and experimental results of each prototype IC's.

3.1. Thresholding

3.1.1. Fabricated IC

For verification of our design, a prototype of 30-channel MPDA-based retinal implant IC excluding the digital controller was fabricated using Towerjazz 0.18 μm CIS process. Figure 3-1 shows the microphotograph of the fabricated prototype and the layout of a unit pixel. The pixel area is 0.021 mm^2, implying that 470-channel
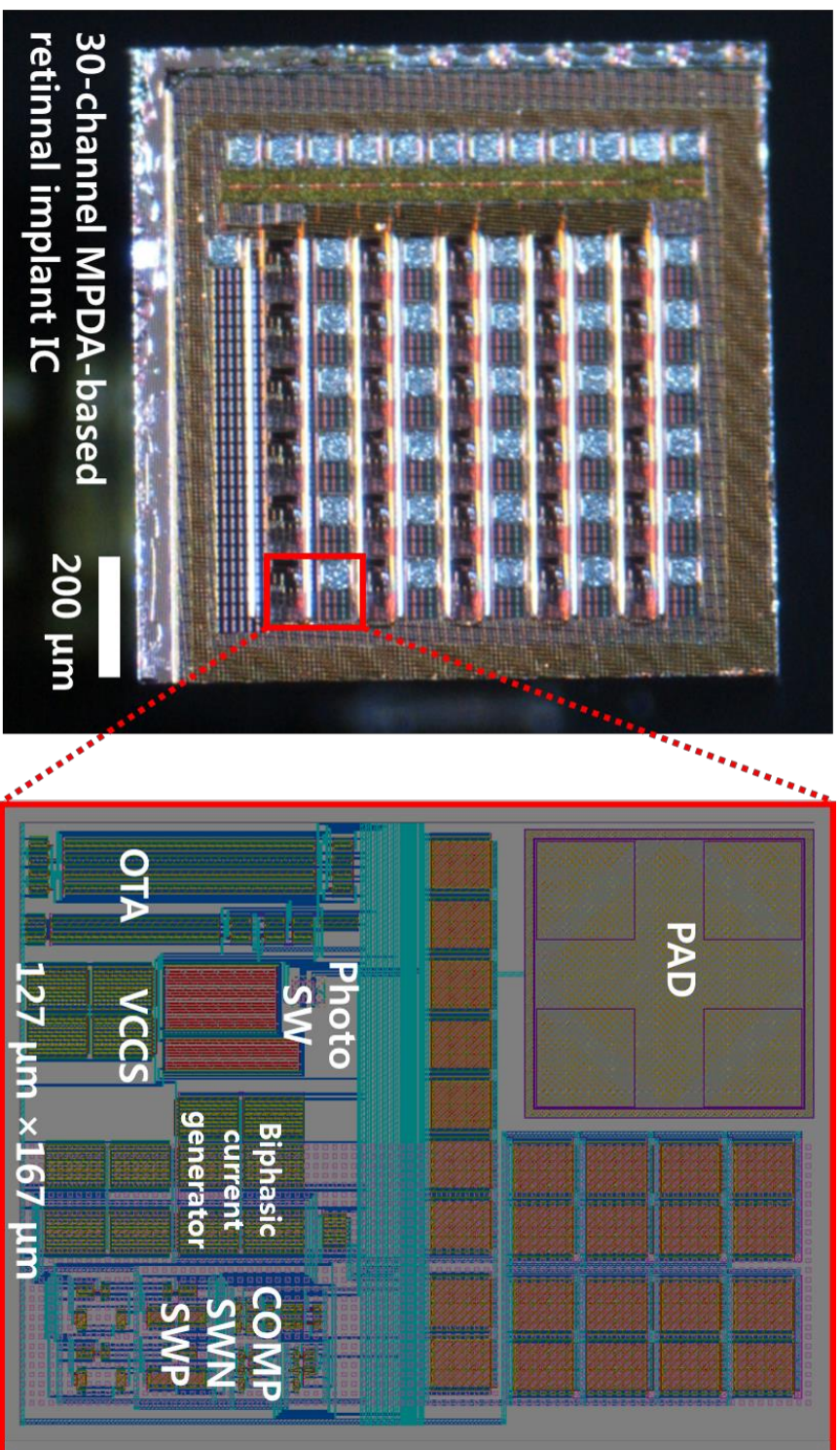
Figure 3-1 Microphotograph of the 30-channel MPDA-based retinal prosthetic IC

59

pixels can be integrated into a macular area of 10 mm^2. 4-tr APS that company provided was used as provided, for the confidential reasons. The characteristics of the 4-tr APS are listed in Table 3-1.

Table 3-1Characteristics of the 4-tr APS

Parameters	Units	Values
Size	μm^2	2.2 ×2.2
Conversion Gain	μV/e-	60
Responsivity,Green	V/ lx · s	0.6
full well capacity	Ke-	10.0
Pixel noise floor	μV	300
Dynamic Range	dB	66

3.1.2. Test Setup

A customized bench top test setup was configured to measure the IC performance,

Figure 3-2 A customized bench top test setup

as shown in Figure 2-2. The IC was connected with a PCB using wire-bonding and protected by transparent epoxy for light transmission. The digital controller was implemented with an FPGA (Spartan 3A, Xilinx Corp., USA). The light source was a digitally-controlled quartz-tungsten-halogen light lamp (66884, Newport, USA), and light intensity was measured by the light meter (TES 1336A, TES Corp., Taiwan). A resistor was connected as a load to the channel output.

3.1.3. Test Results

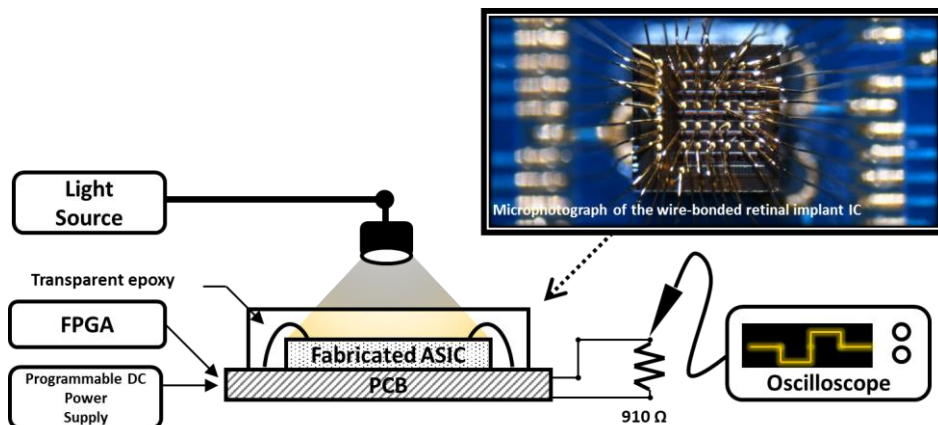Figure 3-3 shows the measurement of the stimulation output in response to light illumination to the IC. Biphasic current pulse burst was measured while light with supra-threshold intensity was illuminated, as shown in Figure 3-3 (a). Otherwise, no biphasic current pulse was measured.

The dependency of the light intensity threshold ($L_{threshold}$) on the TX value was measured. Figure 3-3 (b) shows the measured data (in red lines) together with the design values (in blue lines) where V_{REF1} is 1.65 V, $V_{TH} = 0.7$ V, and k is 0.6 V/ lx · s. The device was designed to operate in a living room lighting condition of under 400 lx. However, the measured values were significantly higher than the design values. The discrepancy was found to be due to the abnormally large offset voltage in the comparator. This fault is under investigation and will be corrected in
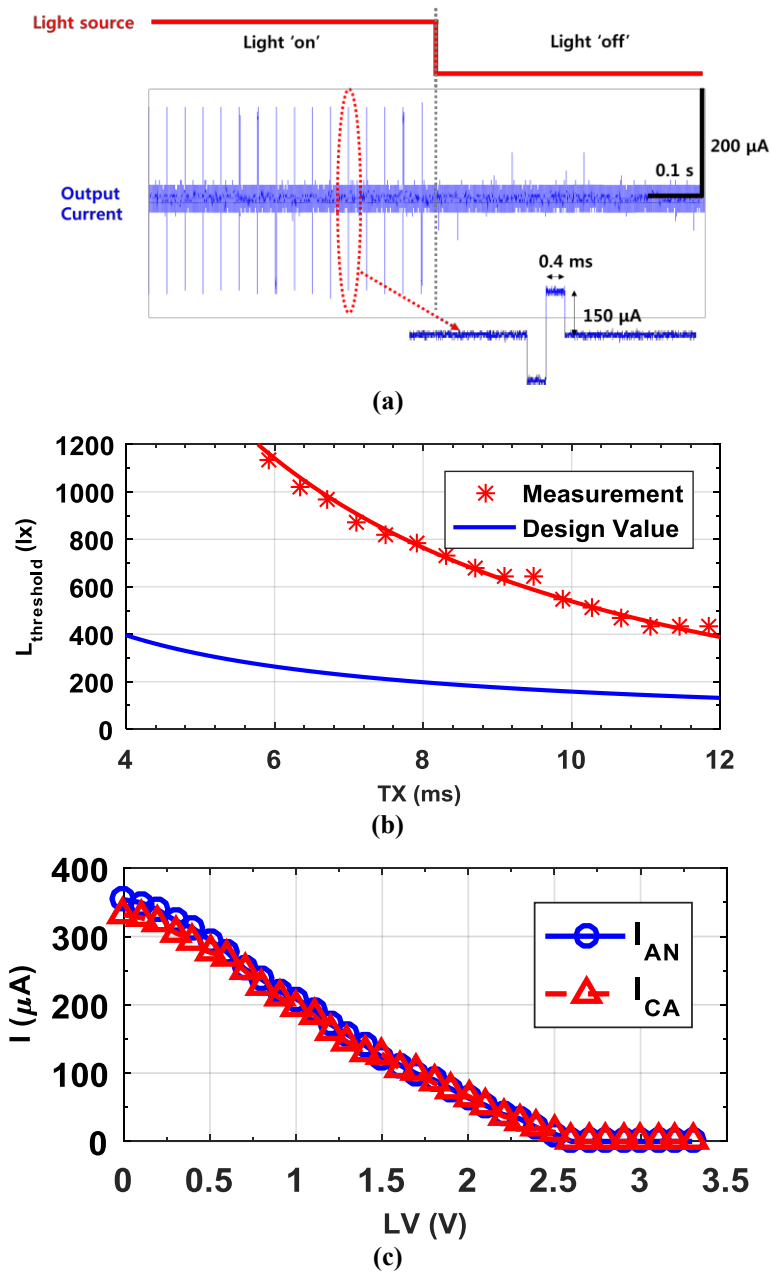
(a)

(b)

(c)

Figure 3-3 Test results of (a) the channel output when light source is on/off, (b) the light intensity threshold along to TX time, and (c) the amplitude of anodic and cathodic current

the next design. We can further increase the light sensitivity by increasing area used by APS for [63], and 3-D structure can be one option without increasing the geometric area [64]. The biphasic currents were measured for the anodic and cathodic phase, respectively, and verified to vary according to the LV (input voltage), as shown in Figure 3-3 (c).   Amplitudes of current in the anodic and cathodic phase were measured to be within the range of 0-354 μA and 0-332 μA, respectively. The average current mismatch was 4.85 % with standard deviation of 3.52 %. The main reason causing the current mismatch is process variation and channel length modulation effect due to varying drain voltages of MOSFETs. A switch connecting between CH and REF can remove the residual current due to the current mismatch in the resting state.

Power consumption was 733 μW per channel when generating a current pulse in the resting state. Primary power consumptions were in the VCCS, mirroring

Table 3-2 Summary of the chip performance

Process	0.18 μm CIS process
Stimulation strategy	Monopolar and simultaneous biphasic current stimulation
Supply voltage	V_{DD} = 1.65 V V_{SS} = -1.65 V
Light intensity threshold	400 lx @TX=12.5 ms 13120 lx @TX=0.79 ms
Stimulus current level	0-354 μA (I_{CA}), 0-332 μA (I_{AN})
Unit pixel area	0.021 mm^2
Power consumption (in the resting state)	733 μW per channel

circuits of the BCG and OTA due to their static currents. This unwanted leak currents can be reduced by the selective operation while generating current pulses. In other words, the VCCS and the BCG in the next version should be activated only when biphasic current pulse are generated for low power consumption, which can significantly reduce the power consumption by 97 % when using the duration of 1 ms and the pulse rate of 30 Hz. Table 3-2 summarized the chip performance.

3.2. Outline Extraction

We simulated the circuit design and fabricated two prototype chips. Fabricated IC's were measured for verification. The first IC was fabricated using 0.18 μm BCDMOS process after simulation. The second IC was fabricated with modification of the first IC.

3.2.1. Simulation Results

The design of the IC was simulated before the chip fabrication using 0.18 μm BCDMOS process parameter for the verification of the chip performance. First, the photosensor output in response to photocurrent was simulated. The pulse rate of the photosensor output is linearly changed by the photocurrent as shown in Figure 3-4 (a). As the light intensity, the photocurrent, and output pulse rate have a linear relationship, the light intensity can be replaced with photocurrent (I_{center}, $I_{surround}$). Figure 3-4 (b) shows the output voltage of the image processor in response to the ratio between photocurrent of the center pixel and those of the surrounding pixels (I_{enter}/ $I_{surround}$). The voltage decreases as the I_{enter}/ $I_{surround}$ increases. Figure 3-4 (c) show the current level of the VCCS. When the input voltage is below 1.2 V that is the same as the I_{enter}/ $I_{surround}$ of 1, current starts to flow up to 650 μA. Figure 3-4 (d) illustrates the current level of the BCG along the I_{enter}/ $I_{surround}$. When the I_{enter}/ $I_{surround}$ is over 1, BCG starts to generate the current pulse. The maximum current

(a)

(b)

(c)

66
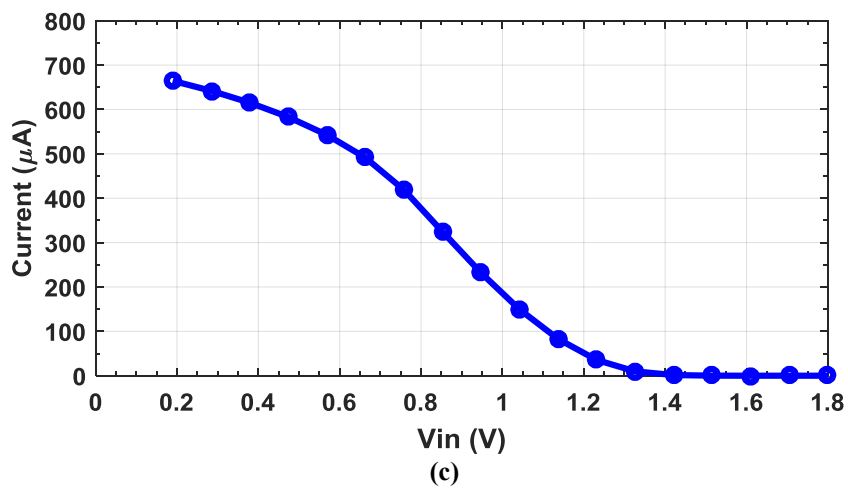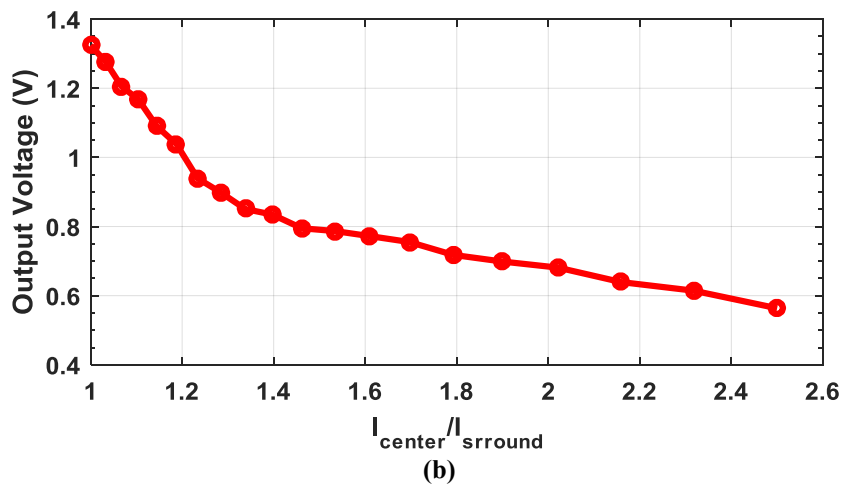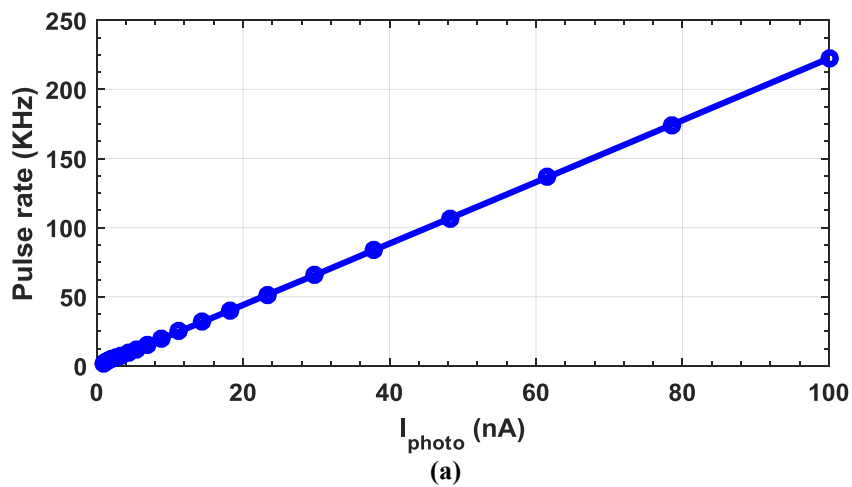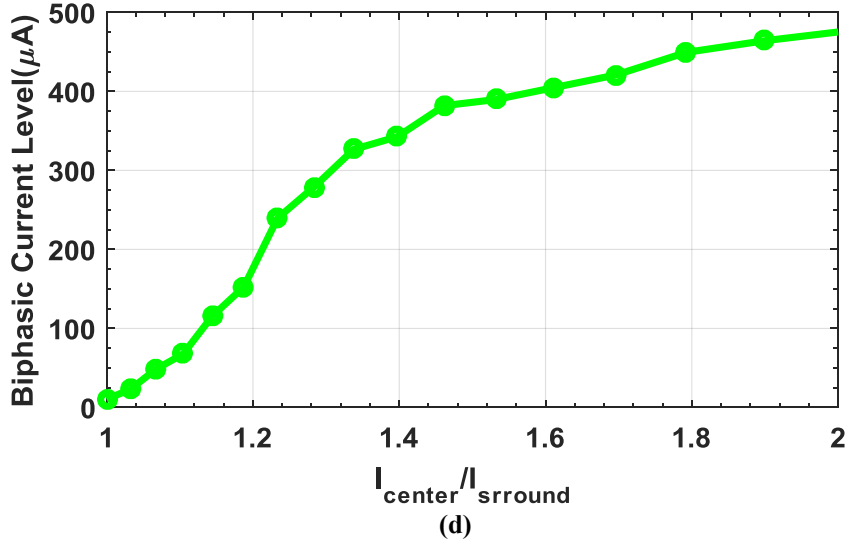
Figure 3-4 Simulation results of (a) pulse rate of the photosensor in response to photo current (I_{photo}), (b) output voltage of image processor in response to current ratio between the center pixel photocurrent (I_{center}) and the surrounding pixel photocurrent ($I_{surround}$), (c) conversion of input voltage into current in VCCS, and (d) biphasic current level of BCG in response to current ratio (I_{center} / $I_{surround}$)

level is 480 μA due to the minimum output voltage of the image processor.

3.2.2. Fabricated IC

For the verification of the design, two prototypes of retinal prosthetic IC's were fabricated. The first IC was fabricated using TowerJazz 0.18 μm BCDMOS process. Figure 3-8 shows the microphotographs of the fabricated ICs. The first IC is the 16-channel retinal prosthetic IC including a digital controller, as illustrated in Figure 3-5 (a). The pixel area is 0.5 mm², implying that 200-channel pixels can be integrated into a macular area of 10 mm². This IC needs a micro-sized light pattern

67

for the verification of outline extraction. Thus 9-channel retinal prosthetic IC with the discrete photodiodes was also fabricated using the same process for test convenience.

The second IC was fabricated using Magna 0.18 μm CMOS process. To solve the limited number of test pads, the second IC has only 1 channel and each block has many test pads. Also, the layout of the second IC was optimized including area-efficient VCCS, resulting in much smaller unit pixel area compared to the first IC. Figure 3-5 (b) shows the microphotograph and layout of the second IC. The unit pixel area is 0.0072 mm^2 due to the area-efficient VCCS and layout optimization, leading that retinal prosthetic IC can integrate 1300-channel pixels into the macular area of 10mm^2 if using circuit under pad (CUP). PAD allocation to be connected with the surrounding IC's was also considered for testing convenience.

3.2.3. Test Setup

Two customized bench top test setup were configured to measure the IC performance. The IC's including the photodiode were connected to a PCB using wire-bonding and protected by transparent epoxy for light transmission, whereas the IC excluding photodiode were protected by black epoxy to minimize noise by the photoelectric effect.

Figure 3-6 shows the bench top test setup of 9-channel retinal prosthetic IC (the
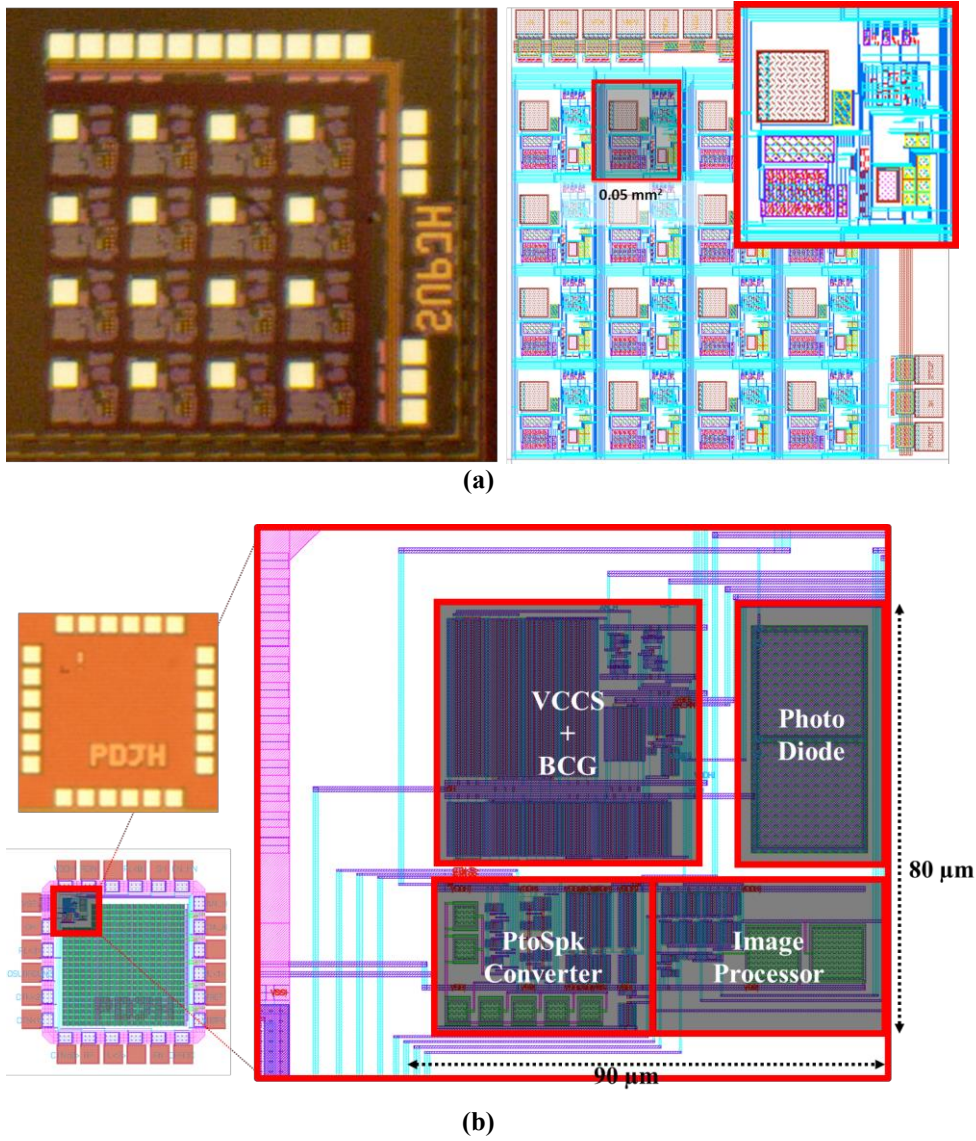
(a)

(b)

Figure 3-5 Microphotographs of the two prototype of retinal prosthetic ICs: (a) the first IC using TowerJazz 0.18 μm BCDMOS process, (b) the second IC using Magna 0.18 μm CMOS process
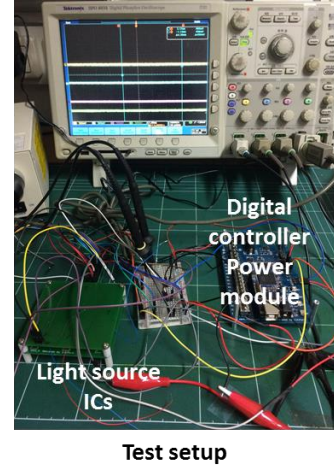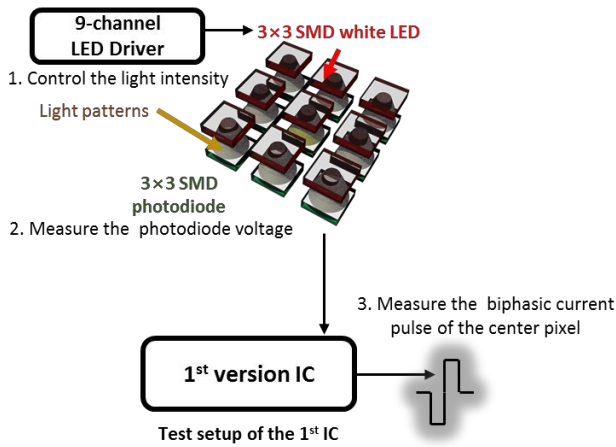
69

Figure 3-6 Test setup of 9-channel retinal prosthetic IC (1st version)

first version). To generate PWM data, we used an FPGA (Spartan 3A, Xilinx Corp., USA). Nine surface-mountable silicon infrared PIN photodiodes (QSB34, Fairchild, USA) were used to generate photocurrent and nine surface-mountable white LEDs were used to illuminate the photodiodes, and the light meter (TES 1336A, TES Corp., Taiwan) measured the light intensity. A resistor was connected as a load to the channel output. Oscilloscope measured the voltage of the center and surrounded photodiodes' plus nodes and biphasic current pulse of the center pixel.

Figure 3-7 illustrates the bench top test for 1-channel retinal prosthetic IC (the second version). FPGA generates all digital signals to control the chips. Two IC's, which represent the center pixel and the surrounding pixel respectively, were connected to measure the effect the N_{center} / $N_{surround}$. The center pixel was illuminated using a digitally-controlled quartz-tungsten-halogen light lamp (66884, Newport, USA) and surround pixel IC with fixed light intensity in order to change

Test setup of the 2nd IC
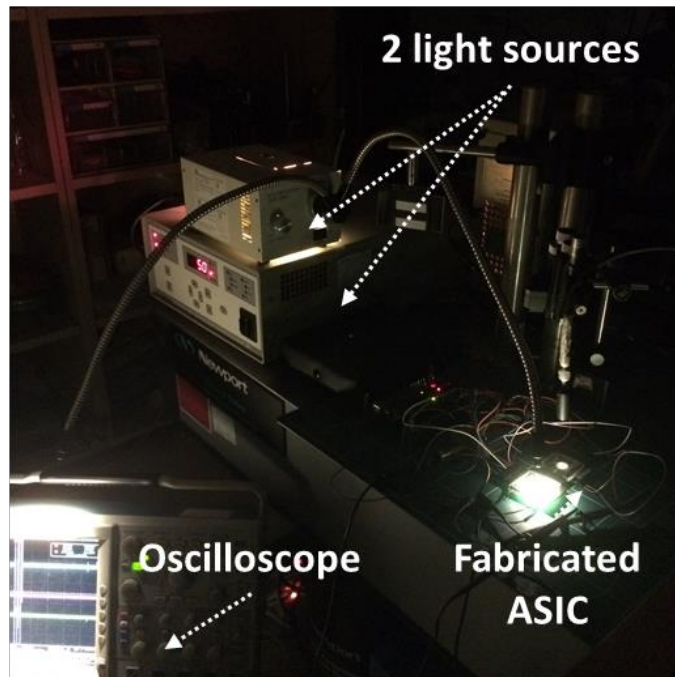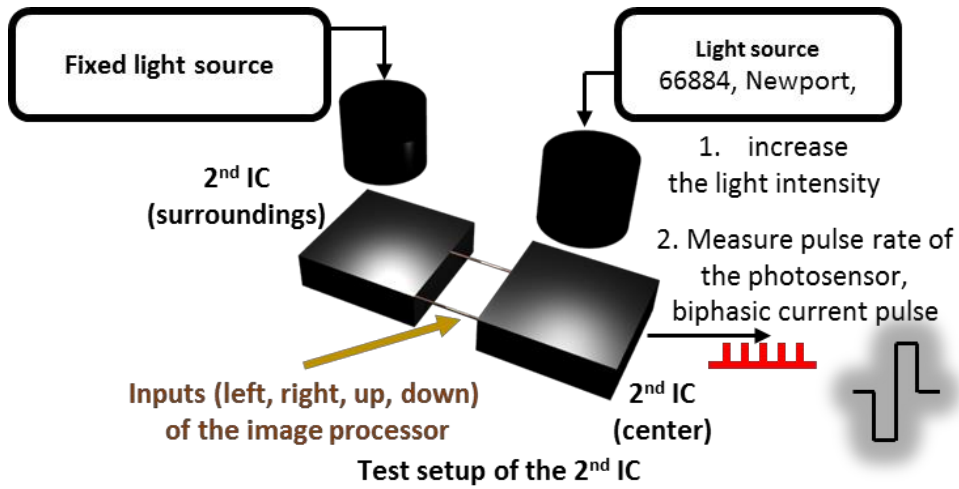
Photograph of the test setup of the 2nd IC

Figure 3-7 Test setup of the 1-channel retinal prosthetic IC (2nd version)

the current L_{center} / $L_{surround}$. The light intensity was measured by the light meter (TES 1336A, TES Corp., Taiwan). A resistor was connected as a load to the channel output.

3.2.4. Test Results

Firstly, we measured the voltage of the photodiode plus node and biphasic current pulse, as shown in Figure 3-8. Due to bright illumination of the center compared to the surrounding, the voltage change of the center pixel is higher than that of the surrounding pixel. As the light intensity of the center region is more than that of the surrounding, biphasic current train was measured. Due to the limited number of test
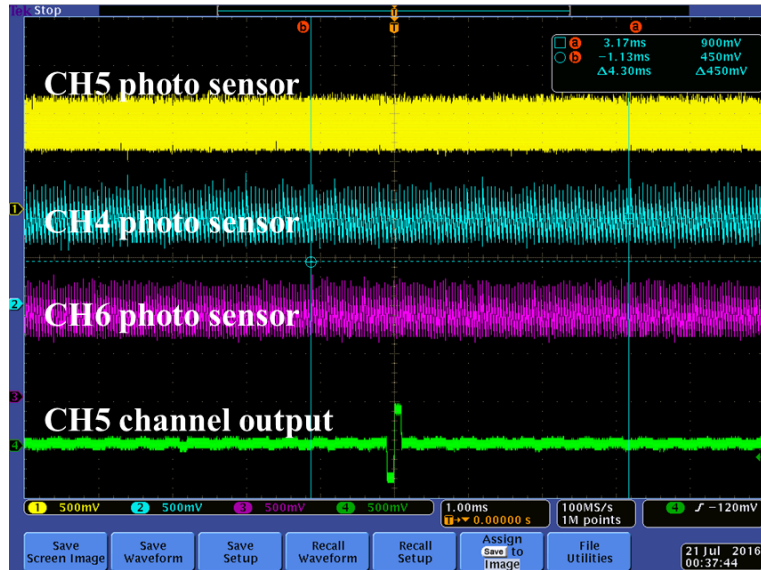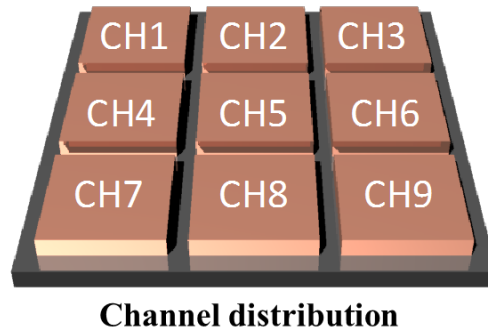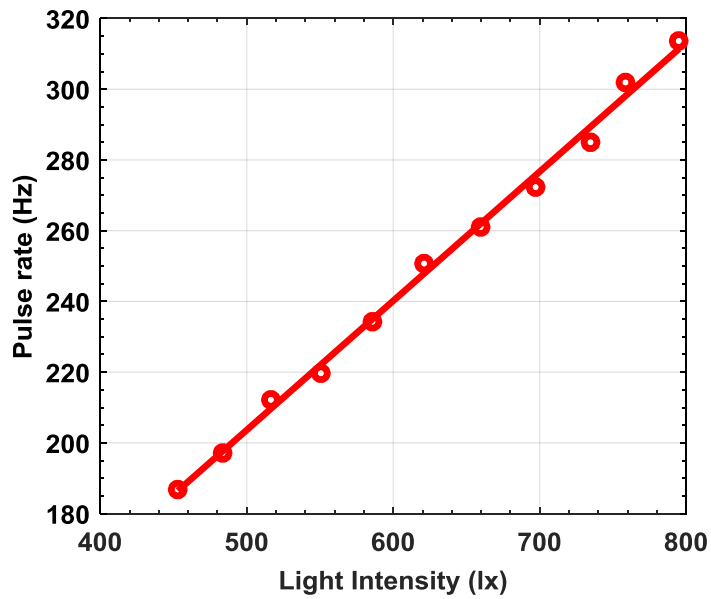

Channel distribution

Figure 3-8 Test result of the 9-channel retinal prosthetic IC (the voltage of the photodiode plus node, biphasic current pulse of the center pixel (CH5))

(a)

(b)

Figure 3-9 (a) Pulsatile output and (b) Pulse rate of the photosensor in response to light intensity

pads and the integrated digital controller that can not change the digital logic, various tests could not be conducted using this chip. Thus each block test were performed using the second IC. The sensitivity of the photosensor and contrast changing was measured with the second IC. Figure 3-9 shows the pulse output and pulse rate of the photosensor. A representative pulse has the pulse rate of 125 Hz (period of 8 ms) and the pulse duration of 200 ns. The image processor consumed power during pulse generation of 200 ns. The pulse rate of the photosensor linearly increased as the light intensity increased. Pulse shape was triangle due to the capacitance of the output capacitor of the photosensor.

Biphasic current level by the change of the current ratio between the light intensity of the center pixel (L_{center})and those of the surrounding pixels ($L_{surround}$) are shown in Figure 3-10. When the light intensity ratio (L_{center} / $L_{surround}$) was 0.55, current level started to increase and was saturated at the light intensity ratio of 1.2. The

Table 3-3Summary of the chip performance

Process	0.18 μm CMOS process
Stimulation strategy	Monopolar simultaneous biphasic current stimulation
Supply voltage	V_{DD} = 1.65 V V_{SS} = -1.65 V
threshold ($L_{center}/L_{surround}$) Saturation ($L_{center}/L_{surround}$)	0.55 1.2
Stimulus current level	0-400 μA
Unit pixel area	0.0072 mm^2
Power consumption (in the resting state)	224 μW per channel (Schmitt trigger) 0.5 μW per channel (image processor, pulse rate 300 Hz, charge amount per pulse: 0.34 nC)
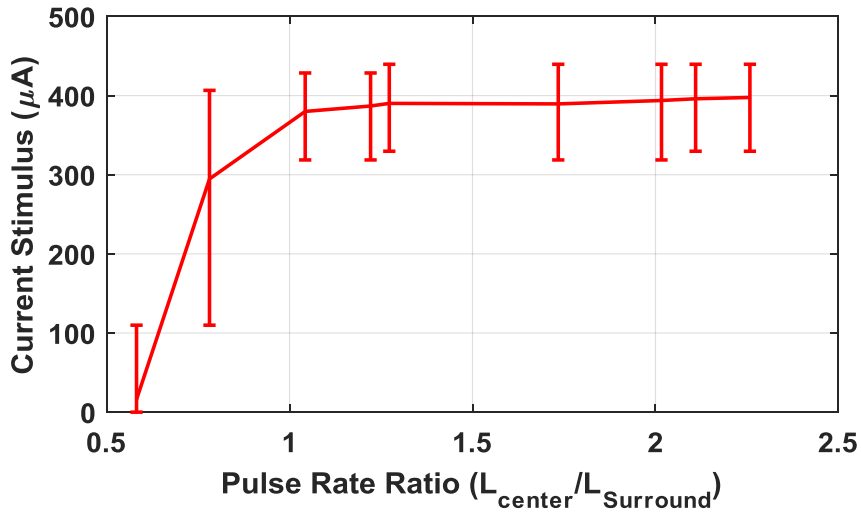
Figure 3-10 Current level of the BCG in response to current ratio (I_{center} / $I_{surround}$)

maximum average current level was 400 μA. One light intensity ratio had multiple current levels in the measurement. This result was due to the output voltage range of the image processor. The image processor has two switches where one is for charging voltage, and the other is for discharging voltage. The pulsatile trains of the photosensors control these switches. Thus output voltage decreases and increase repeatedly, which generates the range of the output voltage. As holding time is different, the output voltage is different by the holding time despite the same L_{center} / $L_{surround}$.

Power consumption per channel was 238 μW, and the most power was consumed in Schmitt trigger, and image processor consumed low power of 0.5 μW. The Schmitt triggers with lower power consumption of up to 50 nW were reported in [65], [66]. Next version should use these low power Schmitt triggers for low-power

75
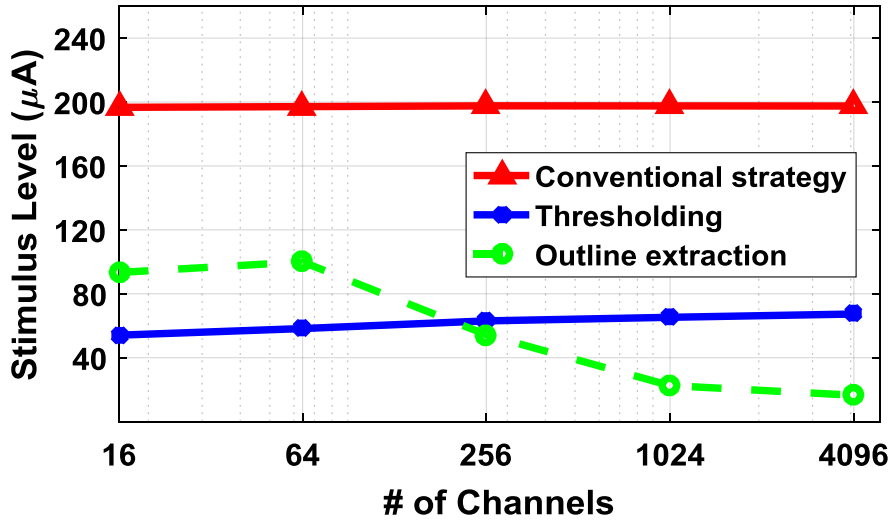
Figure 3-11 Average stimulus power along the number of channels

consumption in the resting state. Chip performance was summarized in Table 3-3.

3.3. Average Stimulus Power Estimation

Average stimulus power in 1024 channels and minimum necessary channels to recognize the images are listed in Table 3-4. Average stimulus levels of the thresholding strategy and outline stimulation strategy need 33 % and 12 % stimulus levels, respectively, of conventional photodiode-based retinal prosthetic strategy. Minimum necessary channels using conventional strategy and thresholding strategy were 60 and 70, respectively, which is similar. Outline strategy needs more channels of 150 than those of other strategies. Figure 3-11 shows the average stimulus of conventional and proposed stimulation strategies along the number of the channels. There were little changes of average stimulus levels in conventional

76

and thresholding strategies. On the other hands, outline extraction strategy decreases the average stimulus level as the number of channels increases.

In the 256 channels, average stimulus level of the outline extraction is the same as that of the thresholding strategy, which means that outline extraction is the most efficient solution among three strategies in above 256 channels.

Table 3-4 Average stimulus level and minimum channels to recognize

Input Image	Minimum Channels to Recognize			Stimulus Level of 1024 channels (μA)		
	Conventional	Thresholding	Outline	Conventional	Thresholding	Outline
A	64	208	64	197.2	65.1	20.4
B	64	64	112	182.9	55.8	26.4
C	16	28	208	200.3	66.6	25.0
D	52	160	64	191.1	60.8	21.9
E	52	64	352	192.3	64.1	23.7
F	52	64	160	206.9	68.9	14.0
G	52	40	160	186.8	59.1	28.3
H	64	64	340	194.8	62.6	20.0
I	16	64	208	228.0	83.5	8.9
J	52	64	64	216.6	76.0	15.1
K	52	112	160	193.6	63.0	27.3
L	16	28	64	217.3	77.2	13.8
M	64	64	112	168.5	49.3	33.4
N	112	64	112	187.9	60.2	26.9
O	16	40	112	189.7	61.0	27.0
P	40	64	64	201.1	67.5	19.8
Q	40	112	160	185.1	59.0	29.8
R	64	112	160	189.4	59.7	23.1
S	208	64	64	193.2	62.4	29.1
T	16	64	112	213.6	73.8	12.7
U	64	112	160	195.6	64.2	21.1
V	160	112	160	207.7	70.2	17.9
W	64	64	352	172.0	52	32.7
X	64	64	112	200.4	66.6	29.8
Y	64	64	64	212.6	73.3	20.4
Z	40	52	208	198.3	65.8	23.6
Average	60±43	77±40	150±87	197.0±13.7	64.9±7.7	22.8±6.4

3.4. Virtual Channels

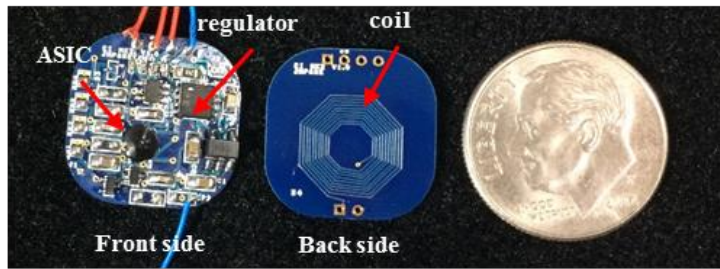### 3.4.1. Fabricated IC

Designed current stimulator IC was fabricated using 0.18 μm BCDMOS process as shown in Figure 3-12 (a). The total area was 0.3 mm², and minimum length was 500 μm which is compatible with the commercial DBS electrode diameter (1.27
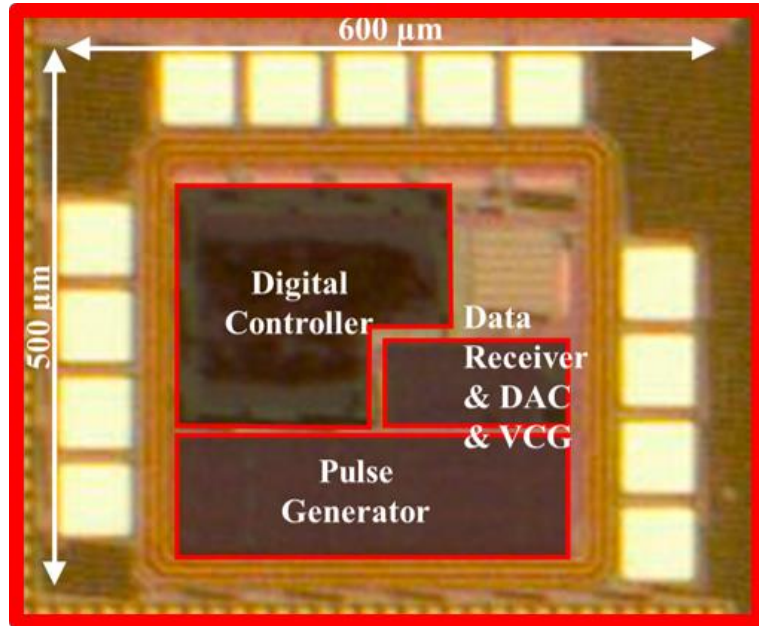
(a)

(b)

Figure 3-12 (a) Microphotograph of the fabricated current stimulator IC (b) Photograph of the prototype for the bench-top test
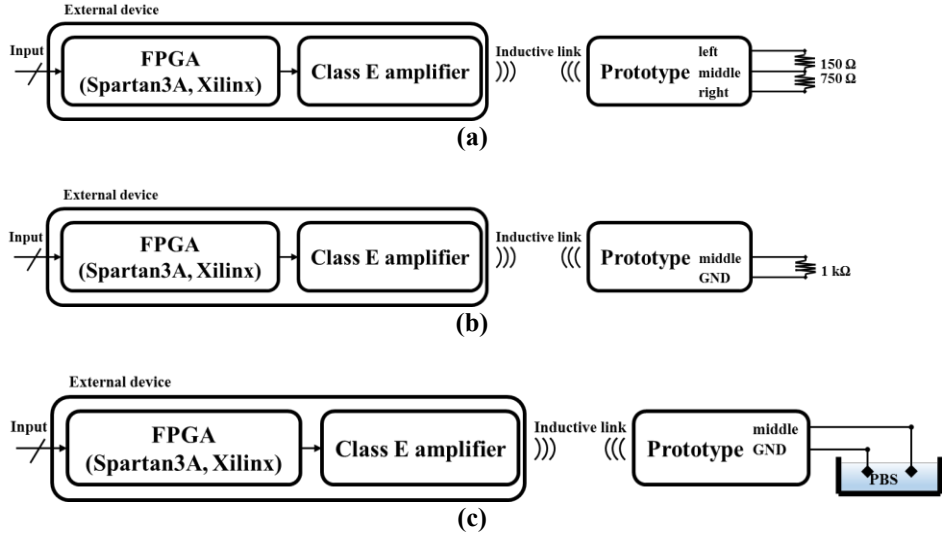
Figure 3-13 Bench-top test setup: (a) while virtual channel mode is active, (b) while virtual channel mode is inactive, and (c) while output is located in PBS solution

mm, DBS Lead Model 3387, Medtronic, USA) [67]. Figure 3-12 (b) shows the fabricated prototype for the bench-top test using the current stimulator IC. The power management module (TPS77118, Texas Instruments, USA) and the inductive link composed of the PCB coil and the passive components were assembled on PCB within the diameter of 15 mm.

3.4.2. Test Setup

The bench-top test was conducted to validate the IC performance as shown in Figure 3-13. An external device was composed of an FPGA (Spartan3A, Xilinx, USA) and a Class-E amplifier to transmit power and data through inductive link modified by [54]. Figure 3-13 (a) shows a block diagram of the virtual channel mode test that left and middle are connected by resistors of 150 Ω and middle and

80

Table 3-5 Summary of the chip performance

Description	Value
Technology	0.18 um BCDMOS (3 Metal)
Area	0.3 mm^2
Number of Channels	1 (Virtual channel: 8), Expandable up to 16 (Virtual channel: 108)
Supply voltage	V_{DD} = 1.8 V, V_{DDH} = 5 V
Current mode	Polarity: Monopolar, bipolar, Phase: Monophasic, biphasic
Current level scale	98 – 3227 μA
Duration	6.4 – 204.8 μs (32 steps)
Supply Current (resting state)	34 μA (V_{DD}), 117 μA (V_{DDH})

right are connected by a resistor of 750 Ω to verify current level ratio regardless of output impedance. If the virtual mode is inactive, one resistor was connected between the middle node and the GND as shown in Figure 3-13 (b), and phosphate buffered saline (PBS) solution was used to measure the effect of biological environment, as shown in Figure 3-13 (c).
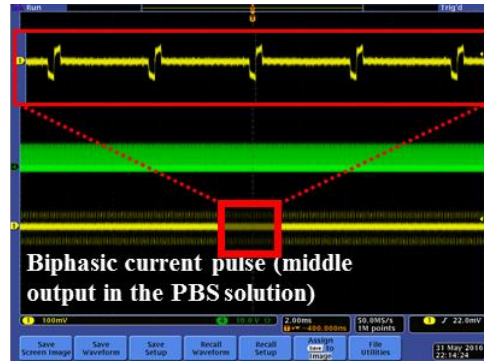
3.4.3. Test Results

Figure 3-14 shows the bench-top test result. We measured received data voltage and left, middle, and right output voltage using an oscilloscope (DPO 4034, Tektronix, USA). In Figure 3-14 (a), voltage of the received data of 0 to 5 V and biphasic current pulse were measured. Balanced charge delivery was confirmed in

PBS solution, as shown in Figure 3-14 (b). Changing Level [5:0], the output current of the middle pulse generator when virtual channel mode was off was measured from 98 to 3227 μA as shown in Figure 3-14 (c). The measured currents of the left pulse generator and the right pulse generator were presented in Figure 3-14 (d), changing Virtual CH [2:0]. Thus the stimulator IC can control current level despite the change of pulse generator output impedance. IC performance of stimulator IC is summarized in Table 3-5.
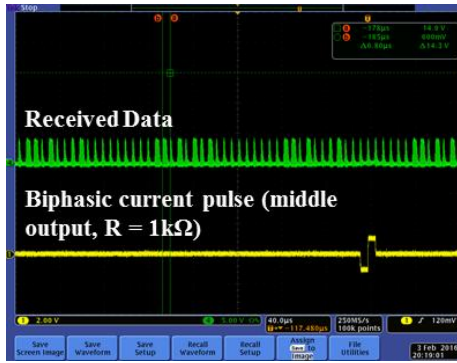
(a)

(b)
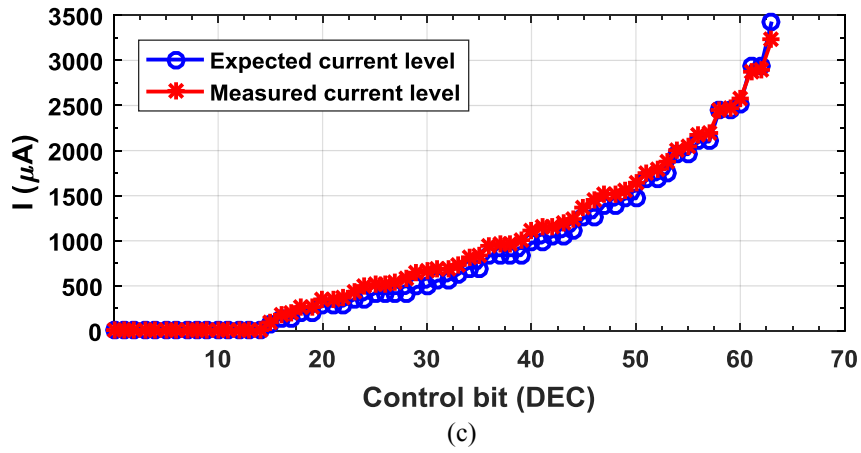
(c)

(d)

Figure 3-14 Ben-top test result: Oscilloscope waveform of (a) received data and middle output of prototype (virtual channel mode is inactive) and (b) received data and middle output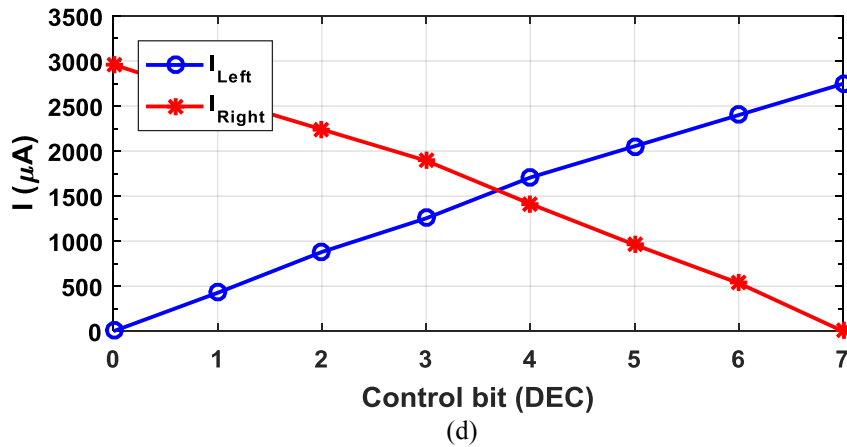 in the PBS solution (virtual channel mode is inactive) (c) Current level vs. control bit (Level [5:0]) while virtual mode is inactive (d) Current level vs. control bit (Virtual CH [2:0]) while virtual channel mode is active

3.4.4. Two-dimensional Virtual Channel Generator– Test setup and Its Result

Figure 3-15 shows the test setup of the two-dimensional virtual channel generator. Digital controller was fabricated using FPGA to be integrated into ASIC in the future. Command language of the FPGA is HDL that is easily converted into the digital logic of the IC. Digital logic has two conditions: PWM data setting and PWM data generating. As the simultaneous generation of the PWM data is needed,
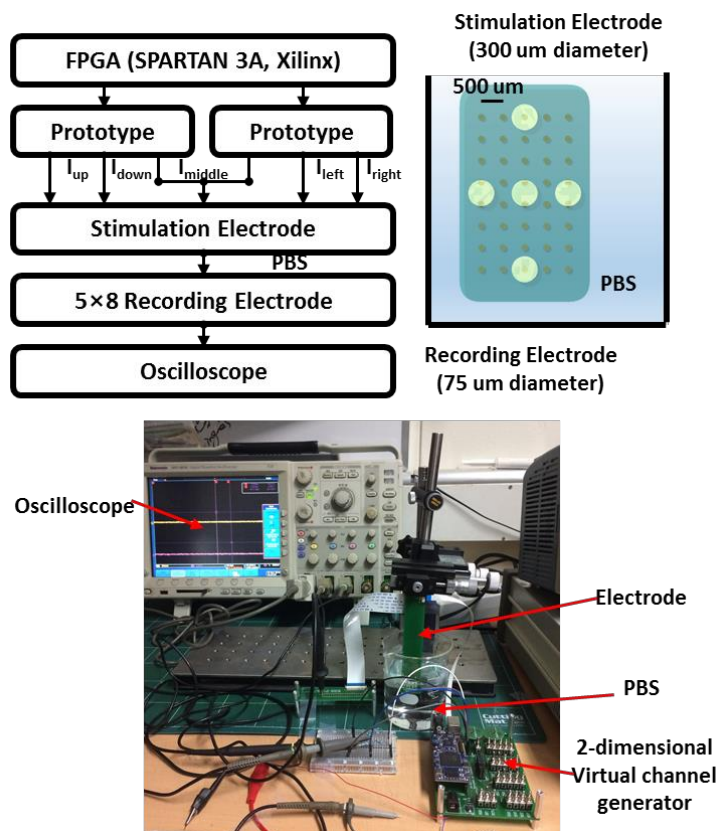

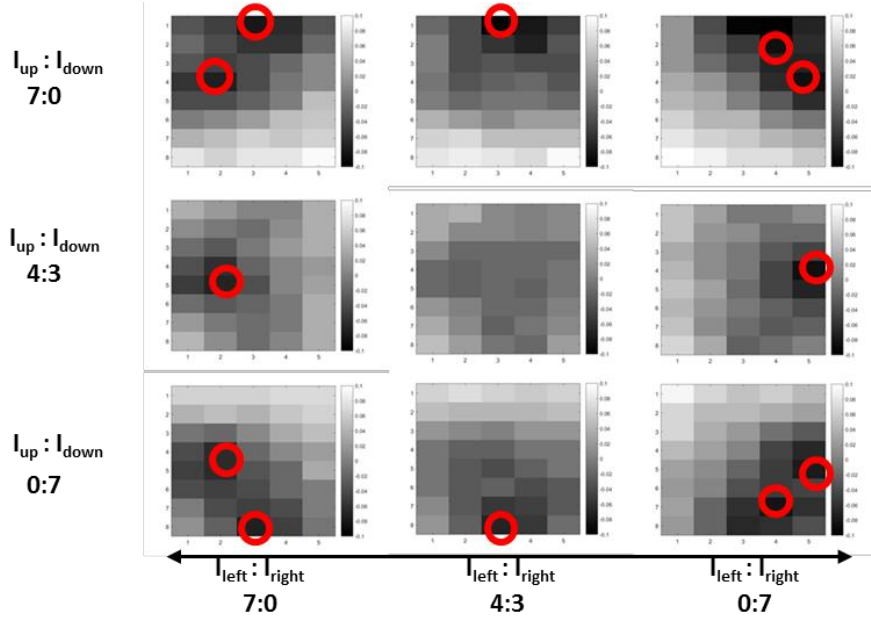Figure 3-15 Test setup of the two-dimensional virtual channel generator

Figure 3-16 Test result of the two-dimensional virtual channel generator

we set the two control parameters of the IC's before generating the PWM data.

To measure the virtual stimulus, the current level that was generated by each channel, was measured with the resistor network. And then, stimulator electrode made by PCB is used. The stimulator electrode includes geometrically distributed five channels (Left, Right, Middle, Up, Down) with a diameter of 300 μm. The electrode delivers the stimulus to PBS solution that is similar to biological environments. And then, the electrical field distribution was measured using a recording electrode made by PCB. A recording electrode has 5×8 channels with a diameter of 75 μm. The distance between stimulating electrode and recording electrode was also changed from 100 μm to 300 μm with 100 μm step.

Figure 3-16 show the test result of the two-dimensional virtual generator. The digital controller adjusts the current ratios of each stimulator IC linearly. As the

current levels of the two IC's (I_{left}, I_{right}, I_{up}, I_{down}) was changed, the high electrical

field was also changed as expected.

3.5. Polymer Packaging

3.5.1. Light Transmittance according to LCP Thickness

The calculated absorption coefficient of LCP film decreased with increasing wavelength within a range of 280 - 2500 cm^{-1} for visible light and infrared (400 – 1200 nm) as shown in Figure 3-17 (a). Figure 3-17 (b) shows a minimum thickness of LCP films to guarantee the transmittance of 10 % and 20 %, respectively. For example, at the wavelength of green, minimum LCP thickness line to guarantee the transmittance of 10 % and 20 % was 10.6 μm and 7.4 μm, respectively. The maximum root mean squared error (RSME) of the fitted values using absorption coefficient and measured values was 0.29 %.

It could be found that the LCP films thinner than 10.6 μm are required to achieve a minimum light transmittance of 10 % excluding scattered light. In the condition of adding scattered light, the film thickness can be thicker, and spatial resolution should be considered in this situation. Conventional MPDA based retinal prosthesis can be used in the broad range of incident light illuminance (0.01 – 100000 lx) by adjusting threshold and calibrating dynamic range [22].

Considering the normal illuminance of ~100 lx in room lighting and ~20000 lx in daylight, 10 % of transmittance is required to operate MPDA-based retinal
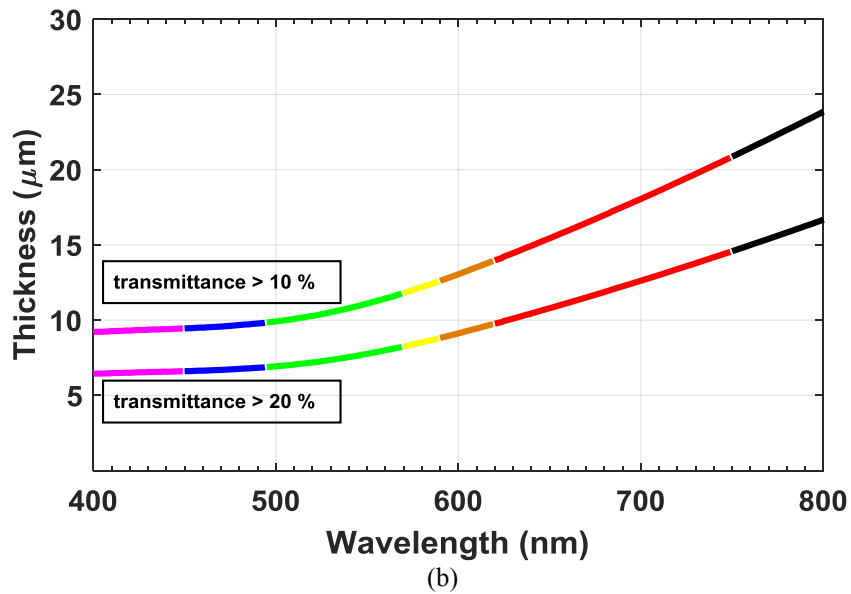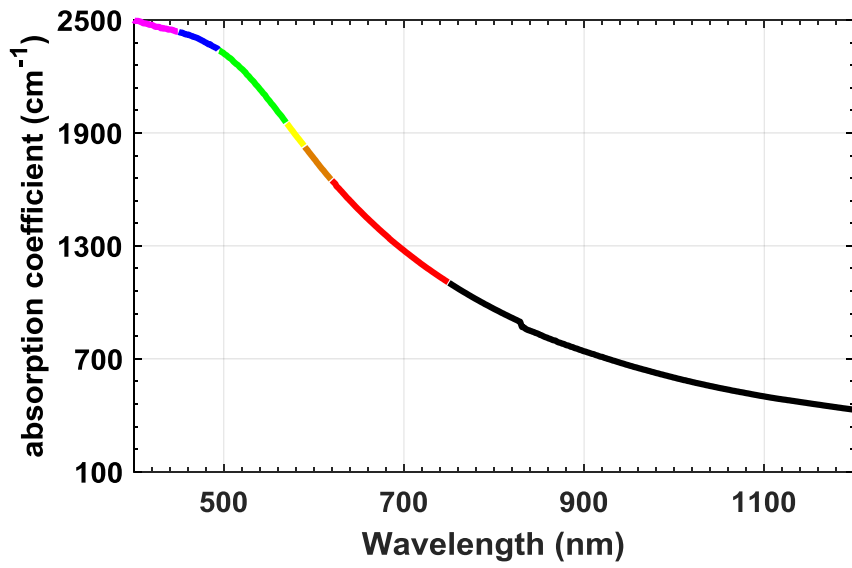
Figure 3-17 (a) The calculated absorption coefficient of LCP film decreased with increasing wavelength within a range of 280 - 2500 cm^{-1} for visible light and infrared (400 – 1200 nm) (b) Minimum thickness of LCP films to guarantee the transmittance of 10 % and 20 %,

Table 3-6 Thickness of plasma etched LCP films

Etching time (min.)	40	45	50	55
Thickness (μm)	8.28	5.51	2.39	1.51
Standard deviation (μm)	0.81	0.18	0.4	0.33

prosthesis with 1 % light resolution in room lighting. Thus 10 % of transmittance is expected to be a tolerable value for the photodiode-based retinal prosthesis.

3.5.2. Thickness Control of LCP

The thickness of the etched film was measured by scanning electron microscope (SEM) as shown in Figure 3-18 and summarized in Table 3-6. Longer etching time resulted in thinner film thickness, but at the same time, more uneven film surface. Furthermore, the dry etched LCP films thinner than 5 μm were prone to be torn. Considering easy handling and minimum light transmittance of 10 % for the optical window, we chose the etching time of 40 minutes.

3.5.3. Spatial Resolution of LCP

In Figure 3-19 (a), black and white stripes captured by the CMOS image sensor covered with LCP films of various thicknesses are compared with the image from the sensor without a cover layer, as represented by light intensities of pixels along
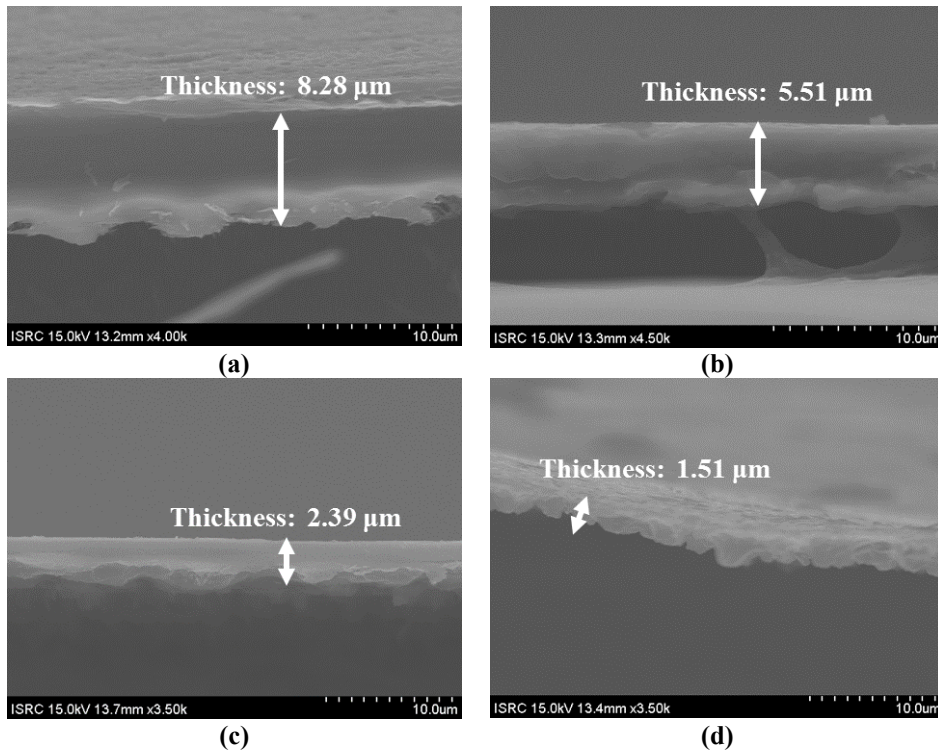
Figure 3-18 Cross-sectional SEM images of etched LCP films with varying etching time: (a) 40 min., (b) 45 min., (c) 50 min., and (d) 55 min

the horizontal direction. The LCP encapsulation of the image sensor degrades the image contrast as a result of light scattering. Thinned LCP film (8.28 μm-thick) could provide higher contrast than that of the original LCP film (25 μm-thick). For quantitative analysis, MTF was evaluated as shown in Figure 3-19 (b). Minimum distinguishable pitches of the original LCP film and the thinned LCP film were 239 μm and 90 μm, respectively. From those results, thinned LCP film based light window could apply to, ideally, 1200-channel MPDA chip in the macular area of 10 mm^2.

(a) **(b)**
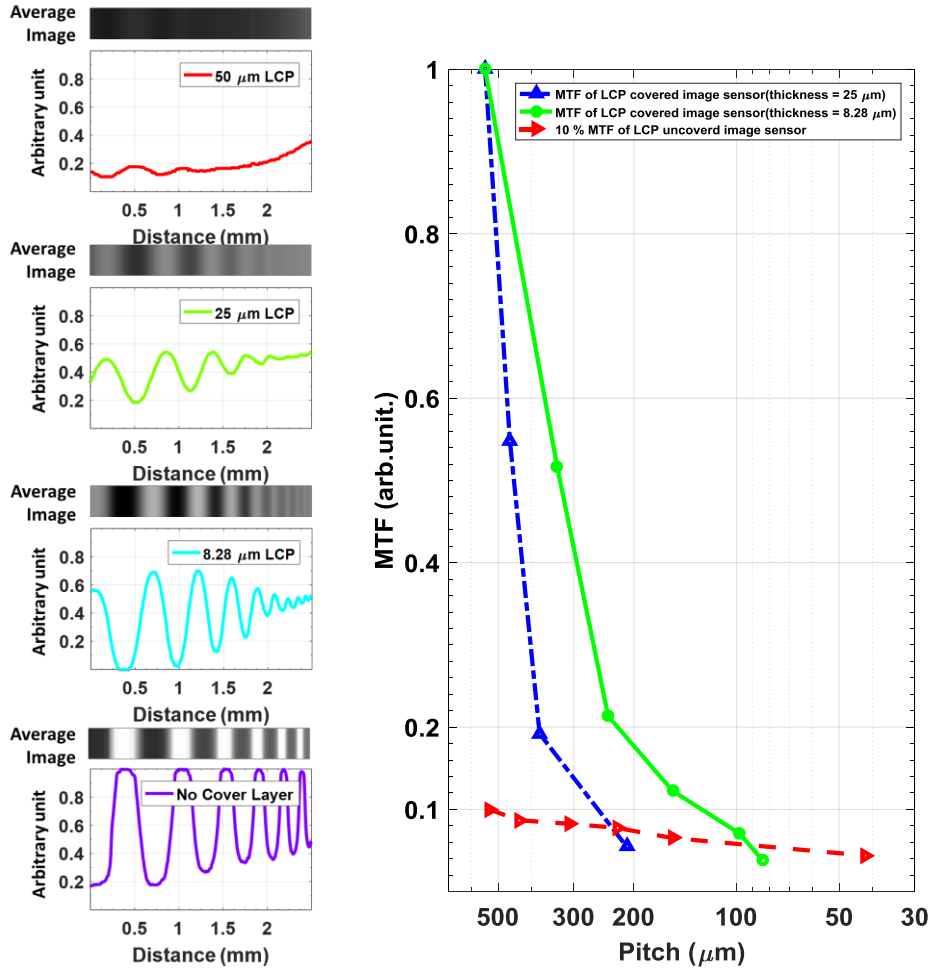
Figure 3-19 (a) Black and white stripe image and relative light intensity of stripe along horizontal direction captured by an image sensor covered by commercial LCP (thickness of 50 μm, 25 μm), thinned LCP (thickness of 8.28 μm), and uncovered (b) MTFs from the LCP (thickness of 25 μm, 8.28 μm) covered images and an uncovered image with a threshold line represented by 10 % of MTF of the uncovered image (intersections at 90 μm for 8.28 μm-thick LCP and at 239 μm for 25 μm-thick LCP films).

Chapter 4: Discussion

In this chapter, we discuss the pitting parameter ($I_{center}/I_{surround}$) change in outline extraction, and the relationship between minimum distinguishable channels and average stimulus power. Also, the effect of current spread was discussed for visual acuity. Hermeticity of the thinned LCP was dealt with in this chapter.

4.1. Average Stimulus Power

The fitting parameter of the generated stimulus patterns using outline extraction is crucial. We used fitting parameters from the simulation result of the stimulus power estimation. As the fitting parameters from simulation result and measurement result are different, we tested that the light intensity ratio threshold (L_{center} / $L_{surround}$) is changed from 1 to 0.55 to know the effect of pitting parameter change. The result shows
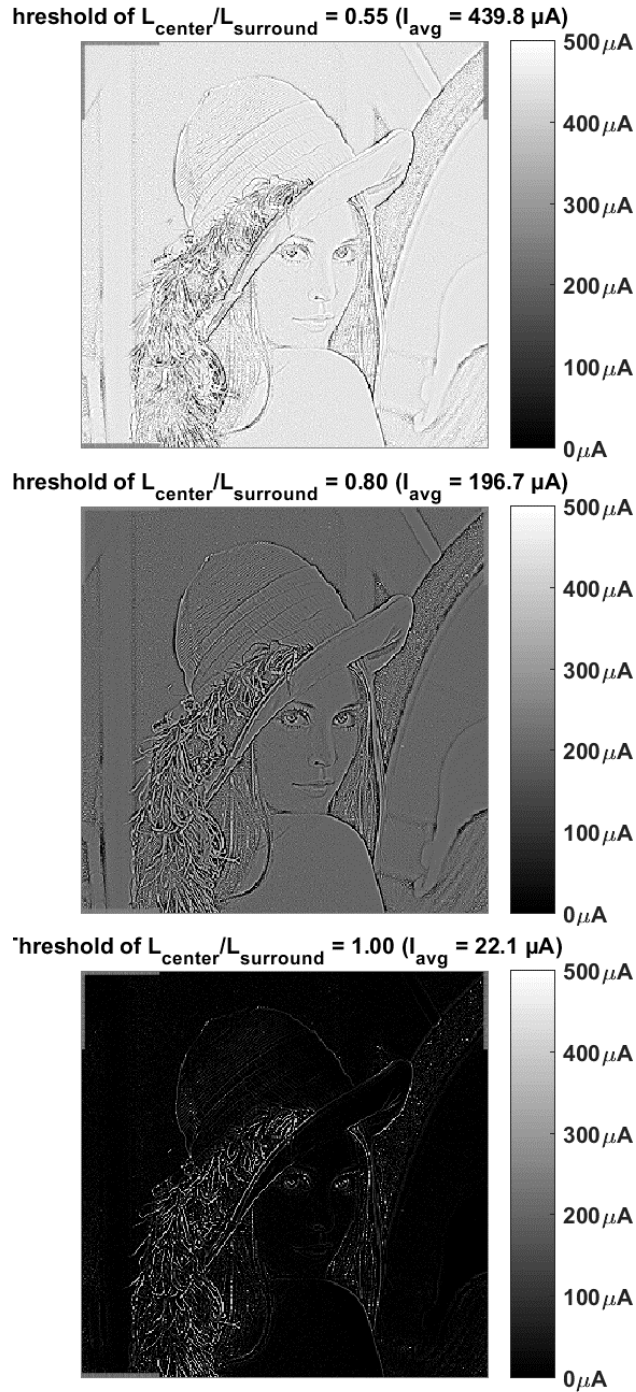
Figure 4-1 Stimulus patterns of outline extraction varying threshold of $L_{center}/L_{surround}$ (4096 channels)

that it takes more power consumption as the decrease of the light intensity ratio (L-center / $L_{surround}$) threshold, as shown in Figure 4-1. This result demonstrated that L-center / $L_{surround}$ should be above 1 to reduce power with generation of stimulus including sufficient visual information. Tuning circuits such as binary weight current source with switches for varying ratio (W/L) can be one of the solutions to change L_{center} / $L_{surround}$.

Minimum distinguishable channels of conventional, thresholding, and outline extraction were 64, 64, 256, respectively. The average stimulus powers of conventional, thresholding, and outline extraction were 197.1 μA, 58.2 μA, 54.4 μA, respectively. Hence, if we operate with the minimum distinguishable channels, the thresholding strategy was the best option in case of recognition of the letters. However, face recognition and other images need more channels, which means that the number of channels needs more than that used to reading letters.

Our preliminary tests show that the proposed strategy reduces stimulus power as an increase of the number of channels. With the modification for low power consumption in the resting state, we can achieve the low-power and high-resolution photodiode-based retinal prosthetic IC. The delicate question investigation to recognize the face and other images should be conducted.
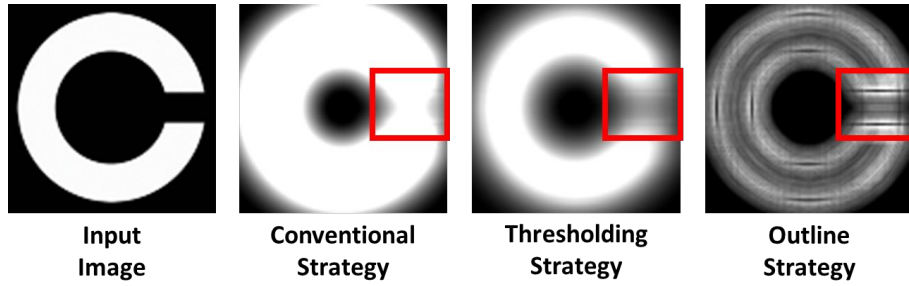
Figure 4-2 The expected Landolt-C images that patients will perceive using thresholding and outline extraction as increasing current crosstalk.

4.2. Visual Acuity

The first thing to consider is the current spread. Excessive current stimulus can cause the large phosphene that the makes the image distorted. There was a report that phosphene size that patients decrease as the stimulus level decrease [68]. Based on this physiological result, we generate the distorted image patterns of the thresholding and outline extraction by increasing current stimulus level, as shown in Figure 4-2. As the current spread increases, Landolt-C that is distorted by an excessive current stimulus can not be recognized. Thus thresholding and outline extraction can help reduce the inter-channel crosstalk which otherwise prohibits achieving desired spatial resolution in the retinal stimulation as well as reducing stimulus power.
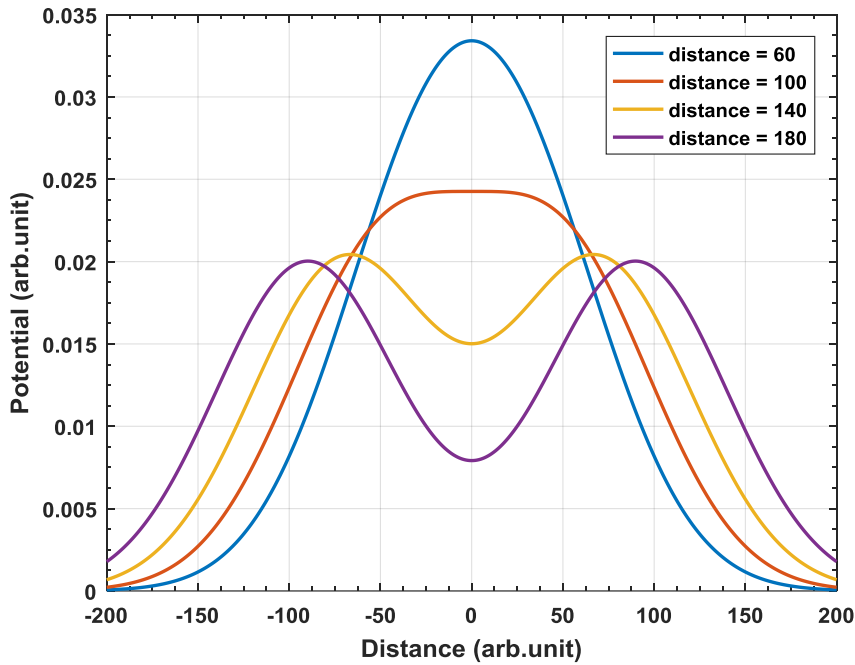
Figure 4-3 Expected steered potential along the distance between two stimulation electrodes

The second one is pulse duration. Recent retinal experiments verified that long duration over 25 ms improves visual acuity of 20 / 312 [69]. If we use stimulus with long duration of 25 ms, there is no option but to use simultaneous stimulation. The BCG, which was used in thresholding, outline extraction, and the two-dimensional virtual channel, is dual independent current supply structure to activate all pixels simultaneously.

The last one is the two-dimensional virtual channels. In the PBS test, some virtual channels generated two potential peaks. This resut was due to the long distance between stimulation electrodes. Figure 4-3 is the expected steered potentials along the different distance between two stimulation electrodes. Thre result shows that

potential from the middle point of distance between two stimulation electrode should be a half of the potential from the center of one stimulation electrodes. Electrode materials are also important. As we use gold electrode, most electrical fields existed in the metal-electrolyte interface due to the double layer capacitance. Thus the electrode material would be changed into other materials with faradaic reaction. In the future, the theoretical analysis and the measurement of the electrical field distribution along the distance between the electrode and the target should be conducted.

4.3. Hermeticity of the Thinned LCP Film

The effect of thinned LCP film upon reliability of the encapsulation could be estimated from the approximated inversely proportional relationship of the barrier thickness and helium diffusion leak rate (R) as

$$R = K \cdot A \cdot \Delta P / d , \qquad (16)$$

where K is the permeability, A is the surface area, ΔP is the pressure difference, and d is the barrier thickness [70], the typical values of which are listed in Table II as referred from [71]. The calculated leak rate of thinned LCP optical window is 1.12×10^{-8} atm· cm^2/s, that is smaller than the failure criteria (5×10^{-8} atm· cm^2/s) described by the method 1014, MIL-STD-883 [71]. In a previous study on

accelerated soak test [40], [72], LCP encapsulation failed after 378 days in 75 ˚C saline as a result of water penetration through thermally bonded LCP-LCP interface, rather than water permeation through LCP film surface. While water penetration through LCP surface is governed by intrinsic permeability and barrier thickness of LCP, water leakage through adhesive interface depends on the integrity of LCP-LCP bonding which depends on various fabrication factors that can be further improved by process optimization for creating stronger interlayer adhesion [72].

As the water leakage through adhesive bonding seems more likely to be the limiting factor than the permeation through LCP surfaces, it is expected the reliability of the 8 μm-thick LCP encapsulation could be at least as good as the previous result with 25 μm -thick encapsulation. Nevertheless, the reliability of the 8 μm-thick LCP encapsulation should be experimentally verified.

Chapter 5: Conclusion and Future Directions

A novel photodiode-based retinal implant IC was fabricated with thresholding stimulation strategy and tunable light intensity threshold for the various light environments. The prototype of retinal implant IC was fabricated with an area of 0.021 mm^2 per unit pixel which can expand up to 470 channels in the macular area of 10 mm^2. Biphasic current pulse ranging from 0 μA to 354 μA was measured with the light intensity threshold from 400 lx to 13120 lx. Power consumption was W733 μW per channel in the resting state, and activation of VCCS only when generating the biphasic current pulse should be adopted in the next generation.

Two prototypes of photodiode-based retinal prosthetic IC's using outline extraction that leads to low power consumption and minimization of current spread were fabricated. The fabricated chips were verified by simulation, then partially confirmed by measurement. The first version manufactured by TowerJazz 0.18 μm

BCDMOS process can integrate 200 pixels with an area of 0.5 mm^2 into the macular area of 10 mm^2. The second one fabricated by Magna 0.18 μm CMOS process can integrate more than 1300 pixels with an area of 0.0072 mm^2 into the macular area. Power consumption was 238 μW per channel in the resting state, and most of the powers was consumed in the Schmitt trigger. Also, $L_{center}/L_{surround}$ was 0.55 that leads to consuming more stimulus power. For those reasons, low-power Schmitt trigger in [65], [66] and tuning circuits such as binary weight current source with switches should be integrated into the next version.

Two-dimensional virtual channels were explored using fabricated current stimulator IC for the high-resolution retinal prosthesis. The simplified VCG using current steering can make more stimulation channel and simple internal digital controller, compensating for deficient channel due to the chip area. Two-dimensional virtual channel scheme was designed and 64 virtual channels were designed using 4 physical electrodes. The measurement of the 9 virtual channels in PBS solution shows its feasibility. A delicate theorem and FEM simulation should be conducted more precise virtual channel formation.

The feasibility of LCP film as an encapsulation material of photodiode-based retinal prosthesis was explored. The transmittance measurement indicated that LCP film should be thinner than 10.6 μm to guarantee 10 % of light transmittance, which was achieved by applying oxygen dry etching to thin the commercially available 25 μm-thick film down to 8.28 μm thickness. The minimum

distinguishable line pitch that can be attained from an image sensor covered by the thinned LCP layer was 90 μm, which is equivalent to ideally 1200-channels in the macular area of 10 mm^2. Based on these results on feasibility test, future works for process optimization and reliability tests are ongoing. Table 5-1 summarize the comparison between previous work and this dissertation, and modification in next generation.

All the technologies and design were fabricated and verified separately. For this reason, integration with proposed photodiode-based retinal prosthesis IC with LCP encapsulation for the high-resolution retinal prosthesis and animal experiments remain for the future work.

Table 5-1 Comparison between previous work and this work, and future work

1. Stimulation strategy

Parameter	Conventional strategy	Proposed strategies (This work)	
	(Light intensity)	**Thresholding**	**Outline Extraction**
Average Stimulus level (Alphabet Image, 1024 channels)	197.6 µA Minimum 100 µA[28]	**65.27 µA**	**22.54 µA**
channel area	0.0051 mm^{2}[22] (1500 channels)	0.021 mm^2 (470 channels)	**0.0072 mm^2 (1300 channels)**
Power consumption per channel	1 µW [73]	733 µW (VCCS, BCG)	238 µW (Schmitt trigger) **0.3 µW (Image processor)**
Future work (modification)		Selectively activation of VCCS BCG (21.99 µW)	Low power Schmitt trigger [65], [66] (50 nW)

2. Packaging materials

Device	E. Zrenner et al.	D. Palanker et al.	Borton et al.	**This work**
Package Material	polyimide	SU-8	Metal & sapphire	**LCP**
Advantage	Flexible, thin High transparency	Flexible, thin High transparency	Hermetic High transparency	**Flexible, thin, Low water absorption (< 0.04)**
Disadvantage	High water absorption 2.8 (%)	High water absorption 0.65 (%)	Rigid, bulky (> 1mm)	**Minimum thickness (transmittance of visible light > 10 %): 10.6 µm** **8.28 µm film film fabrication using O$_2$ DRIE** **Minimum pitch :90 µm (1200 channels)**

References

[1]   D. K. Kessler, G. E. Loeb, and M. J. Barker, "Distribution of speech

       recognition results with the Clarion cochlear prosthesis," *Ann Otol Rhinol

       Laryngol*, vol. 104, no. Suppl 166, pp. 283–285, 1995.

[2]   B. S. Wilson and M. F. Dorman, "The surprising performance of present-

       day cochlear implants," *IEEE Trans. Biomed. Eng.*, vol. 54, no. 6, pp. 969–

       972, 2007.

[3]   B. S. Wilson, C. C. Finley, D. T. Lawson, R. D. Wolford, D. K. Eddington,

       and W. M. Rabinowitz, "Better speech recognition with cochlear implants,"

       Nature, vol. 352, no. 6332, pp. 236–238, 1991.

[4]   F.-G. Zeng, "Trends in cochlear implants," *Trends Amplif.*, vol. 8, no. 1, pp.

       1–34, 2004.

[5]   F. G. Zeng, S. Rebscher, W. Harrison, X. Sun, and H. Feng, "Cochlear

       implants: system design, integration, and evaluation.," *IEEE Rev. Biomed.

       Eng.*, vol. 1, no. dc, pp. 115–142, 2008.

[6]   M. D. Johnson, S. Miocinovic, C. C. McIntyre, and J. L. Vitek,

       "Mechanisms and targets of deep brain stimulation in movement disorders,"

       Neurotherapeutics, vol. 5, no. 2, pp. 294–308, 2008.

[7]   S. I. Park, J. H. Oh, Y. S. Hwang, S. J. Kim, and J. W. Chang, "Electrical

       stimulation of the anterior cingulate cortex in a rat neuropathic pain model,"

       in *Advances in Functional and Reparative Neurosurgery*, Springer, 2006,

       pp. 65–71.

[8]   V. Voon, C. Kubu, P. Krack, J. Houeto, and A. I. Tröster, "Deep brain

stimulation: neuropsychological and neuropsychiatric issues," *Mov. Disord.*, vol. 21, no. S14, pp. S305–S327, 2006.

[9]   B. Linderoth and R. D. Foreman, "Physiology of spinal cord stimulation: review and update," *Neuromodulation Technol. Neural Interface*, vol. 2, no. 3, pp. 150–164, 1999.

[10]   T. Cameron, "Safety and efficacy of spinal cord stimulation for the treatment of chronic pain: a 20-year literature review," *J. Neurosurg. Spine*, vol. 100, no. 3, pp. 254–267, 2004.

[11]   M. Haim, "The epidemiology of retinitis pigmentosa in Denmark," *Acta Ophthalmol. Scand.*, vol. 80, no. s233, pp. 1–34, 2002.

[12]   W. Smith *et al.*, "Risk factors for age-related macular degeneration: pooled findings from three continents," *Ophthalmology*, vol. 108, no. 4, pp. 697–704, 2001.

[13]   Y. H. L. Luo and L. Da Cruz, "A review and update on the current status of retinal prostheses (bionic eye)," *Br. Med. Bull.*, vol. 109, no. 1, pp. 31–44, Feb. 2014.

[14]   T. T. Kien, T. Maul, and A. Bargiela, "A review of retinal prosthesis approaches," *Int. J. Mod. Phys. Conf. Ser.*, vol. 9, pp. 209–231, 2012.

[15]   E. Zrenner, "Fighting blindness with microelectronics.," *Sci. Transl. Med.*, vol. 5, no. 210, p. 210ps16, Mar. 2013.

[16]   J. D. Weiland and M. S. Humayun, "Retinal prosthesis," *IEEE Trans. Biomed. Eng.*, vol. 61, no. 5, pp. 1412–1424, Aug. 2014.

[17]   M. S. Humayun *et al.*, "Interim results from the international trial of second sight's visual prosthesis," *Ophthalmology*, vol. 119, no. 4, pp. 779–788, Apr.

2012.

[18]   Y. H. L. Luo and L. da Cruz, "The Argus® II Retinal Prosthesis System,"
       Prog. Retin. Eye Res., vol. 50, pp. 89–107, 2016.

[19]   D. D. Zhou, J. D. Dorn, and R. J. Greenberg, "The Argus® II retinal
       prosthesis system: An overview," *Electron. Proc. 2013 IEEE Int. Conf.
       Multimed. Expo Work. ICMEW 2013*, Jul. 2013.

[20]   T. Fujikado *et al.*, "Testing of semichronically implanted retinal prosthesis
       by suprachoroidal-transretinal stimulation in patients with retinitis
       pigmentosa," *Investig. Ophthalmol. Vis. Sci.*, vol. 52, no. 7, pp. 4726–4733,
       2011.

[21]   S. K. Kelly *et al.*, "Developments on the Boston 256-channel retinal
       implant," *Electron. Proc. 2013 IEEE Int. Conf. Multimed. Expo Work.
       ICMEW 2013*, pp. 7–12, 2013.

[22]   E. Zrenner *et al.*, "Subretinal electronic chips allow blind patients to read
       letters and combine them to words.," *Proc. Biol. Sci.*, vol. 278, no. 1711, pp.
       1489–97, 2011.

[23]   K. Stingl *et al.*, "Artificial vision with wirelessly powered subretinal
       electronic implant alpha-IMS.," *Proc. Biol. Sci.*, vol. 280, no. 1757, p.
       20130077, Feb. 2013.

[24]   K. Mathieson *et al.*, "Photovoltaic retinal prosthesis with high pixel
       density," *Nat. Photonics*, vol. 6, no. 6, pp. 391–397, 2012.

[25]   L. Wang *et al.*, "Photovoltaic retinal prosthesis: implant fabrication and
       performance," *J. Neural Eng.*, vol. 9, p. 46014, 2012.

[26]   E. V Bagshaw and M. H. Evans, "Measurement of current spread from

microelectrodes when stimulating within the nervous system.," *Exp. Brain Res.*, vol. 25, no. 4, pp. 391–400, 1976.

[27]   R. R. Harrison and C. Charles, "A low-power low-noise CMOS amplifier for neural recording applications," *IEEE J. Solid-State Circuits*, vol. 38, no. 6, pp. 958–965, 2003.

[28]   L. Theogarajan, "Strategies for restoring vision to the blind: Current and emerging technologies," *Neurosci. Lett.*, vol. 519, no. 2, pp. 129–133, 2012.

[29]   S. Kim, P. Tathireddy, R. A. Normann, and F. Solzbacher, "In vitro and in vivo study of temperature increases in the brain due to a neural implant," *2007 3rd Int. IEEE/EMBS Conf. Neural Eng.*, pp. 163–166, 2007.

[30]   G. J. Chader, J. Weiland, and M. S. Humayun, *Artificial vision: needs, functioning, and testing of a retinal electronic prosthesis*, vol. 175, no. 9. Elsevier, 2009.

[31]   M. N. Shivdasani *et al.*, "Factors affecting perceptual thresholds in a suprachoroidal retinal prosthesis," *Investig. Ophthalmol. Vis. Sci.*, vol. 55, no. 10, pp. 6467–6481, 2014.

[32]   K. Gosalia, J. Weiland, M. Humayun, and G. Lazzi, "Thermal elevation in the human eye and head due to the operation of a retinal prosthesis," *IEEE Trans. Biomed. Eng.*, vol. 51, no. 8, pp. 1469–1477, 2004.

[33]   G. Jiang and D. D. Zhou, "Technology Advances and Challenges in Hermetic Packaging for Implantable Medical Devices," in *Implantable Neural Prostheses 2: Techniques and Engineering Approaches*, D. Zhou and E. Greenbaum, Eds. New York, NY: Springer New York, 2010, pp. 27–61.

[34]   D. a Borton, M. Yin, J. Aceros, and A. Nurmikko, "An implantable wireless
        neural interface for recording cortical circuit dynamics in moving
        primates.," *J. Neural Eng.*, vol. 10, no. 2, p. 26010, 2013.

[35]   G. Jiang and D. D. Zhou, "Implantable Neural Prostheses 2: Techniques and
        Engineering Approaches," D. Zhou and E. Greenbaum, Eds. New York,
        NY: Springer New York, 2010, pp. 27–61.

[36]   J. B. Firszt, D. B. Koch, M. Downing, and L. Litvak, "Current Steering
        Creates Additional Pitch Percepts in Adult Cochlear Implant Recipients,"
        Otol. Neurotol., vol. 28, no. 5, pp. 629–636, 2007.

[37]   D. M. Landsberger and A. G. Srinivasan, "Virtual channel discrimination is
        improved by current focusing in cochlear implant recipients," *Hear. Res.*,
        vol. 254, no. 1–2, pp. 34–41, 2009.

[38]   S. F. Cogan, "Neural stimulation and recording electrodes.," *Annu. Rev.
        Biomed. Eng.*, vol. 10, pp. 275–309, 2008.

[39]   S. Shin *et al.*, "High Charge Storage Capacity Electrodeposited Iridium
        Oxide Film on Liquid Crystal Polymer-Based Neural Electrodes," *Sensors
        Mater.*, vol. 28, no. 3, pp. 243–260, 2016.

[40]   S. W. Lee, K. S. Min, J. Jeong, J. Kim, and S. J. Kim, "Monolithic
        encapsulation of implantable neuroprosthetic devices using liquid crystal
        polymers," *IEEE Trans. Biomed. Eng.*, vol. 58, no. 8, pp. 2255–2263, 2011.

[41]   J. Jeong, S. W. Lee, K. S. Min, S. Shin, S. B. Jun, and S. J. Kim, "Liquid
        crystal polymer (LCP), an attractive substrate for retinal implant," *Sensors
        Mater.*, vol. 24, no. 4, pp. 189–203, 2012.

[42]   C. Lee, A. Kiourti, and J. Volakis, "Miniaturized Fully-Passive Brain

Implant for Wireless Neuropotential Acquisition," *IEEE Antennas Wirel. Propag. Lett.*, vol. 1225, no. 1344825, pp. 1–1, 2016.

[43]   R. A. Dickie, S. S. Labana, R. S. Bauer, A. C. S. D. of Polymeric Materials: Science, and Engineering, *Cross-Linked Polymers: Chemistry, Properties, and Applications*, no. v. 367. American Chemical Society, 1988.

[44]   P. M. Figueiredo and J. C. Vital, "Kickback noise reduction techniques for CMOS latched comparators," *IEEE Trans. Circuits Syst. II Express Briefs*, vol. 53, no. 7, pp. 541–545, 2006.

[45]   M. Bigas, E. Cabruja, J. Forest, and J. Salvi, "Review of CMOS image sensors," *Microelectronics J.*, vol. 37, no. 5, pp. 433–451, 2006.

[46]   M. Ghovanloo and K. Najafi, "A compact large voltage-compliance high output-impedance programmable current source for implantable microstimulators," *IEEE Trans. Biomed. Eng.*, vol. 52, no. 1, pp. 97–105, 2005.

[47]   P. Jespers, *THE GM/ID METHODOLOGY, A SIZING TOOL FOR LOW-VOLTAGE ANALOG CMOS CIRCUITS*, 1st ed. Boston, MA, 2010.

[48]   K. Iniewski, *VLSI Circuits for Biomedical Applications*. 2007.

[49]   D. Purves *et al.*, *Neuroscience*, vol. 3. 2004.

[50]   R. Jain, R. Kasturi, and B. G. Schunck, *Machine vision*, vol. 5. McGraw-Hill New York, 1995.

[51]   Y. Leblebici, M. Ingenieur, and S. M. Kang, *CMOS Digital Integrated Circuits: Analysis and Design*. 2003.

[52]   Y. K. Lo, K. Chen, P. Gad, and W. Liu, "A fully-integrated high-compliance voltage SoC for epi-retinal and neural prostheses," *IEEE Trans.*

Biomed. Circuits Syst., vol. 7, no. 6, pp. 761–772, 2013.

[53]   V. Valente, A. Demosthenous, and R. Bayford, "A tripolar current-steering stimulator ASIC for field shaping in deep brain stimulation," *IEEE Trans. Biomed. Circuits Syst.*, vol. 6, no. 3, pp. 197–207, 2012.

[54]   S. K. An *et al.*, "Design for a simplified cochlear implant system," *IEEE Trans. Biomed. Eng.*, vol. 54, no. 6, pp. 973–982, 2007.

[55]   K. Chen, Z. Yang, L. Hoang, J. Weiland, M. Humayun, and W. Liu, "An integrated 256-channel epiretinal prosthesis," *IEEE J. Solid-State Circuits*, vol. 45, no. 9, pp. 1946–1956, 2010.

[56]   M. Sivaprakasam, M. S. Humayun, W. Liu, and J. D. Weiland, "A variable range Bi-phasic current stimulus driver circuitry for an implantable retinal prosthetic device," *IEEE J. Solid-State Circuits*, vol. 40, no. 3, pp. 763–770, 2005.

[57]   J. J. Sit and R. Sarpeshkar, "A low-power blocking-capacitor-free charge-balanced electrode-stimulator chip with lesst than 6 nA DC error for 1-mA: Full-Scale Stimulation," *IEEE Trans. Biomed. Circuits Syst.*, vol. 1, no. 3, pp. 172–183, 2007.

[58]   S. H. Bae *et al.*, "In vitro biocompatibility of various polymer-based microelectrode arrays for retinal prosthesis," *Investig. Ophthalmol. Vis. Sci.*, vol. 53, no. 6, pp. 2653–2657, 2012.

[59]   J. Jeong, S. H. Bae, K. S. Min, J. M. Seo, H. Chung, and S. J. Kim, "A miniaturized, eye-conformable, and long-term reliable retinal prosthesis using monolithic fabrication of liquid crystal polymer (LCP)," *IEEE Trans. Biomed. Eng.*, vol. 62, no. 3, pp. 982–989, 2015.

[60] F. A. Jenkins and H. E. White, *Fundamentals of Optics*. McGraw-Hill, 1976.

[61] J. Ge, M. P. K. Turunen, and J. K. Kivilahti, "Surface modification of a liquid-crystalline polymer for copper metallization," *J. Polym. Sci. Part B Polym. Phys.*, vol. 41, no. 6, pp. 623–636, Mar. 2003.

[62] G. D. Boreman, *Modulation Transfer Function in Optical and Electro-optical Systems*. Society of Photo Optical, 2001.

[63] J. Farrell, F. Xiao, and S. Kavusi, "Resolution and Light Sensitivity Traedoff with Pixel Size," p. 60690N–60690N–8, 2006.

[64] T. Lulé *et al.*, "Sensitivity of CMOS based imagers and scaling perspectives," *IEEE Trans. Electron Devices*, vol. 47, no. 11, pp. 2110–2122, 2000.

[65] S. Kundra and P. Soni, "Low power Schmitt trigger."

[66] S. F. Al-Sarawi, "Low power Schmitt trigger circuit," *Electronics Letters*, vol. 38, no. 18. pp. 1009–1010, 2002.

[67] D. A. Malone *et al.*, "Deep brain stimulation of the ventral capsule/ventral striatum for treatment-resistant depression.," *Biol. Psychiatry*, vol. 65, no. 4, pp. 267–75, Feb. 2009.

[68] R. Wilke *et al.*, "Spatial resolution and perception of patterns mediated by a subretinal 16-electrode array in patients blinded by hereditary retinal dystrophies," *Investig. Ophthalmol. Vis. Sci.*, vol. 52, no. 8, pp. 5995–6003, Jul. 2011.

[69] A. C. Weitz *et al.*, "Improving the spatial resolution of epiretinal implants by increasing stimulus pulse duration," *Sci. Transl. Med.*, vol. 7, no. 318, p. 318ra203-318ra203, 2015.

[70]   H. Greenhouse, *Hermeticity of Electronic Packages*. Elsevier Science, 2011.

[71]   M. J. Chen *et al.*, "Design and development of a package using LCP for RF/microwave MEMS switches," *IEEE Trans. Microw. Theory Tech.*, vol. 54, no. 11, pp. 4009–4015, 2006.

[72]   J. Jeong, S. Hyun Bae, J.-M. Seo, H. Chung, and S. June Kim, "Long-term evaluation of a liquid crystal polymer (LCP)-based retinal prosthesis.," *J. Neural Eng.*, vol. 13, no. 2, p. 25004, Apr. 2016.

[73]   A. Rothermel *et al.*, "A CMOS chip with active pixel array and specific test features for subretinal implantation," *IEEE J. Solid-State Circuits*, vol. 44, no. 1, pp. 290–300, 2009.

Appendix − Generated Stimulus Patterns of Various the Number of Channels

4 Subjects recognized the input image by showing the stimulus patterns with conventional and proposed strategies, increasing the number of channels (4×4, 8×8, 16×16, 32×32, 64×64). The alphabet was used. Average current levels are also described in each figure.

Appendix 1 – Alphabet
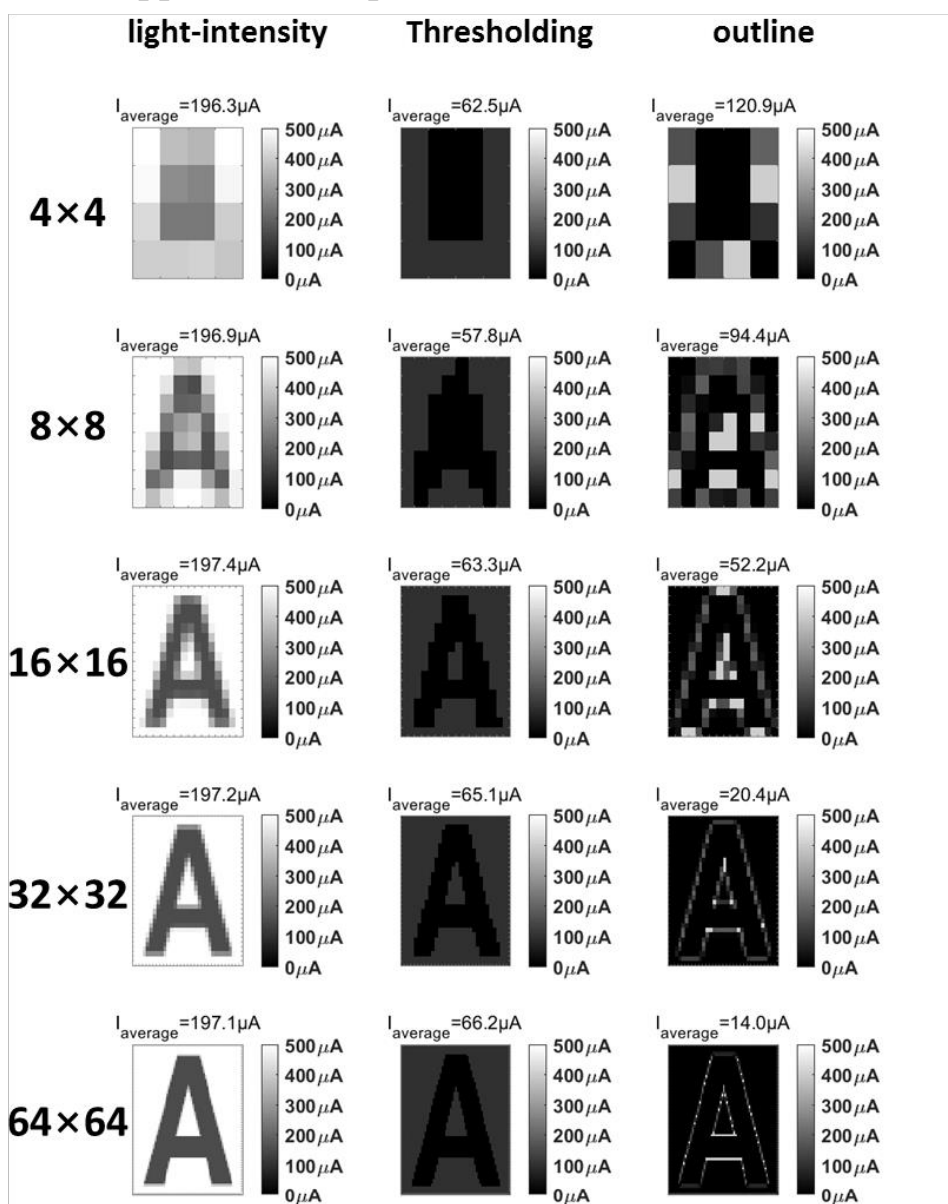
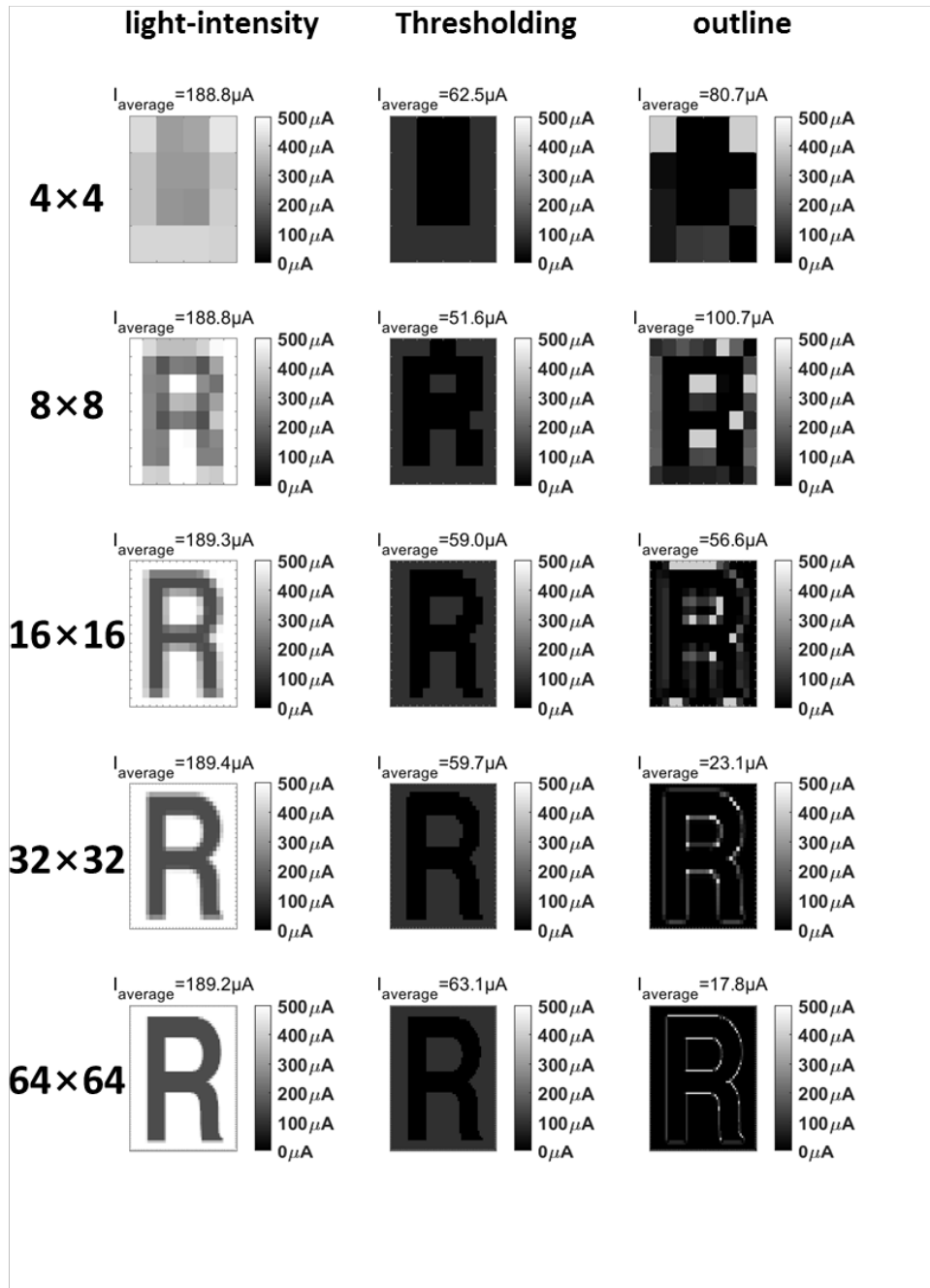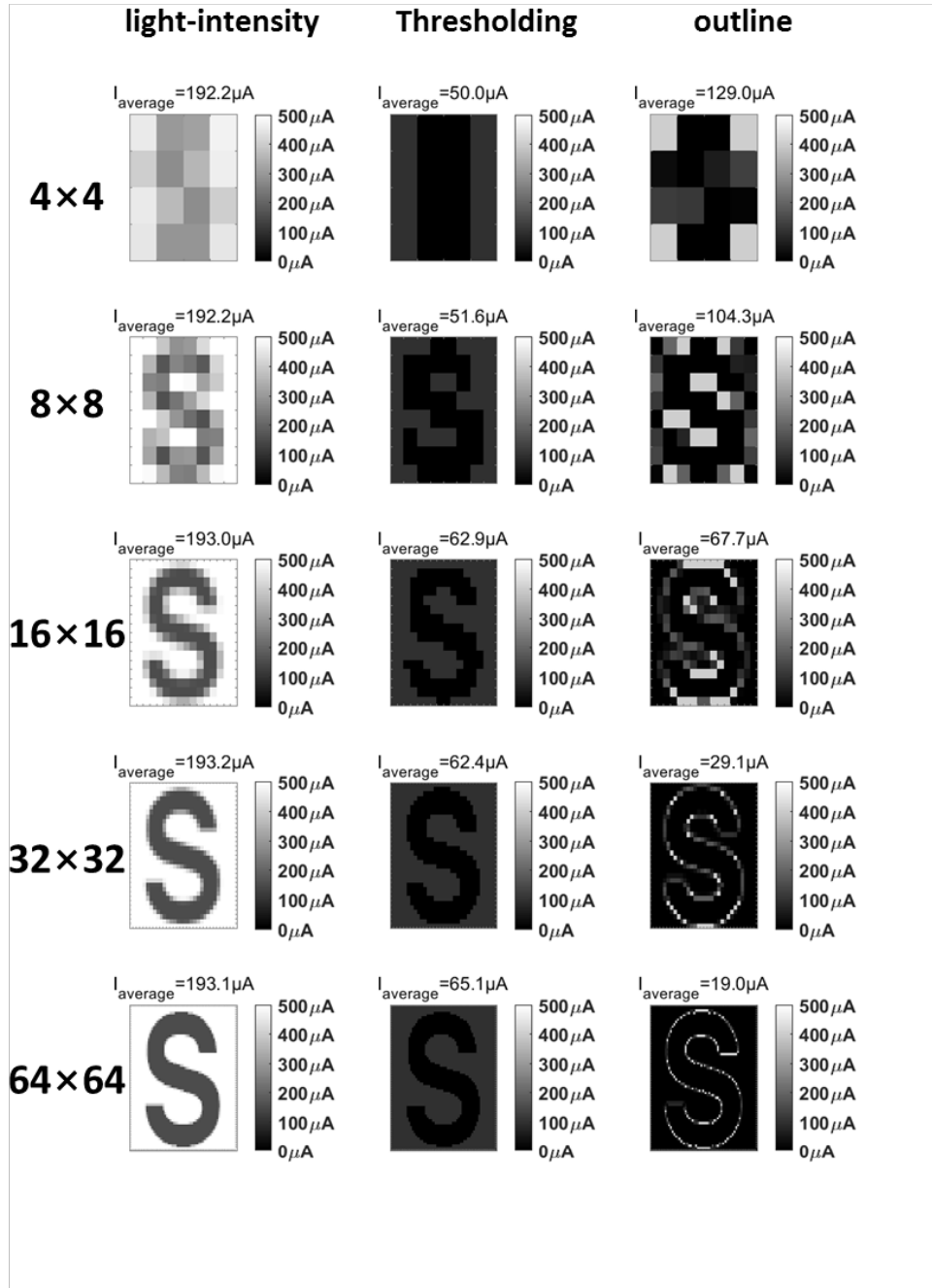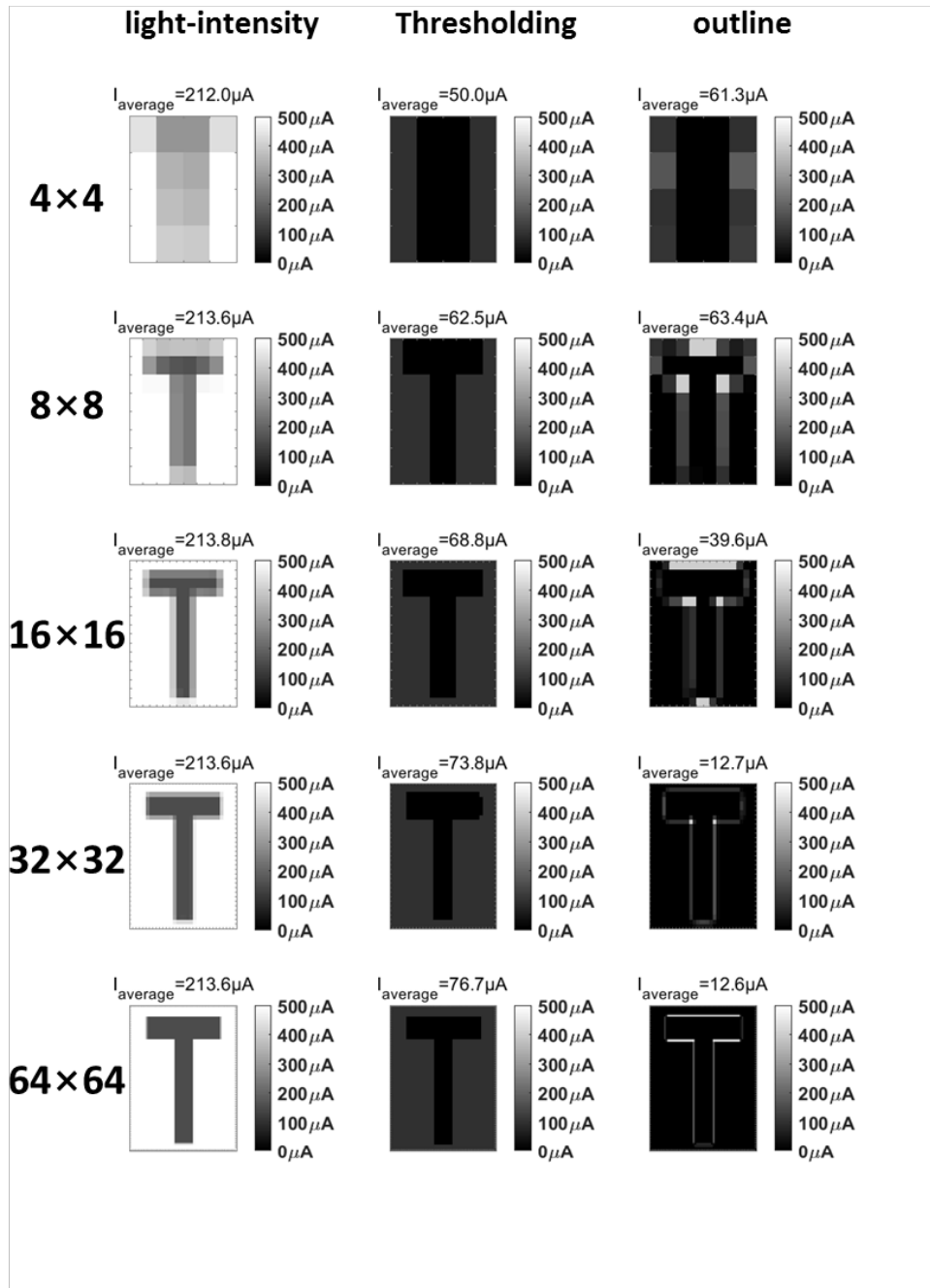Appendix 1 Stimulus patterns of Character 'A'
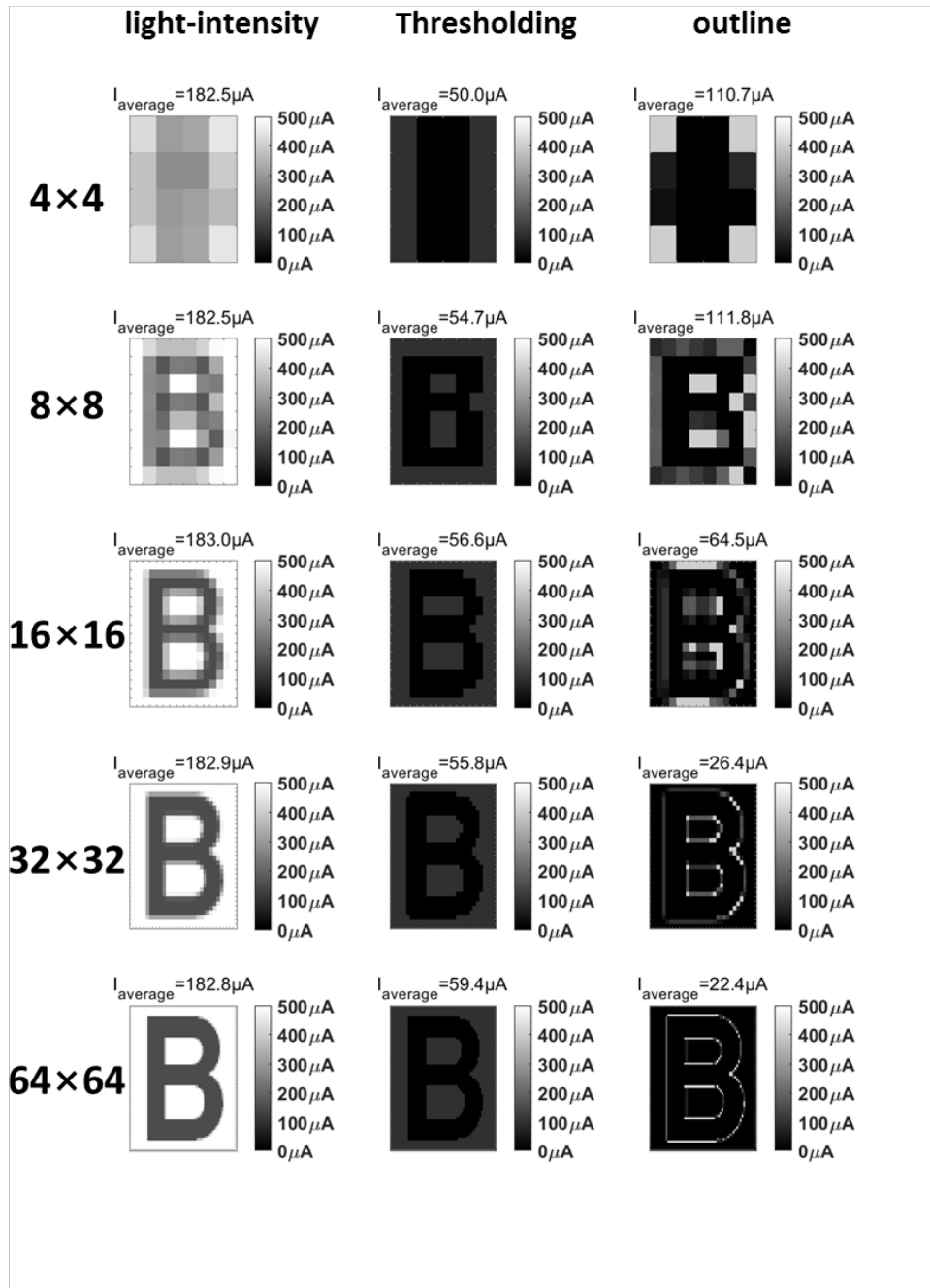
Appendix 2 Stimulus patterns of Character 'B'
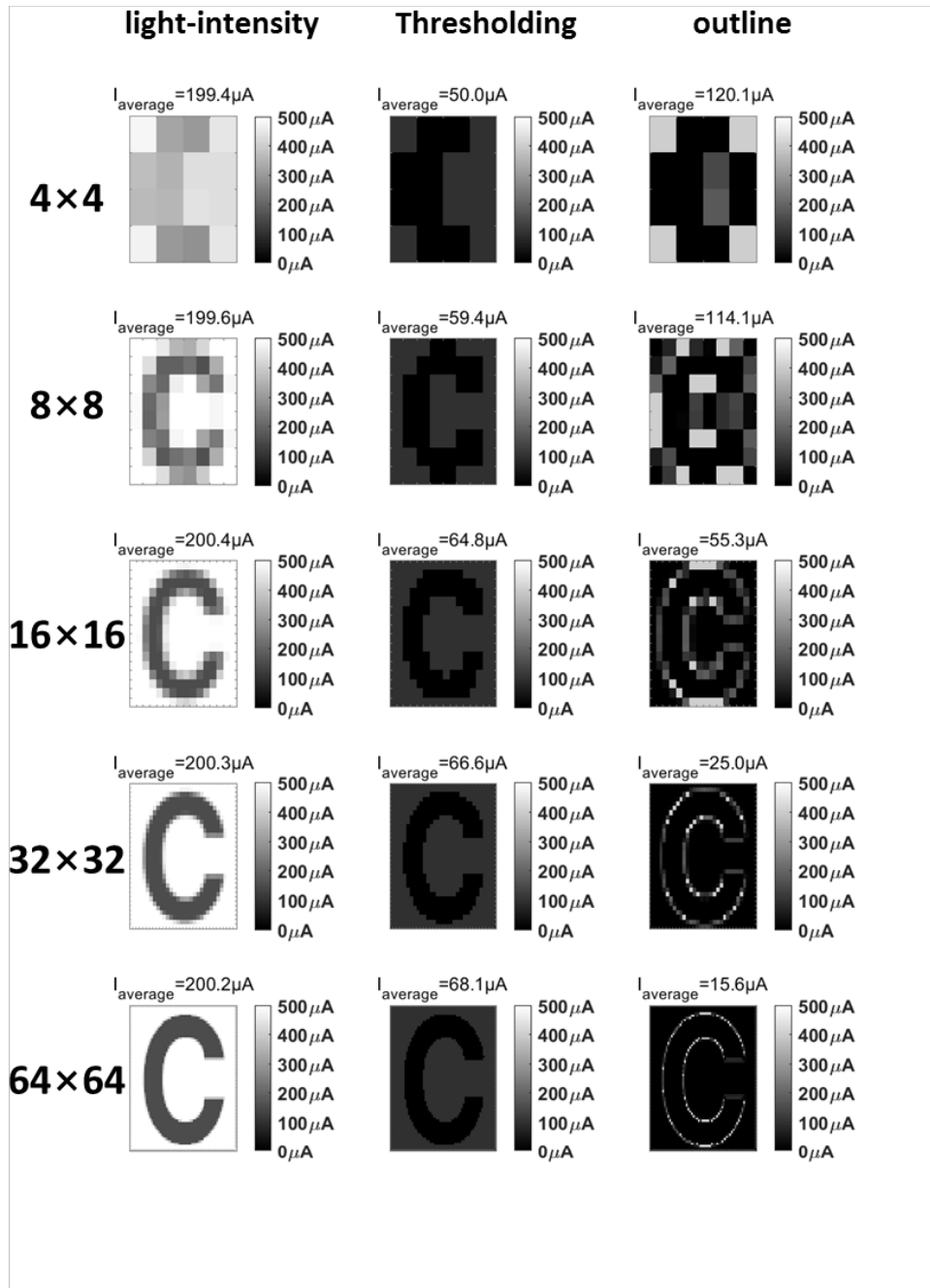
Appendix 3 Stimulus patterns of Character 'C'
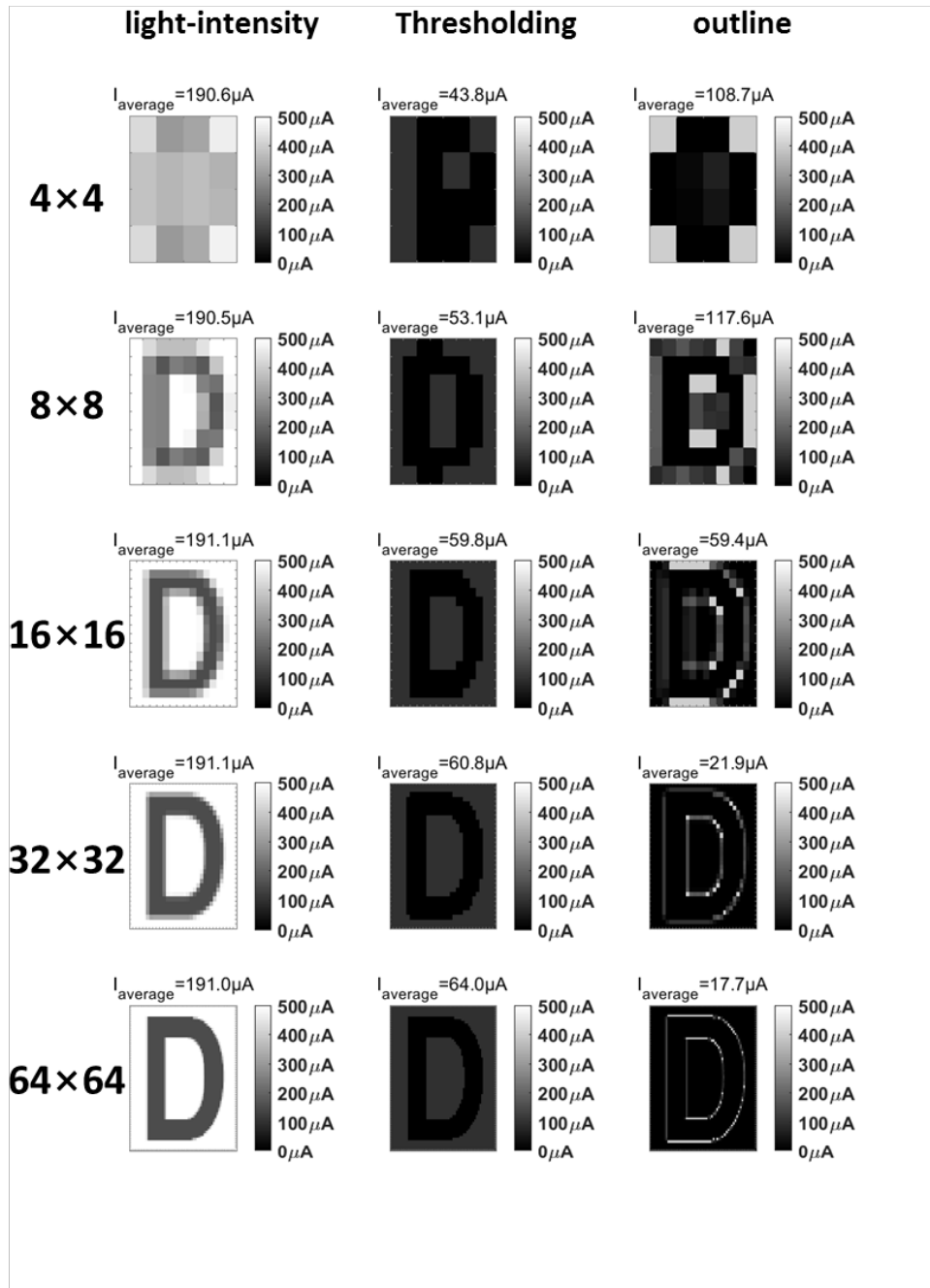
Appendix 4 Stimulus patterns of Character 'D'
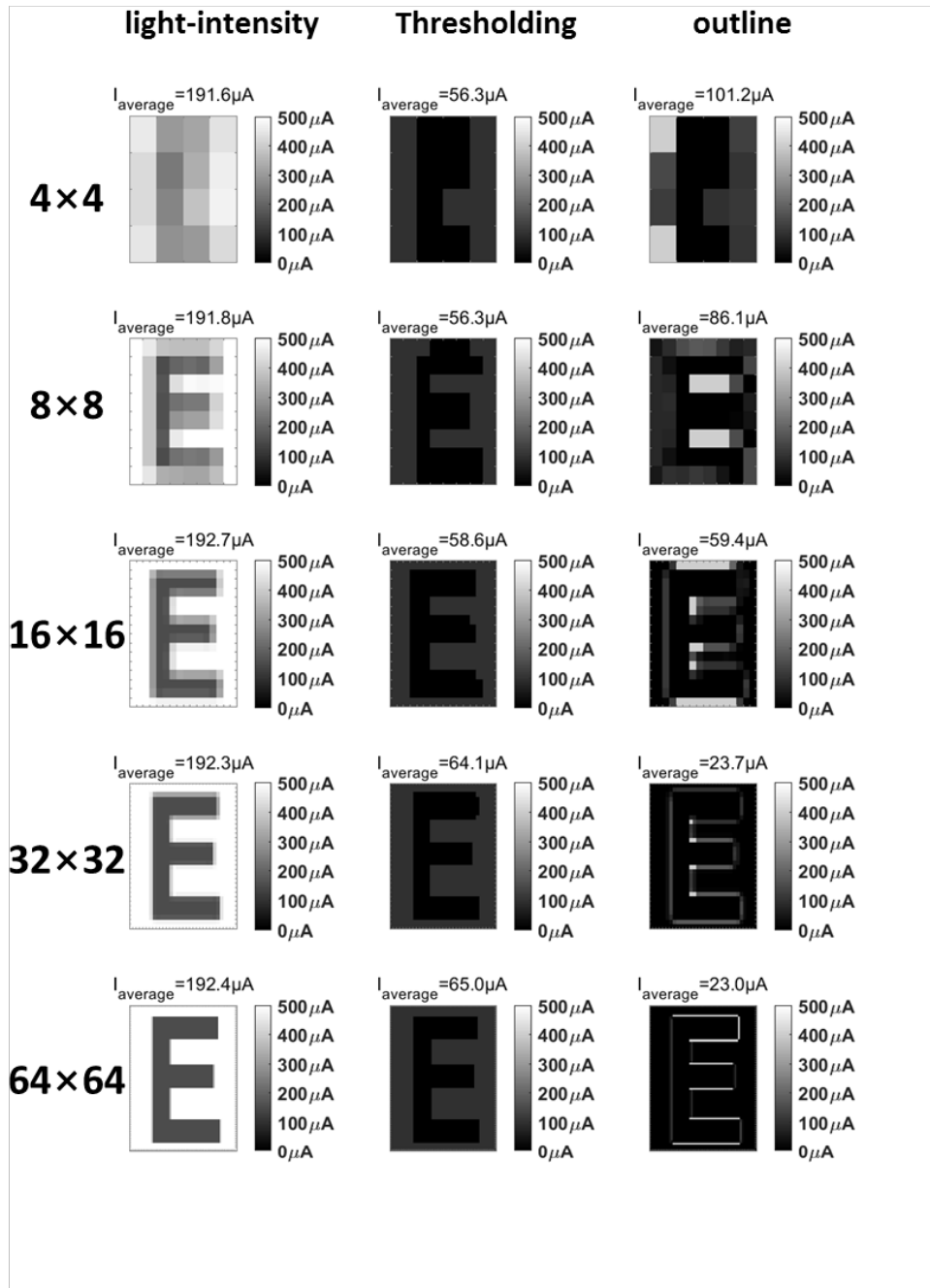
Appendix 5 Stimulus patterns of Character 'E'
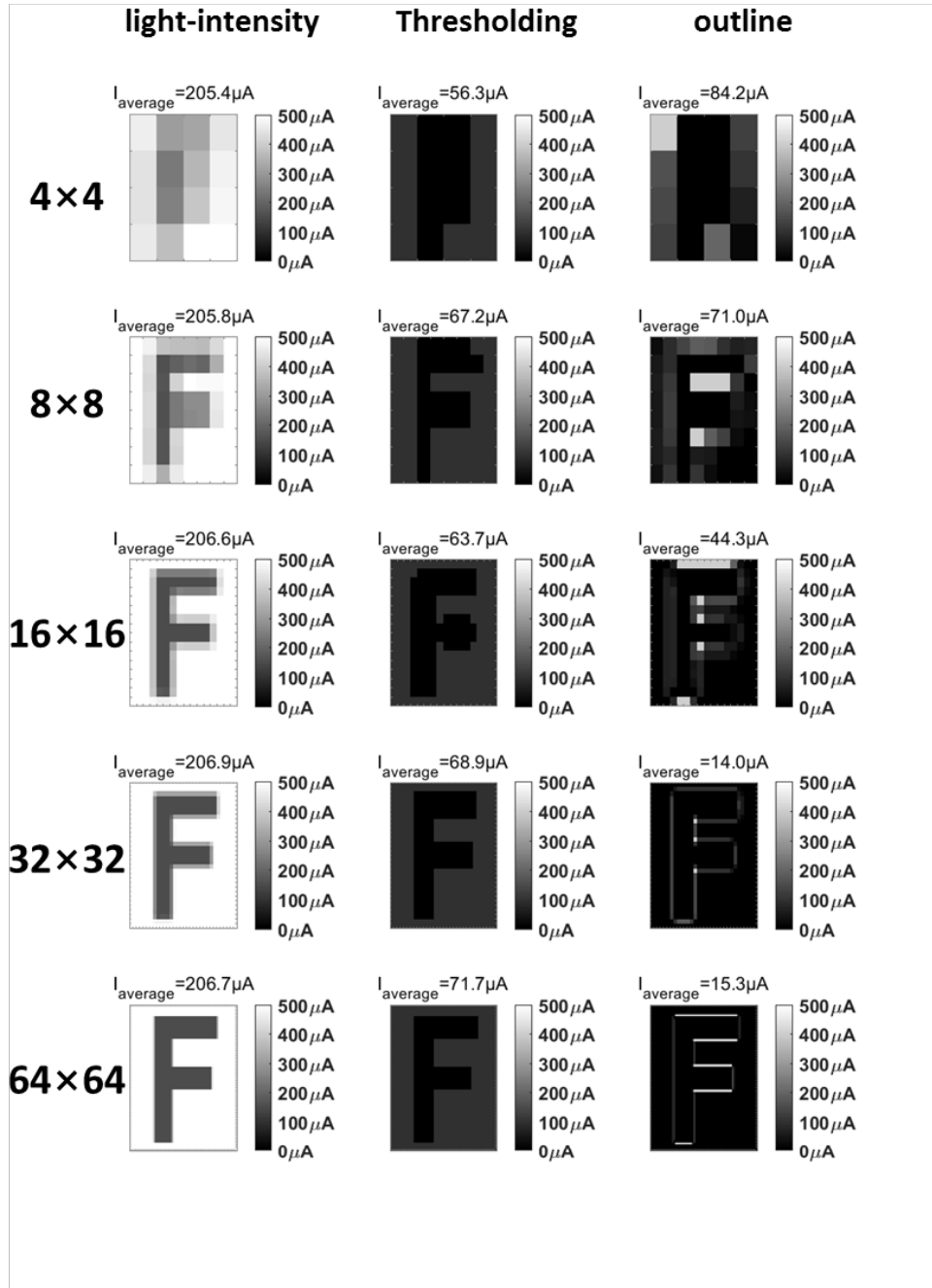
Appendix 6 Stimulus patterns of Character 'F'
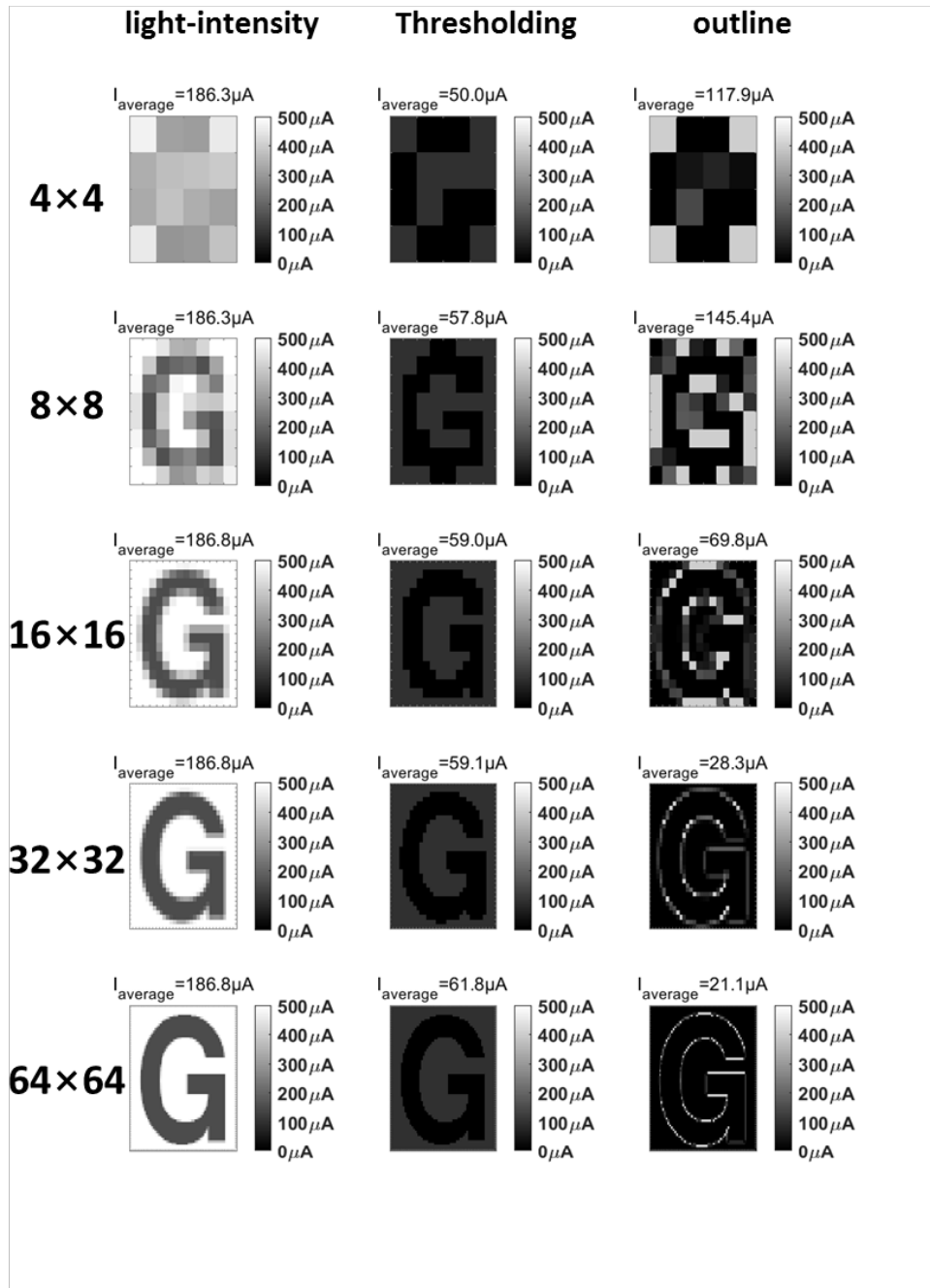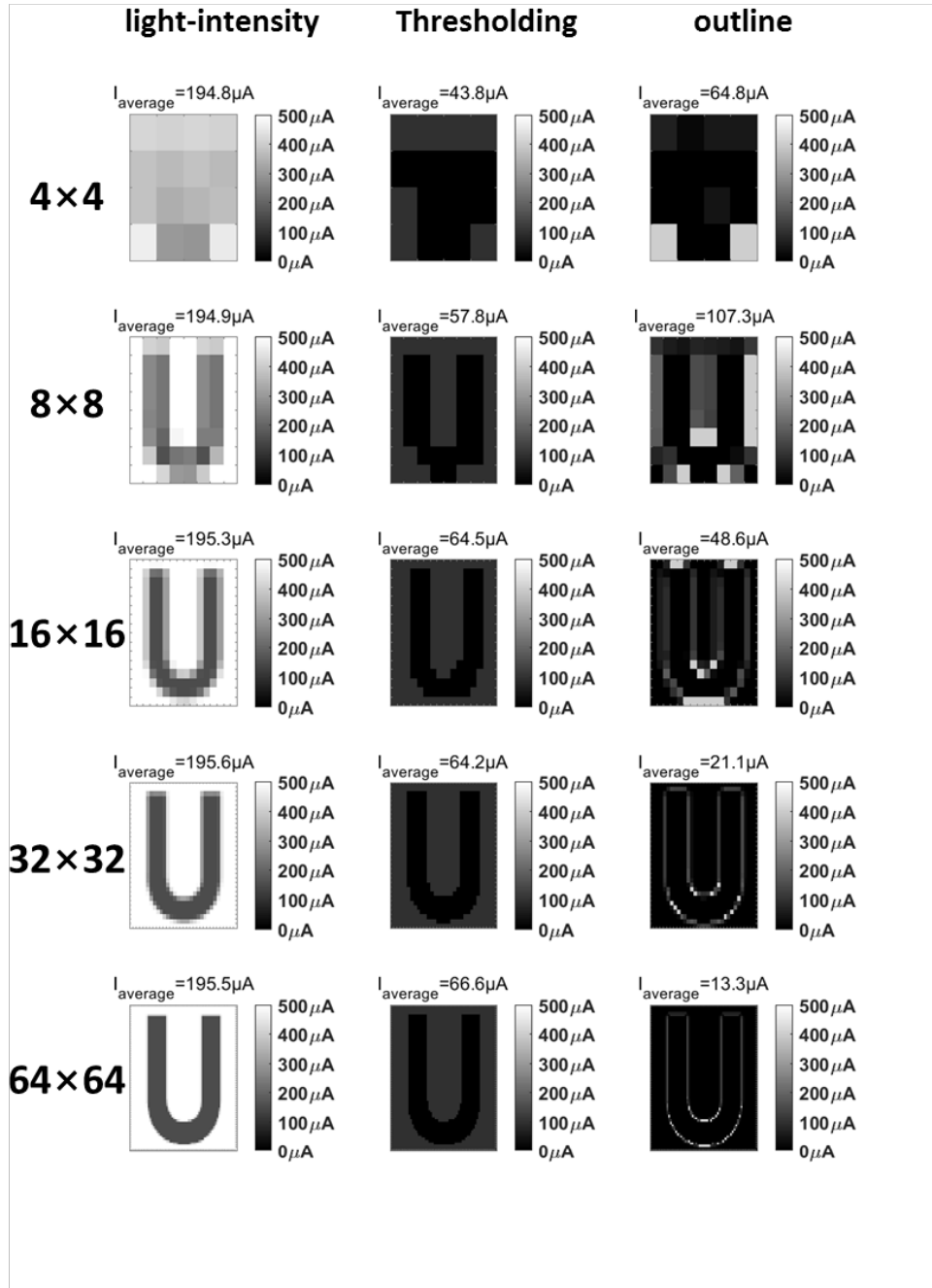
Appendix 7 Stimulus patterns of Character 'G'
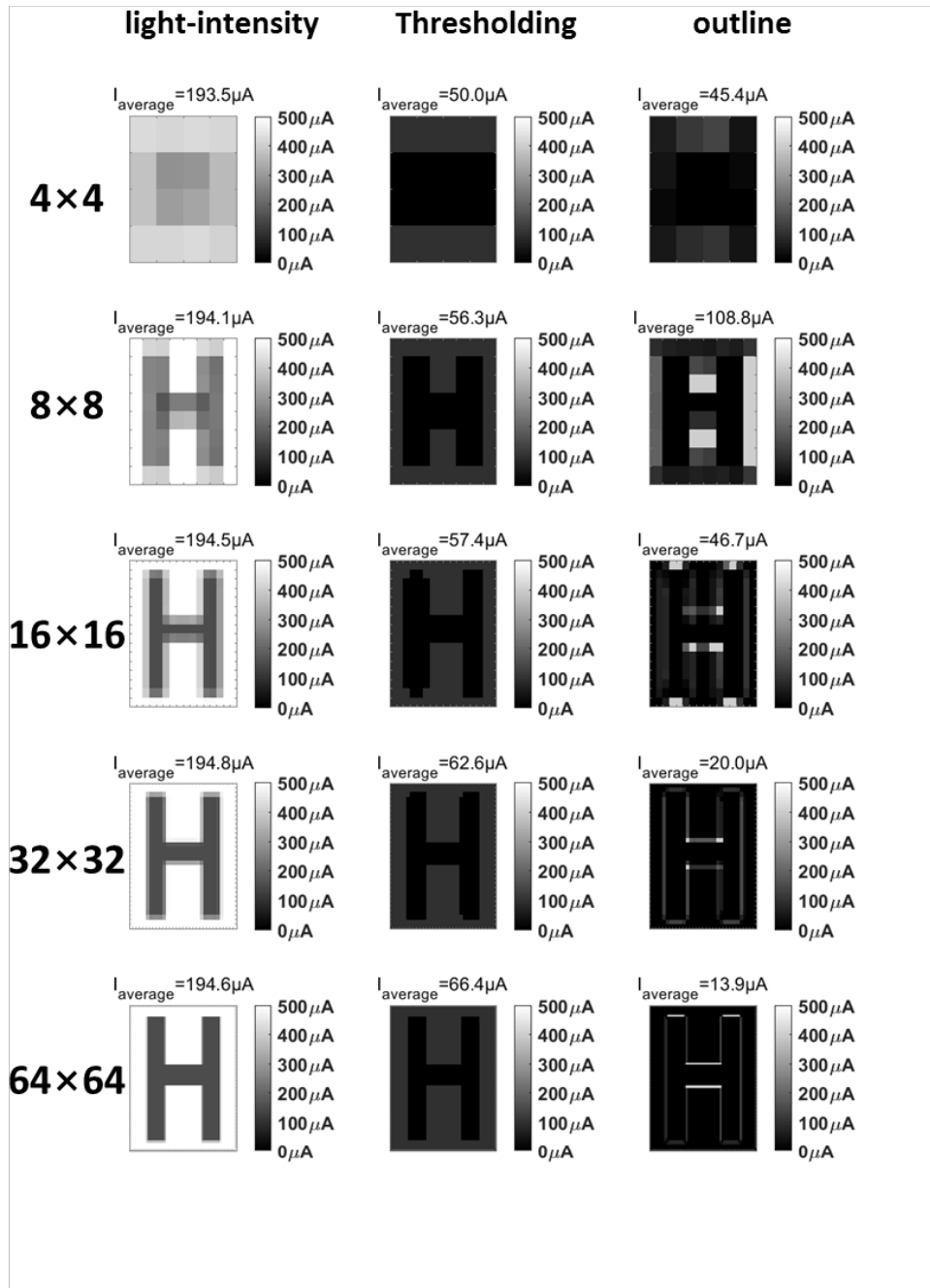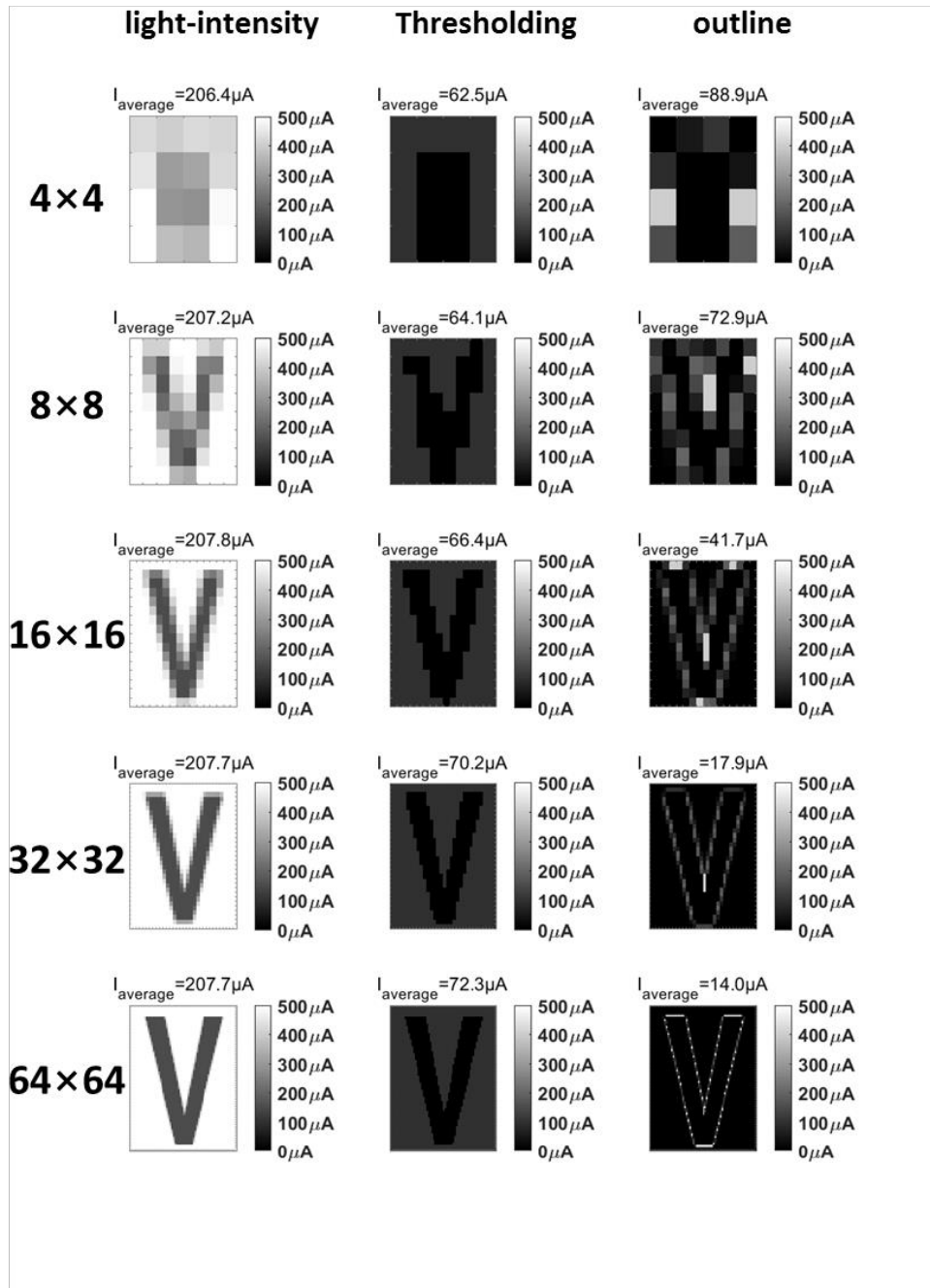
Appendix 8 Stimulus patterns of Character 'H'
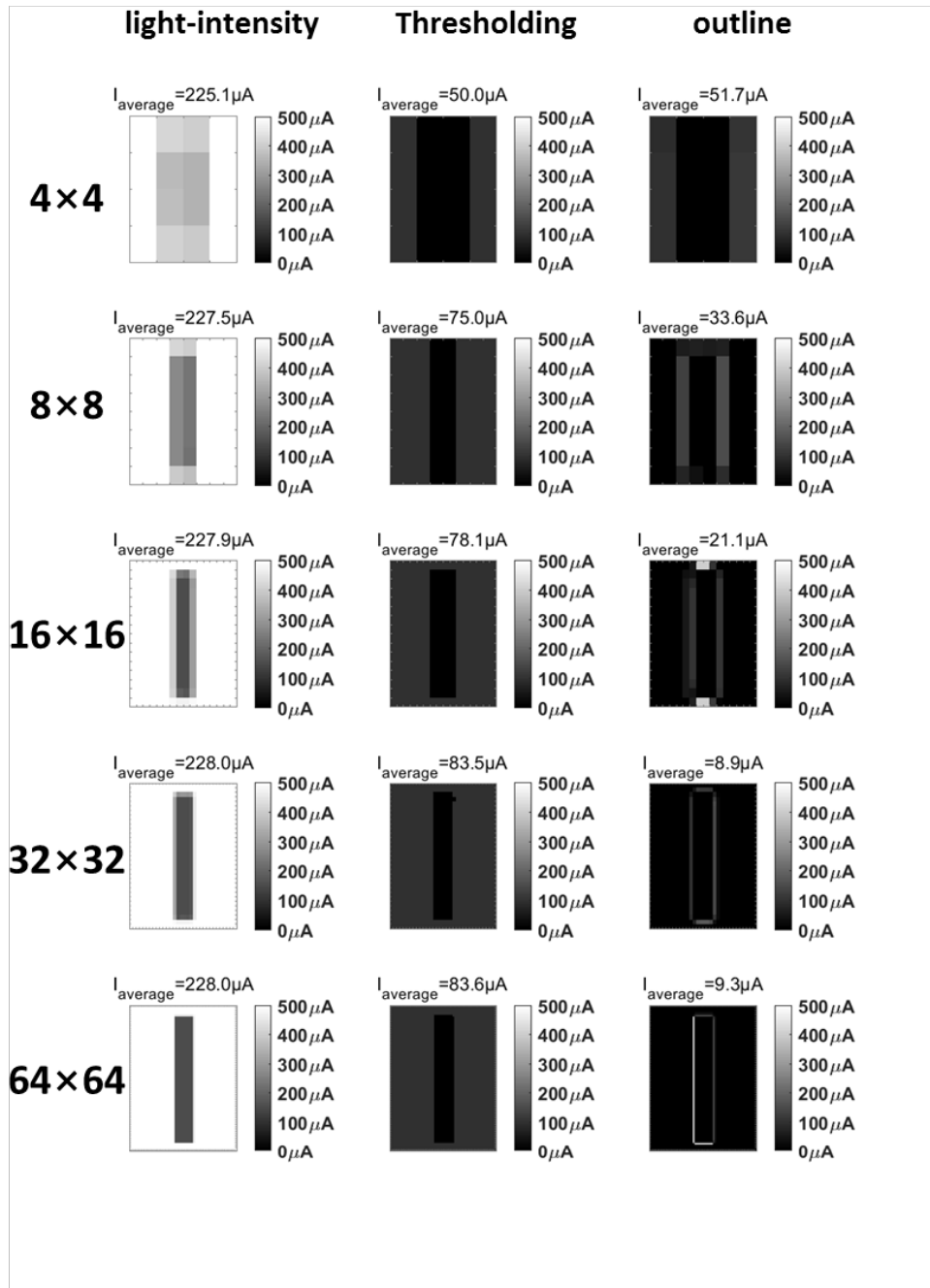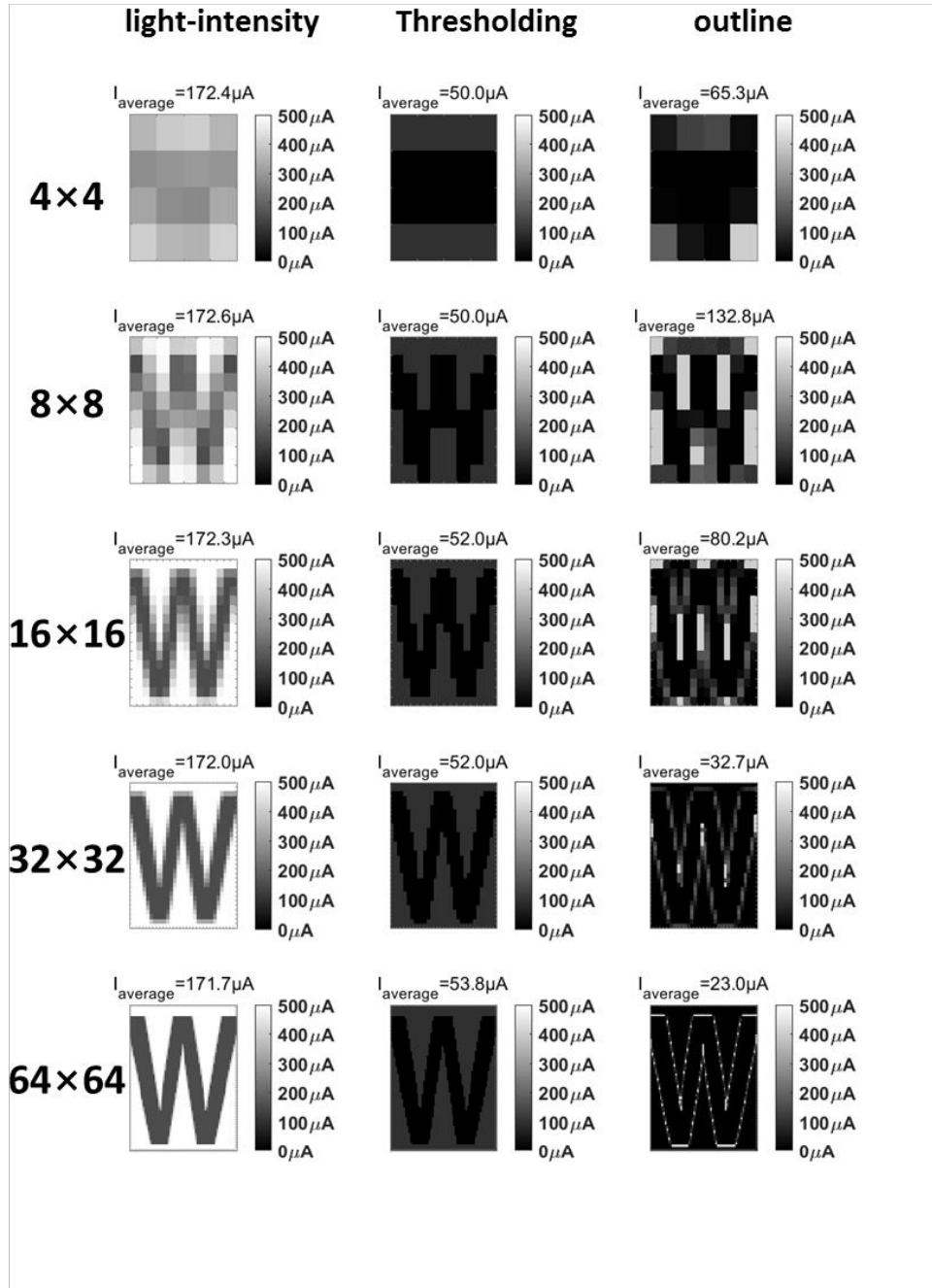
Appendix 9 Stimulus patterns of Character 'I'
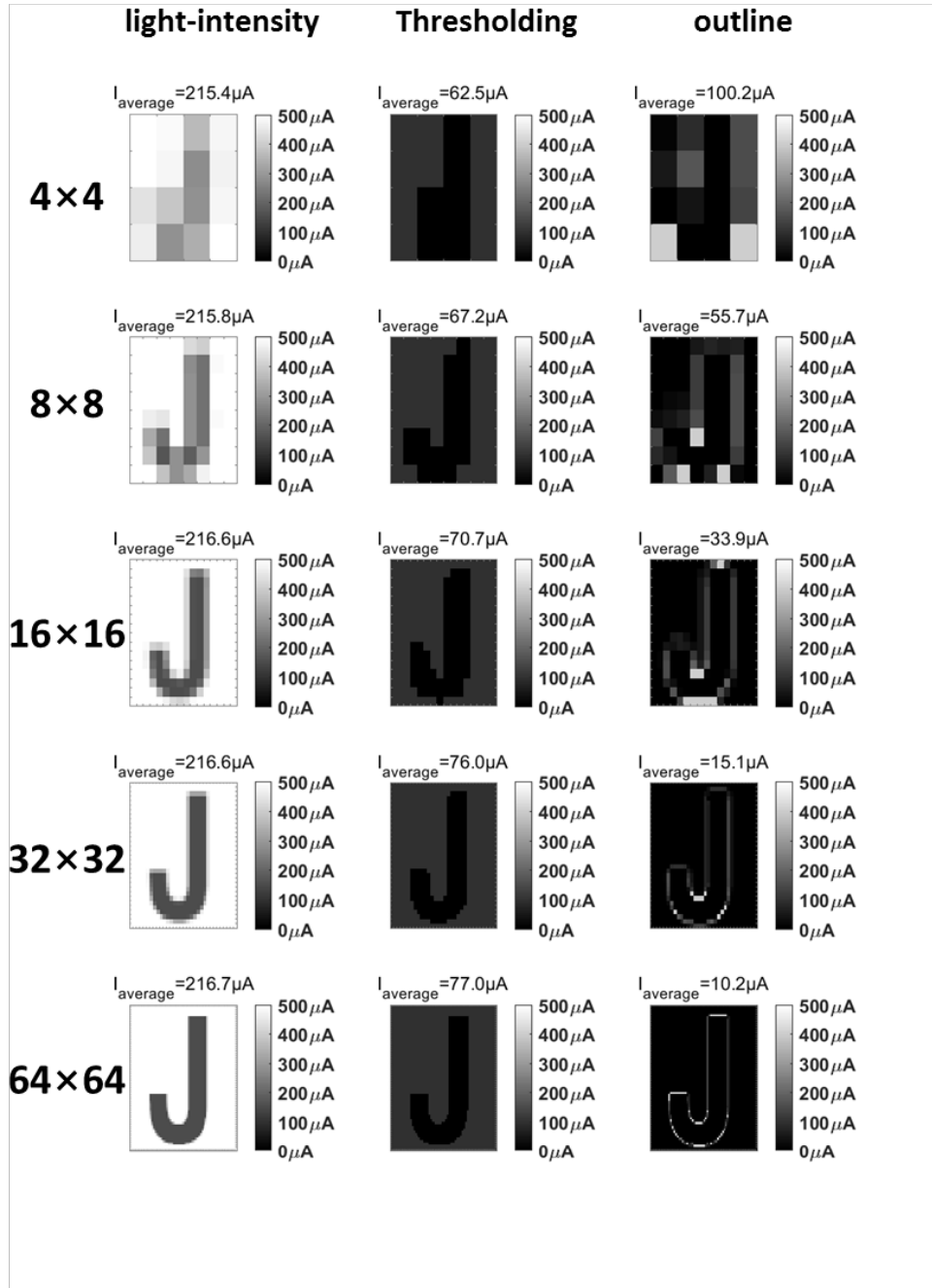
Appendix 10 Stimulus patterns of Character 'J'
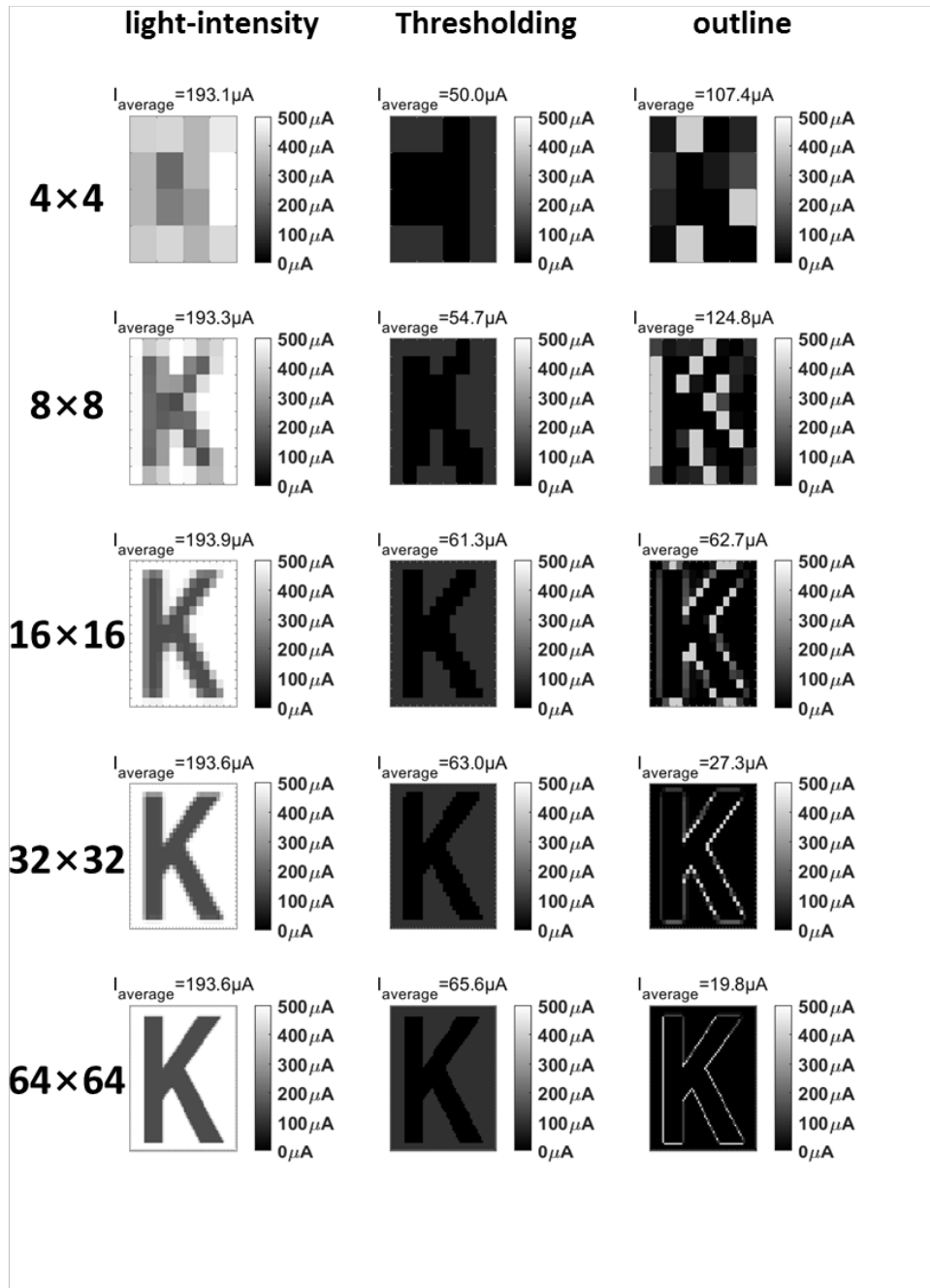
Appendix 11 Stimulus patterns of Character 'K'
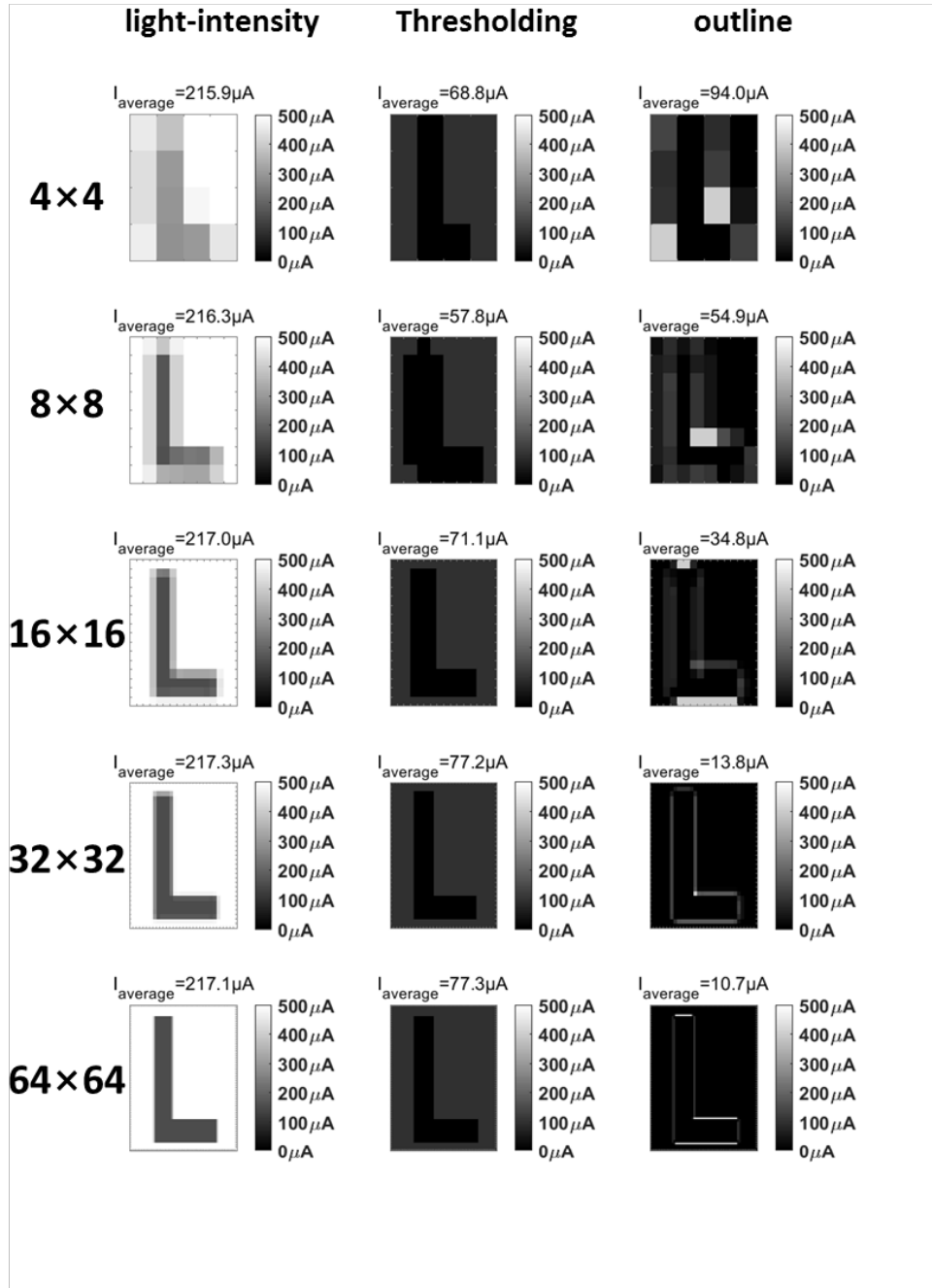
Appendix 12 Stimulus patterns of Character 'L'
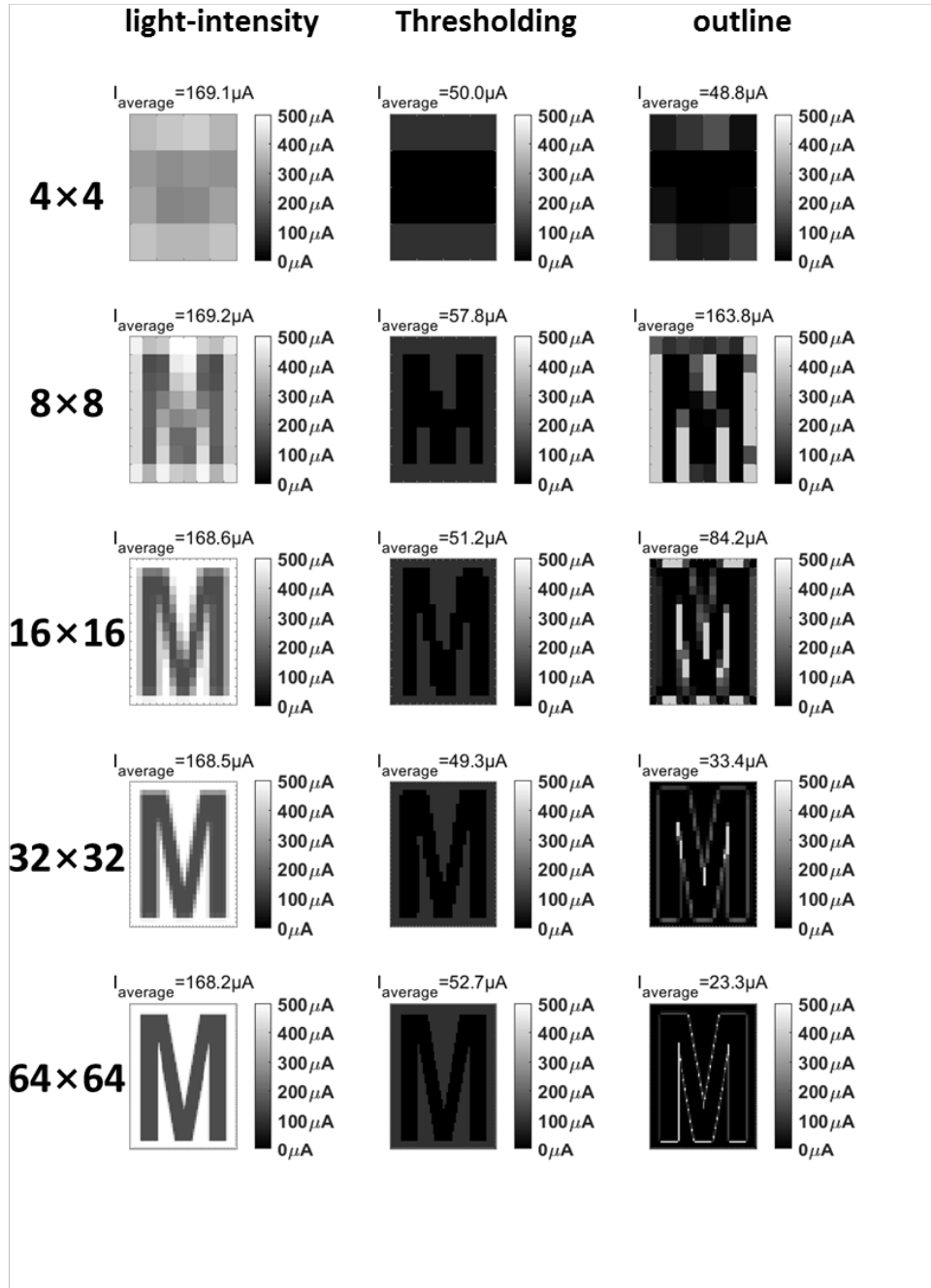
Appendix 13 Stimulus patterns of Character 'M'
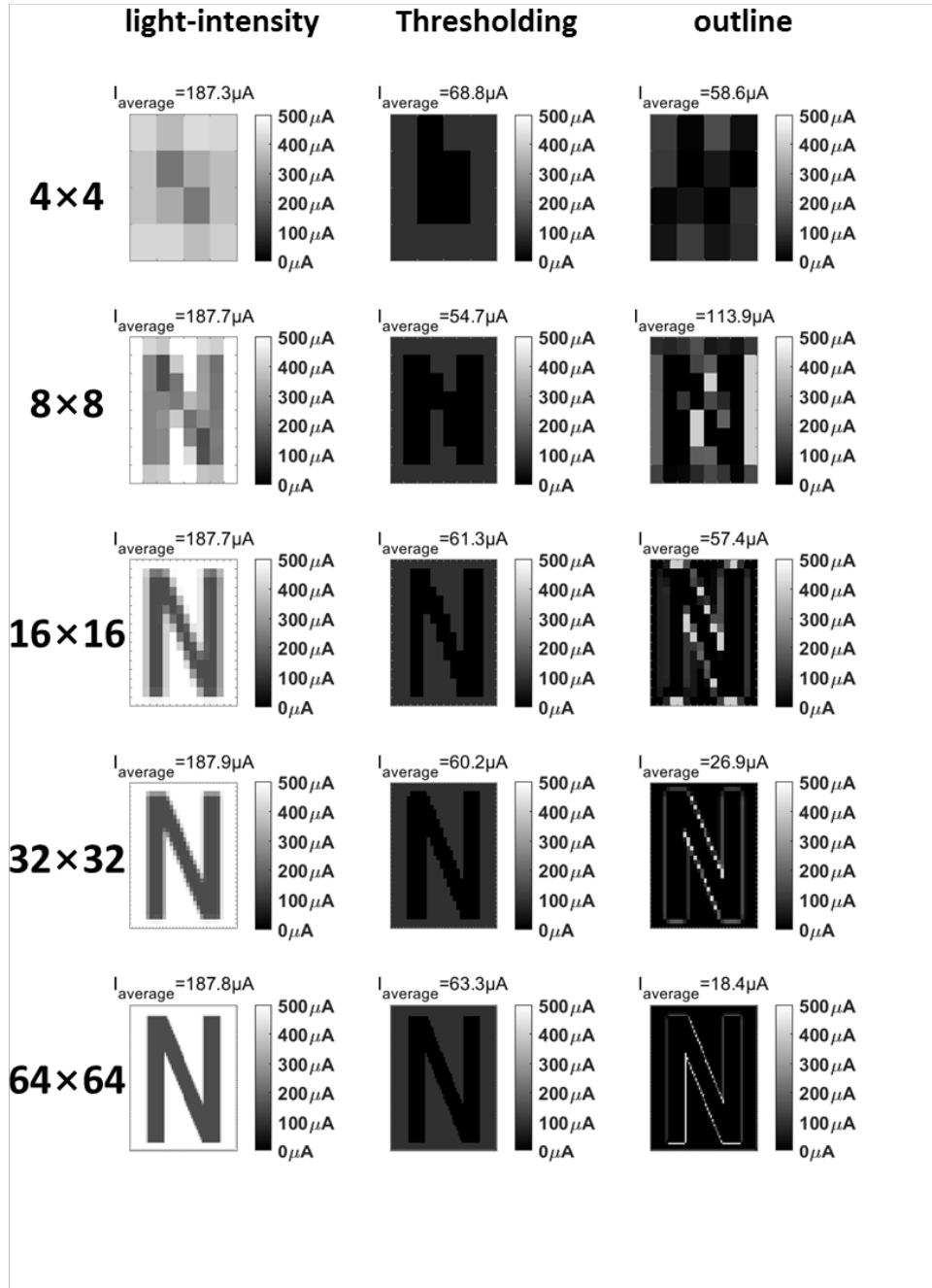
Appendix 14 Stimulus patterns of Character 'N'
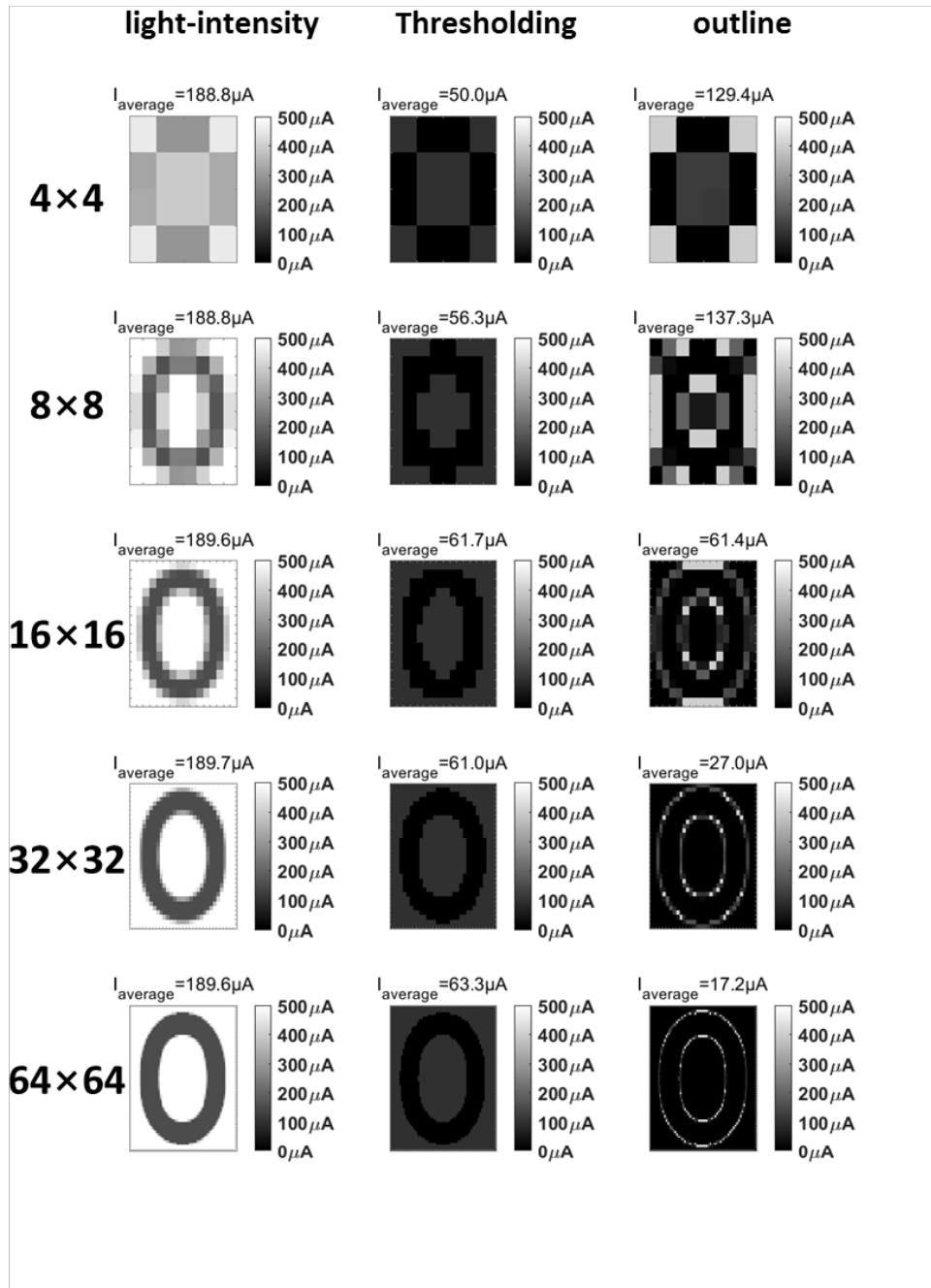
Appendix 15 Stimulus patterns of Character 'O'
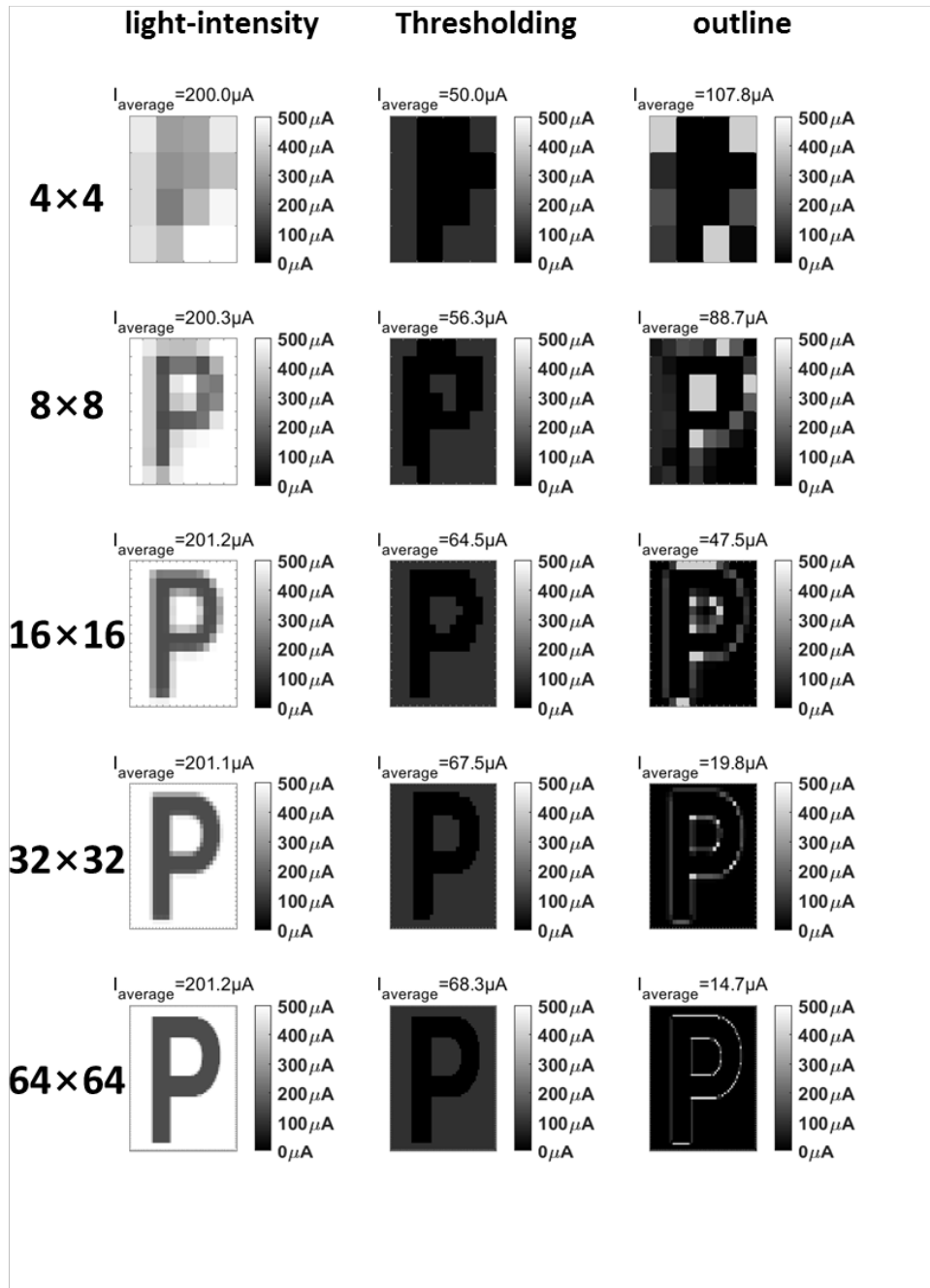
Appendix 16 Stimulus patterns of Character 'P'
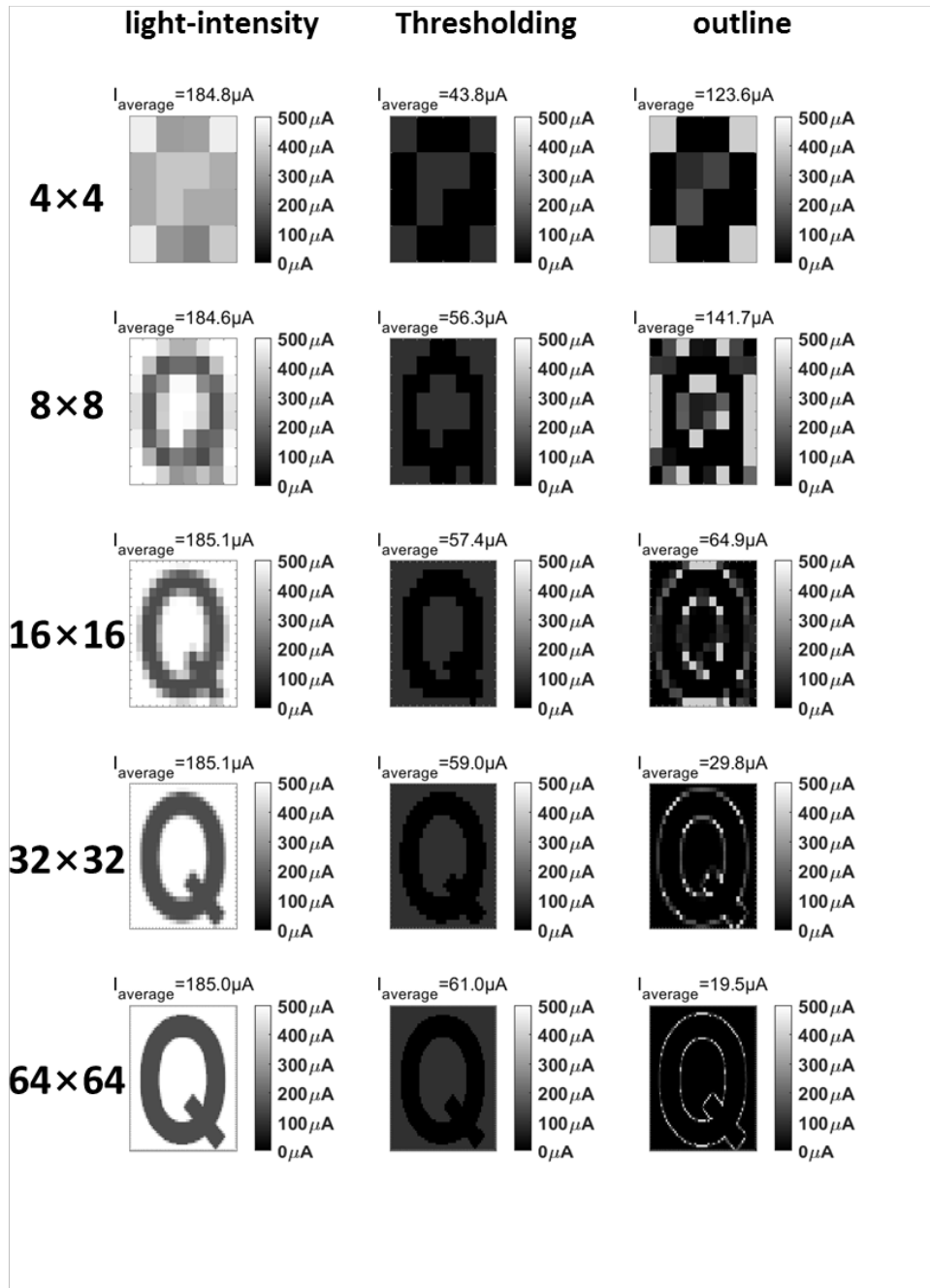
Appendix 17 Stimulus patterns of Character 'Q'

Appendix 18 Stimulus patterns of Character 'R'

Appendix 19 Stimulus patterns of Character 'S'
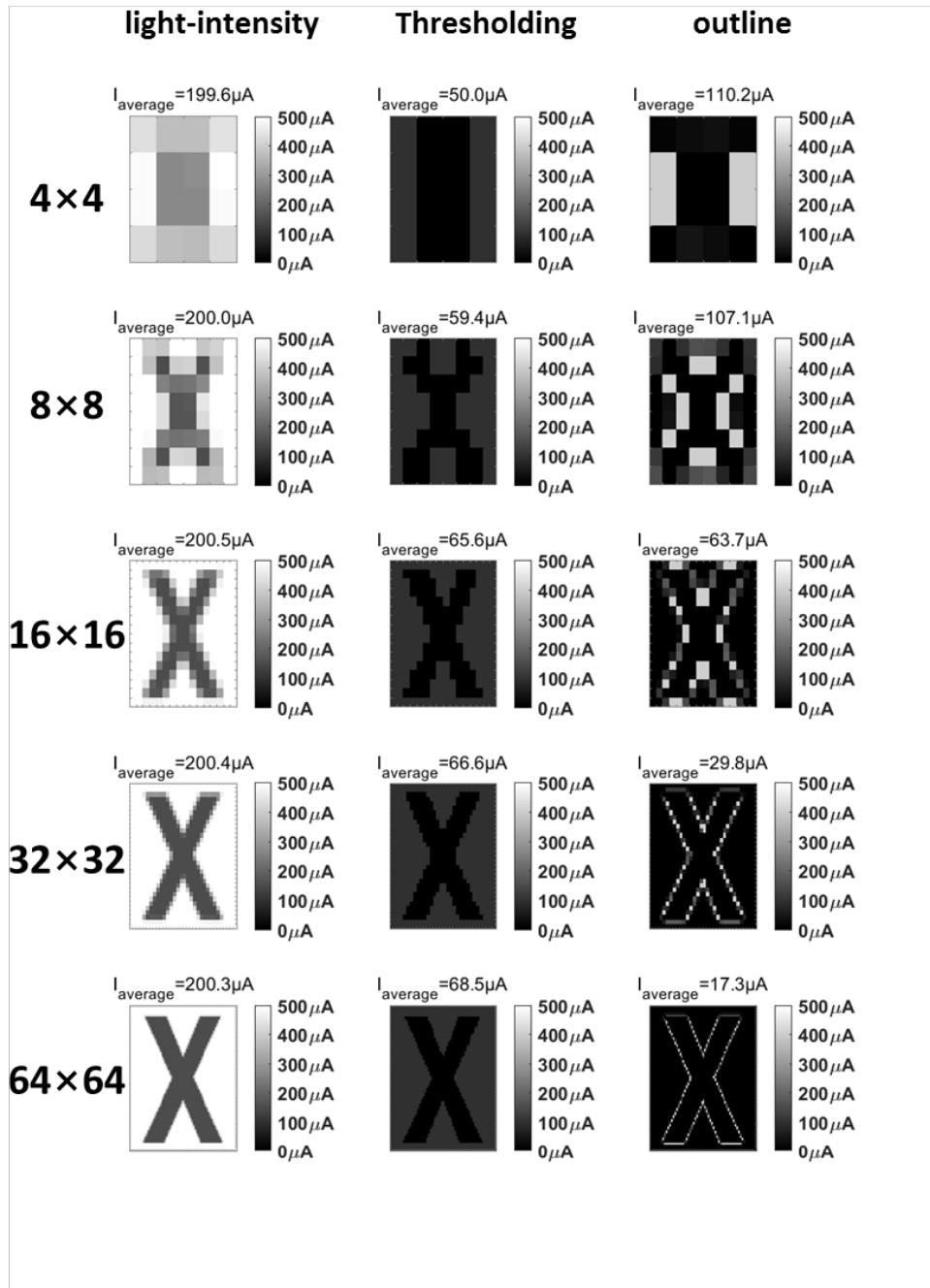
Appendix 20 Stimulus patterns of Character 'T'

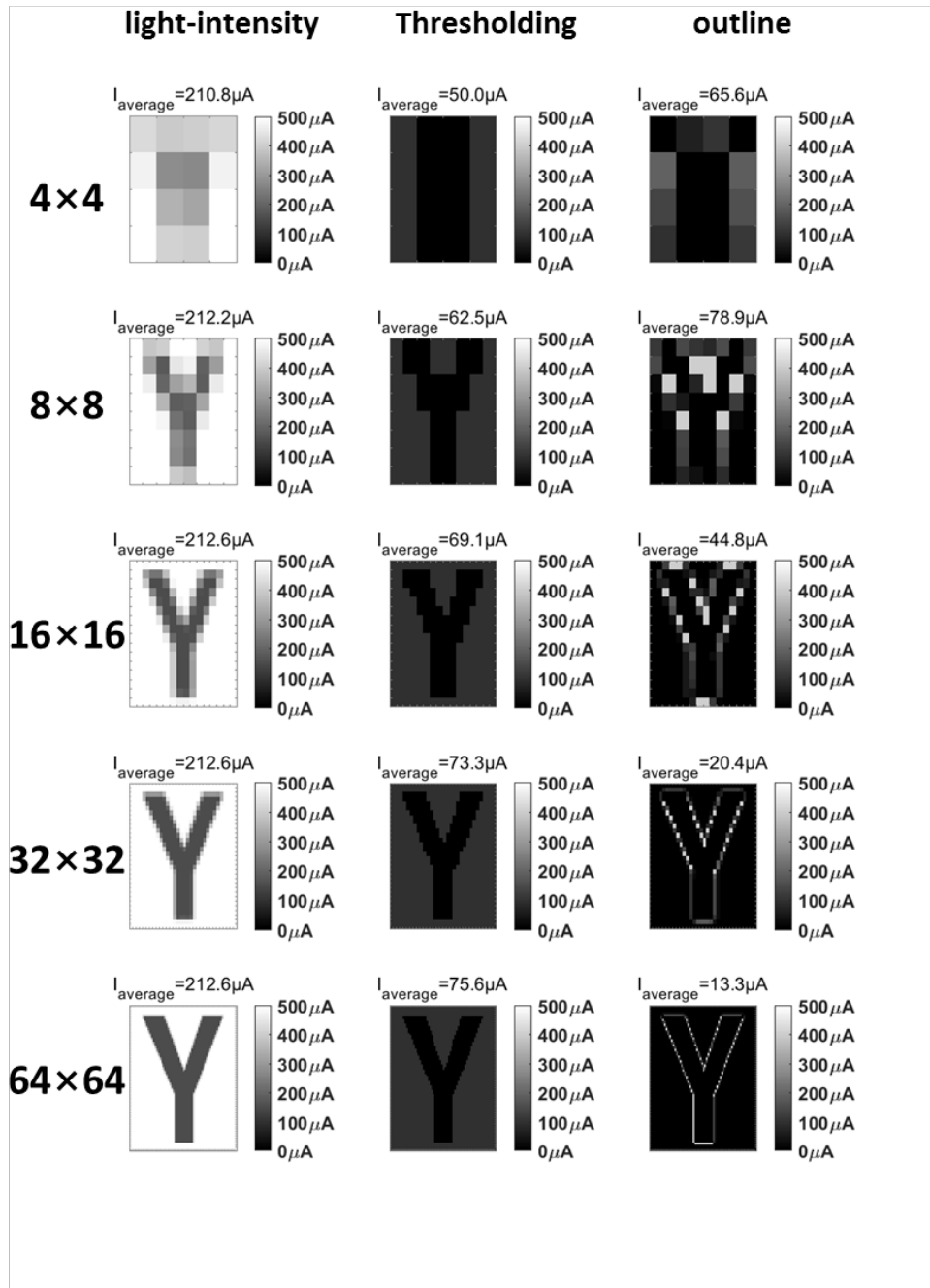Appendix 21 Stimulus patterns of Character 'U'
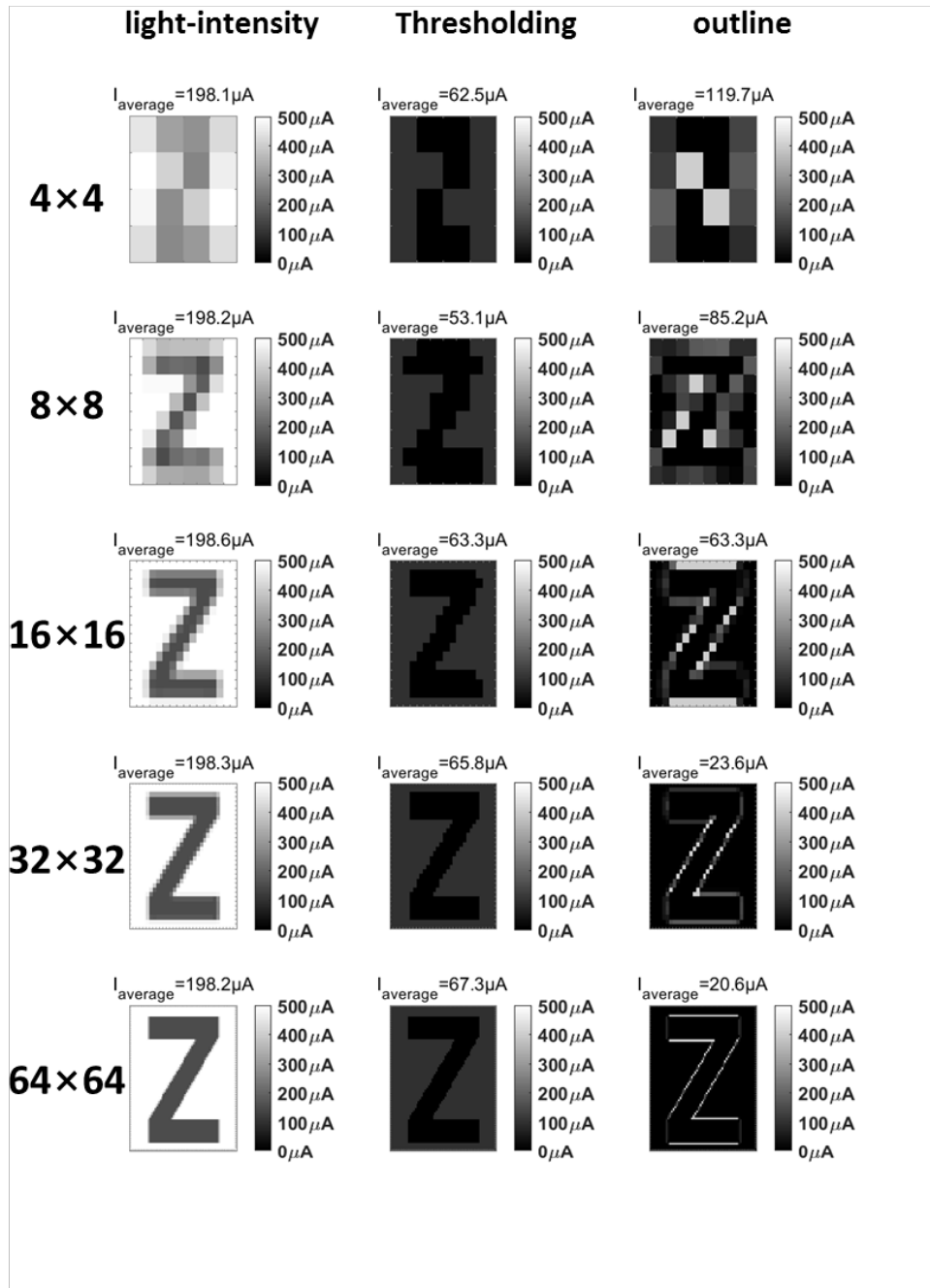
Appendix 22 Stimulus patterns of Character 'V'

Appendix 23 Stimulus patterns of Character 'W'

Appendix 24 Stimulus patterns of Character 'X'

Appendix 25 Stimulus patterns of Character 'Y'

Appendix 26 Stimulus patterns of Character 'Z'

국 문 초 록

인공 망막 장치는 빛 정보가 함유된 전기 신호를 살아있는 망막 세포절에 전달하여 손실된 시력을 회복시켜주는 전자 장치이다. 현재 이용 가능한 인공 망막 장치는 픽셀수와 관련하여 몇 가지 문제점을 지니고 있는데, 그 중 하나로 제한된 필셀 수로 발생하는 시각정보 전달제약이다. 따라서 많은 연구자들은 자극 채널수를 증가시키는 방향으로 연구를 진행하고 있다. 하지만, 이를 진행하기 위해선 다른 문제점들이 있는데 그 중 하나로 전력소모가 있다. 현재 인공 망막 장치는 1000 채널의 자극파형을 생성하기 위해서 20 mW의 전력이 필요로 한데, 이는 체내 온도 상승을 야기하기 때문에 채널당 자극파형을 생성하는데 필요한 전력소모를 줄이는 것이 바람직하다. 다른 문제는 장기 이식가능한 광학 창이 내장된 패키징 부재로, 현재 사용되는 사파이어 글래스 메탈 패키징은 크기가 크고, 단단한 단점을 가지고 있으며, polyimide, parylene-C와 같은 투명한 폴리머는 높은 흡습률을 가지고 있어 장기이식에 부적합하다.

 이 학위논문은 위에서 언급한 문제들을 해결하기 위한 전략 및 방법을 제시하고 있다. 저 전력소모를 위한 두 가지 자극 전략을 제시하는데, 하나는 신경세포가 활성화 될 정도의 자극크기로 자극전류를 제한하는

것이다(문턱 자극 전략). 다른 하나는 이미지의 윤곽선만 자극하여 활성화되는 채널의 수를 줄이는 것이다 (윤곽선 자극 전략). 두 자극 전략을 검증하기 위해 집적회로를 설계 및 제작을 하였다. 시뮬레이션과 측정결과는 상용 자극 전략에 비해 1/3 이하의 자극파형을 생성하기 위한 전력소모를 가진다. 채널수 집적도를 높이기 위해 면적 효율이 좋은 전압전류변화기를 설계 및 제작하였으며, 이를 적용한 픽셀은 면적이 0.0072 mm² 로 약 1200 채널을 망막영역에 삽입할 수 있을 것으로 기대된다.

장기 이식 가능한 광학 창이 포함된 패키징 물질로 액정 폴리머(LCP)를 제안하고, 이를 검증하기 위해서 광학적 성질을 측정하였다. LCP 필름은 비활성, 생체친화적인 유연한 폴리머 물질로 흡습성도 Pylex 유리와 비슷하여 장기이식 가능한 물질로 각광받고 있다. 우리는 가시광선 투과율을 10 % 보장하기 위해 최대 10 μm 이하의 두께의 LCP 필름이 필요하다는 사실을 알아내고, 빛 산란성을 줄이기 위해 표면의 거침이 적도록 하는 O2 DRIE 기법을 이용하여 LCP 필름을 식각하였다. 제작한 8.28 μm 두께의 LCP필름의 분해능을 측정한 결과 90 μm를 얻을 수 있었고, 이는 망막영역에 1200 채널의 인공 망막 장치를 삽입할 수 있음을 보였다.